

## Response to Anonymous Referee #1

We would like to thank the referee for their review of this manuscript and their useful comments which have helped to improve the paper. Below we provide our response to the comments. Text in blue refers to text that has been added to or adjusted in the manuscript.

1) In Section 3.2.1 the methodology for the comparison between FRP-PIXEL product and other geostationary fire products is described. For FIR and WFABBA products, the less conservative classes of fire detections are excluded by the analysis. (For WFABBA, only filtered fire detections have been used in the analysis. This product has also different classes of outputs (Processed, Saturated, Cloud Contaminated, High Probability, Medium Probability, Low Probability). Have all of them been included in the analysis?). This comparison analysis shows that in general the FRP-PIXEL product generates a much higher number of fires detections with respect to the other geostationary fire products. In the light of this, do the authors think that it would be of interest to include in this comparative analysis also the less conservative detections for the other satellite fire products? If not related to the exclusion of the less probable classes of detection, what are, according to the authors, the main reasons of the differences observed with the other active fire products derived from the same Meteosat SEVIRI observations.

As suggested by the reviewer, we have updated the comparison between the different SEVIRI active fire datasets and now include all four variations of the WFABBA dataset. These are the inclusion of all active fire detections, all fire detections WFABBA 'filtered' dataset (where SEVIRI fire pixels that area only detected once during 24 hrs are removed) and WFABBA 'filtered' detections keeping only the higher probability fires (WFABBA flags 0 to 3) and high and medium probability fires (WFABBA flags 0 to 4). Figure 5 (in the manuscript; and shown below) has been updated to show the diurnal cycle of fire pixel detections which now includes the different variations of the active fire datasets. The full WFABBA dataset provides a marginally greater number of active fire detections than the filtered WFABBA dataset using all detections irrespective of detection confidence. Both of these datasets detects fewer active fire pixels than even the LSA SAF FRP-PIXEL dataset screened to only include pixels with an FRP >50 MW (which are generally the high confidence detections). Table 2 in the manuscript (and shown below) has been adjusted to include this new analysis :

**Table 2** : Summary of active fire pixel detection errors of omission and commission of the four SEVIRI-derived active fire products explored herein (LSA SAF FRP-PIXEL product; Wooster *et al.*, 2015, WF-ABBA; Prins *et al.*, 1998, Fire Detection and Monitoring - FDeM; Amraoui *et al.*, 2010, and FIR Active Fire Monitoring; Joro *et al.*, 2008). Data were collected over the LSA SAF southern Africa geographic region during August 2014, when fire activity is widespread in this area. The MODIS active fire products (MOD14 and MYD14; Giglio *et al.*, 2003) acted as the independent data source for the comparison.

	<u>FRP-PIXEL</u>	<u>WFABBA</u>	<u>WFABBA</u>	<u>WFABBA</u>	<u>WFABBA</u>	<u>FDeM</u>	<u>FIR</u>
		<u>All detection</u>	<u>Filtered</u>	<u>Filtered (flags 0-4)</u>	<u>Filtered (flags 0-3)</u>		
<u>SEVIRI fire pixels at</u>	<u>33414</u>	<u>15610</u>	<u>13008</u>	<u>9736</u>	<u>8832</u>	<u>7664</u>	<u>7151</u>

<u>coincident MODIS overpasses</u>							
<u>SEVIRI fire pixels detected by MODIS</u>	<u>29037</u>	<u>14521</u>	<u>12284</u>	<u>9369</u>	<u>8496</u>	<u>7260</u>	<u>6730</u>
<u>Commission error (%)</u>	<u>13</u>	<u>7</u>	<u>6</u>	<u>4</u>	<u>4</u>	<u>5</u>	<u>6</u>
<u>Omission error (%)</u>	<u>77</u>	<u>82</u>	<u>84</u>	<u>87</u>	<u>88</u>	<u>92</u>	<u>95</u>

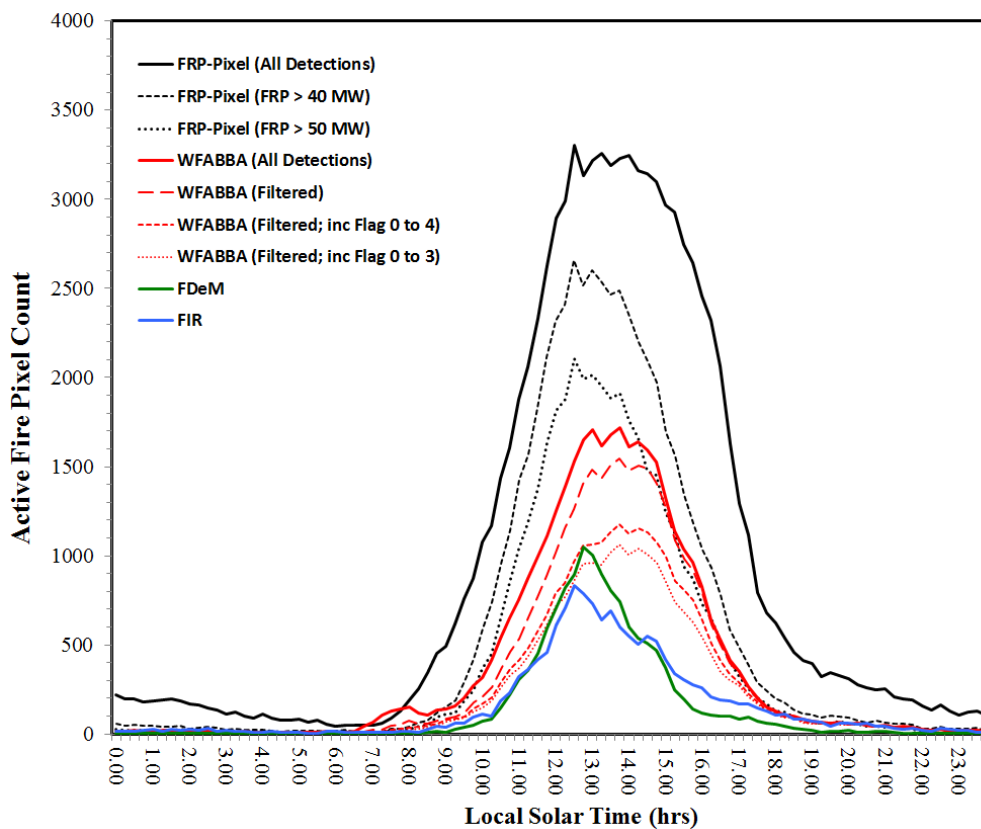


**Figure 5:** Diurnal cycle of active fire detections made by the four SEVIRI active fire products discussed herein over the LSA SAF southern Africa geographic region (Figure 1) on a single day (30<sup>th</sup> August 2014). The products are the LSA SAF FRP-PIXEL product (Wooster *et al.*, 2015), Wildfire-ABBA (WFABBA; Prins *et al.*, 1998), Fire Detection and Monitoring (FDeM; Amraoui *et al.*, 2010) and Active Fire Monitoring (FIR; Joro *et al.*, 2008). All confirmed active fire detections made in each product are included here for completeness, and results are shown in terms of the local solar time of detection. For the FRP-PIXEL product, three active fire time-series are shown; 1) all detections, and those only those detections from fire pixels with FRP magnitudes 2) >40 MW and 3) >50 MW since it is known that increasing undercounting of active fire pixels occurs around these limits (Roberts

and Wooster, 2008). For the WFABBA active fire detections, four versions of the dataset are included 1) all active fire detections, 2) the WFABBA 'filtered' detections where active fire pixels only detected once during 24 hrs are removed; and the WFABBA filtered detections keeping only 3) the high probability fires (flags 0 to 3) and 4) high and medium probability fires (flags 0 to 4). The LSA SAF FRP-PIXEL product detects a total of 89781 active fire pixels over the day which reduces to 53561 and 39461 when restricted to fire pixels with FRP magnitudes >40 MW and >50 MW respectively. For the WFABBA detections, the total number of active fire detections is 35759, the WFABBA filtered dataset contains 35759 detections which reduces to 30751 and 23957 when low and medium probability fire detections are removed. The FDeM and FIR detect only 13477 and 14645 active fire pixels respectively.

If not related to the exclusion of the less probable classes of detection, what are, according to the authors, the main reasons of the differences observed with the other active fire products derived from the same Meteosat SEVIRI observations?

As the revised Figure 5 indicates, the exclusion of fire pixel detections which are deemed to have a lower detection confidence reduces the total number of detections significantly. Differences in the number of active fire detections between active fire datasets are also the result of the inputs to the algorithm (e.g. cloud and land cover masks), pre-processing (e.g. atmospheric correction) and the algorithm itself (e.g. the type and value of the thresholds applied to discriminate fire affected pixels from non-fire affected pixels). The majority of the performance difference is very likely due to the detection algorithm methods and thresholds, but other factors are important. For example, Freeborn *et al.* (2014) found that the sensitivity of the SEVIRI cloud mask accounted for 30% of the LSA SAF FRP-PIXEL products omission rate when compared against the MODIS active fire product. It is difficult to exactly partition the cause of the differences in the number of fire pixel detections between the various SEVIRI active fire products, in part because with the exception of the LSA SAF FRP-PIXEL product no additional information is provided with the other products other than that of the detected active fire pixels. Therefore, we are unable to determine the effect of algorithm threshold difference on the numbers of detected fire pixels verses, for example, the different cloud mask used. Nevertheless, it is clear from the results that the LSA SAF FRP-PIXEL product is by far the most sensitive to the presence of active fires.

As a demonstration of the different algorithm sensitivities, we further analysed the per-pixel FRP frequency-magnitude distribution of each SEVIRI active fire product using one month of SEVIRI observations (August 2014). The FDeM and FIR products don't provide FRP estimates for detected active fire pixels, whilst the WFABBA algorithm uses a different approach (Dozier method) to measure FRP. Therefore, for consistency, we used the FRP values from the FRP-PIXEL product that are coincident with MODIS active fire detections as the basis for the assessment, and compared only active fire detections from the FRP-PIXEL, FDeM, FIR and WFABBA datasets that are spatially and temporally coincident with these in the analysis. This approach does not account for active fire detections present in the non FRP-PIXEL products but not in the FRP-PIXEL active fire detections. However, these are small in number since the FRP-PIXEL product delivers by far the greatest number of active fire counts.

Results, shown in Figure 1 below, indicate that the FRP-PIXEL product detects a greater number of low FRP pixels compared to the other products, and can detect fires with an FRP are low as 30 MW with confidence. The "pins" mark the point at which there is a decline in

algorithm fire detection performance, i.e. when the algorithm starts to become obviously weaker at discriminating the thermal radiance emitted from small and/or lower intensity fires. This occurs below around 50 MW for the filtered WFABBA product, around 80 - 100 MW for the FIR and FDeM products respectively. The percentage of pixels from each dataset which are not coincident with a FRP-PIXEL and MODIS active fire detection are 21% (WFABBA), 29% (FDeM) and 19% (FIR). Because this analysis only includes detections coincident with the FRP-PIXEL product and with MODIS fire pixels it includes only ~70 - 80% of the pixels present in all of the analysed SEVIRI active fire datasets, so the results do not fully represent these products and we do not include the analysis in the manuscript. However, it is broadly indicative of performance and we include it here for the benefit of the review and for completeness.

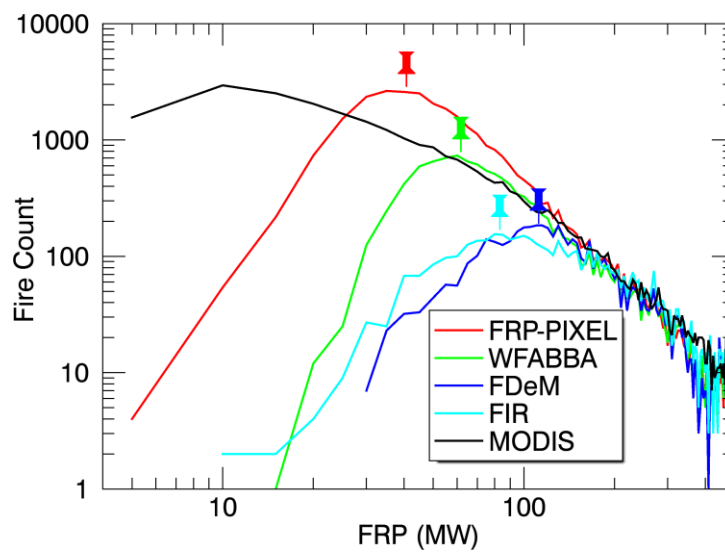


*Figure 1. Frequency-magnitude distributions constructed from coincident active fire pixels detected by the FRP-PIXEL, WFABBA, FDeM and FIR products that are coincident with MODIS active fire detections over the southern Africa region during August 2014. The lower breakpoint of the distribution of each product (shown as a pin), coincides with the decline in each active fire detection product performance as the thermal radiance emitted from small and/or lower intensity fires cannot be distinguished from the background signal in each product. The FRP values at the lower breakpoint are 30 MW, 50MW, 100 MW, 80 MW for FRP-PIXEL, WFABBA, FDeM and FIR respectively.*

2) In Section 5.2.2 and in Table 4 it is not clear which enhancement factor has been used to adjust the bottom-up aerosol emission estimates to those observed in top-down inventories.

We noticed an unnecessary adjustment factor in Equation 3 ( $\beta=1$  in our study) and an unnecessary subscript in Equation 4, that describe the calculation of emissions from the Peloponnese fires. For the Peloponnese region, Table 4 contains the emissions factors ( $\eta_s$ ) for a number of gas and aerosol species for land cover type ( $l$ ). In fact, the extratropical forest of this island is the only landcover type used in this case study. A constant ( $\alpha$ ) is used to adjust the bottom-up aerosol emissions to those observed via top-down inventories. In the manuscript this was given a subscript  $l$  ( $\alpha_l$ ) when, given the constant landcover type a global

constant of 3.1 for aerosol emissions and 1 for gaseous smoke constituent was applied. This enhancement makes our calculation consistent with Ichoku and Kaufman *et al.* (2005) and just 10% lower than Kaiser *et al.* (2012). The unnecessary subscript *l* has been removed:

$$\eta_s = \alpha(s) \times \kappa_l(s) \quad (4)$$

where  $\alpha = 3.1$  for aerosol emissions and  $\alpha = 1$  for gaseous smoke constituents. To make this clearer in the manuscript, the paragraph discussing Equation 4 has been adjusted to :

$$\eta_s = \alpha(s) \times \kappa_l(s) \quad (4)$$

where  $\kappa_l$  is the land cover (*l*) specific emissions factor for species *s* and  $\alpha$  is a constant which is used to adjust bottom-up aerosol emissions estimates to those observed in top-down inventories. A regionally varying bias occurs between bottom-up derived aerosol emissions and MODIS AOD measurements, requiring the former to be adjusted when being used in air quality or climate model simulations (Peterenko *et al.*, 2012). Yang *et al.* (2011) also found smoke emissions ( $PM_{2.5}$ ) derived using the bottom-up approach was underestimated by a factor of three when compared to MODIS AOD retrievals. Kaiser *et al.* (2012) recommend a global aerosol enhancement by a factor of 3.4 as first-order correction. These values are also broadly consistent with differences of up to a factor of three found by Ichoku and Kaufmann (2005) using satellite observations of FRP and AOD compared to measurements of  $c \times \kappa_l(s)$  derived from laboratory measurements. Here, we estimate emissions of organic matter and black carbon in exact agreement with Ichoku and Kaufmann (2005) by enhancing their emission factors for Andreae and Merlet (2001) with a factor of 3.1. According to the GFEDv3 land cover dataset, also used for our calculations in GFAS (Kaiser *et al.*, 2012), the fire affected region of Greece is classed as extratropical forest and the emitted species and relevant emissions factors are given in Table 4.

3) In Section 5.2.2 (pg.15939 line 9) the choice of releasing the smoke emissions in the lowest atmospheric level has not been discussed. Given the magnitude of the modelled fires, how much the authors think, the missing information of the plume penetration above the Planetary Boundary Layer, could have impacted the simulation of the smoke plume evolution?

It is likely that releasing the calculated smoke emissions into the lowest atmospheric layer, rather than at higher altitudes, does have an impact on the modelled concentration and transport. For example, Leung *et al.* (2007) and Guan *et al.* (2008) found that the inclusion of plume injection height information in atmospheric transport models led a reduction in surface CO concentration around the source, since a greater proportion of the smoke emissions were lofted above the planetary boundary layer. However, actually estimating the correct smoke injection height to use in a particular fire simulation is a topic of much current debate and research, and is not yet solved. Even if for a particular event we could know the correct height from independent observations, this is not the case for the vast majority of fires that the Copernicus Atmosphere Service (CAMS) has to model.

Where it is actually attempted, the parameterisation of smoke plume injection height is currently typically achieved using direct EO measurements from stereo-imagery or lidar based methods, and sometimes through using empirical or deterministic models. Paugam *et al.* (2015a) for example provide a review of current methods used to estimate smoke plume injection height. Typically these depend on both the fire behaviour and ambient atmospheric situations. During the Peloponnese fires studied here, Lui *et al.* (2009) have provided an estimate of 2.5 km for the height of the plume closest to the wildfires using MISR observations acquired on the morning of 26<sup>th</sup> August. From Figure 9a in our manuscript, it is evident that the fire emitted FRP on the morning of the 26<sup>th</sup> August was high, but only around half that seen on the 25<sup>th</sup> August. This, coupled with morning image acquisition of MISR, when fire activity is typically less intense, suggests that the injection heights during the Peloponnese wildfires are actually likely to exceed those derived by Lui *et al.* (2009) from MISR; particularly during periods when the fire activity was most intense. However, currently we do not know the true injection height on the different days and times of the Peloponnese fires, and nor is this information available for other fires modelled in the Copernicus Atmosphere Service (CAMS) to which our study is a demonstration. One area of research, discussed by Sofiev *et al.* (2012) and Paugam *et al.* (2015b) is the use of FRP measurements within plume rise models in order to provide estimates of plume injection height over a wider range of fires. To reflect this, the following text has been added to the manuscript (Section 5.2.2) :

Smoke emissions from the Peloponnese fires were calculated using Equations 3 and 4, along with the emissions factors given in Table 4. The smoke emissions must be injected into the atmosphere at a particular height, or distribution of heights, and such injection height assumptions can have implications for the resulting spatio-temporal distribution of the emitted species. Leung *et al.* (2007) and Guan *et al.* (2008) demonstrated that use of more detailed plume injection height assumptions resulted in a reduction in near surface CO concentrations, since more plumes were assumed to be lofted above the boundary layer. Paugam *et al.* (2015a) provided a recent review of approaches to estimate smoke plume injection height, including the methods of Sofiev *et al.* (2012) and Paugam *et al.* (2015b) that use FRP measurements to characterise wildfire thermal properties related to plume rise. This research remains at a relatively early stage, but it appears that FRP measures may indeed have a role to play in characterising smoke plume injection height as well as the rate of emission of chemical and aerosol species. Here we retained the commonly used assumption that the calculated smoke emissions are injected into the lowest atmospheric level, since this is generally what has been assumed in the series of MACC projects thus far (Kaiser *et al.*, 2012). The CAMS is anticipated to use injections heights from Paugam *et al.* (2015b) in the future.

Guan, H., Chatfield, R., B., Freitas, S. R., Bergstrom, R. W., Longo, K. M. (2008) Modeling the effect of plume-rise on the transport of carbon monoxide over Africa with NCAR CAM. *Atmospheric Chemistry and Physics*. 8. 6801–6812.

Leung, F-Y, T., Logan, J. A., Park, R., Hyer, E., Kasischke, E., Streets, S and Yurganov, L. (2007) Impacts of enhanced biomass burning in the boreal forests in 1998 on tropospheric chemistry and the sensitivity of model results to the injection height of emissions. *Journal of Geophysical Research*. 112. D10313, doi:10.1029/2006JD008132

Liu, Y., Kahn, R. A., Chaloulakou, A. and Koutrakis, P. (2009) Analysis of the impact of the forest fires in August 2007 on air quality of Athens using multi-sensor aerosol remote sensing data, meteorology and surface observations. *Atmospheric Environment*. 43. 3310-3318.

Paugam, R., Wooster, M., Freitas, S. R. and Val Martin, M. (2015a) A review of approaches to estimate wildfire plume injection height within large scale atmospheric chemical transport models – Part 1. *Atmospheric Chemistry and Physics Discussions*. 15. 9767-9813.

Paugam, R., Wooster, M., Atherton, J., Freitas, S. R., Schultz, M. G. and Kaiser, J. W. (2015b) Development and optimization of a wildfire plume rise model based on remote sensing data inputs – Part 2. *Atmospheric Chemistry and Physics Discussions*. 15. 9815-9895.

Sofiev, M., Ermakova, T., and Vankevich, R. (2012) Evaluation of the smoke-injection height from wild-land fires using remote sensing data. *Atmospheric Chemistry and Physics*. 12. 1995-2006. doi:10.5194/acp-12-1995-2012.

4) From Section 5.3.1 SEVIRI saturation seems to be a major limitation of the FRPPIXEL product in describing the 2007 Greek fire episodes. Do the authors think that including MODIS-FRP derived emissions in the description of the selected fire episode could help to understand the impact that SEVIRI saturation has in underestimating the magnitude of the studied fire emissions?

The 2007 Peloponnese "mega fires" were very large and extremely intense - the greatest fire event recorded in Greece since the satellite era began we believe. Due to this, and the closely spaced nature of the fires which meant that many could be burning within a single SEVIRI pixel or group of pixels, the MWIR channel saturated on a number of occasions. Analysis shows that a maximum of 23% of the detected SEVIRI fire pixels were saturated in a single timeslot, on the day when the wildfires were at their most intense. Analysis of the total FRP record from the Peloponnese wildfires indicates that, on average, when SEVIRI and MODIS viewed the fires simultaneously SEVIRI measured 58% of the FRP measured by MODIS. Between the 24<sup>th</sup> and 26<sup>th</sup> August, when the wildfires were most intense (Figure 9a), MODIS made 13 overpasses and in total during co-incident observations SEVIRI measured 39% of the total FRP measured by MODIS.

The MODIS instrument offers the advantage of providing mostly unsaturated FRP observations, but is only capable of providing intermittent temporal sampling and thus estimating FRE from MODIS' FRP observations is not trivial. Baldassarre *et al.* (2015) report far better simulations of the Antalya (2008) fire in Turkey using the SEVIRI FRP-PIXEL product than with MODIS-derived FRP data, despite some saturation of the SEVIRI FRP observations. Estimating daily fire radiative energy (FRE) and fuel consumption using the temporally intermittent MODIS FRP measurements has been conducted in a number of



different ways. For example, one approach is via temporal integration of the daily FRP using an assumed diurnal fire cycle model (e.g. Kaiser *et al.*, 2012; Vermote *et al.*, 2009). Freeborn *et al.* (2011) provide a further method based on derived conversion coefficients, but all such approaches are often best suited to coarse spatial (e.g.  $1^\circ \times 1^\circ$  grid cells) and/or temporal resolution (e.g. 1 day, 1 week) derivations, not derivations for single fire events. This is in part evident from Figure 9a in the manuscript, where a fire diurnal cycle is evident for the Peloponeese fires but one that may not be described by an assumed diurnal cycle model (e.g. a modified Gaussian as assumed by some of the above MODIS-based methods). A coarser regional scales, such assumed fire diurnal cycles maybe more realistic fits to the true nature of fire activity. It is also the case that the FRP-to-FRE methods described by Vermote *et al.* (2009), and Freeborn *et al.* (2011), actually tend to underestimate SEVIRI FRE-derived fuel consumption estimates - when the latter have been adjusted to account for the low-spatial resolution bias of SEVIRI (Roberts and Wooster, 2008; Freeborn *et al.*, 2011).

Following the approach used in the Global Fire Assimilation System (GFAS) of the Copernicus Atmosphere Service (CAS; Kaiser *et al.*, 2012), we have adjusted the "raw" dry matter (DM) combustion estimates obtained using our remotely-sensed FRP measures by a land cover specific coefficient (Equation 2 in the manuscript) such that the totals are in line with those provided by the Global Fire Emissions Database (GFED, v3.1). This will aid somewhat aid accounting for the impact of underestimation of FRP caused by sensor saturation, and we have added the following text to Section 5.3.1 of the manuscript to indicate that the SEVIRI estimates are affected by saturation :

Between the 24<sup>th</sup> and 26<sup>th</sup> August, when the wildfires were most intense, MODIS made 13 overpasses and SEVIRI measured 39% of the total FRP measured by MODIS. This demonstrates the massive scale of these fires, particularly given that the SEVIRI's pixel area over the region is  $\sim 14 \text{ km}^2$ .

Due to the aforementioned SEVIRI MWIR channel saturation, the SEVIRI FRP-derived fuel consumption estimate is considered a minimum estimate.

Freeborn, P. H., Wooster, M. J., Roberts, G. (2011) Addressing the spatiotemporal sampling design of MODIS to provide estimates of the fire radiative energy emitted from Africa. *Remote Sensing of Environment*. 115. 2. 475 – 489

Kaiser, J. W., Heil, A., Andrae, M. O., Benedettie, A., Chubarova, N., Jones, L., Morcrette, J.-J., Razinger, M., Schultz, M. G., Suttie, M. and van der Werf, G., R. (2012) Biomass burning emissions estimates with a global fire assimilation system based on observed fire radiative power. *Biogeosciences*. 9. 5125-5142. doi:10.5194/bg-9-5125-2012

Vermote, E., Ellicott, E., Dubovik, O., Lapyonok, T., Chin, M., Giglio, G. and Roberts, G. (2009) An approach to estimate global biomass burning emissions of Organic and Black Carbon from MODIS Fire Radiative Power. *Journal of Geophysical Research*. 114. D18205. doi:10.1029/2008JD011188.

Minor comment: Page 15921, Line 11. “: : further from the Meteosat sub-satellite point (SSP) : : :”

The manuscript has been altered accordingly



## **Response to Anonymous Referee #2**

We would like to thank the referee for their review of this manuscript and their useful comments which have helped to improve the paper. Below we provide our response to the comments. Text in blue refers to text that has been added to or adjusted in the manuscript.

Jenkins et al. (1998): the reference is missing

The reference has now been added to the reference list :

Jenkins, B. M., Baxter, L. L., Miles Jr, T. R., and Miles, T. R. (1998) Combustion properties of biomass. *Fuel Processing Technology*, 54, 17 – 46.

The authors state that the products may omit small and/or low intensity wildfires which are very frequent in the Mediterranean region. What would be the strategy to evaluate carefully this bias? Would the use of “ground truth” information e.g. from EFFIS European fire database be of any interest?

Non-detection of small and/or low intensity fires (i.e. low FRP fires) is an important issue, particularly in regions where SEVIRI’s pixel area is largest (i.e. furthest from the West African sub-satellite point). MODIS obtains FRP measurements using a 1 km<sup>2</sup> pixel area at nadir and is therefore able to detect many of the small fires that are omitted by the SEVIRI ~ 10 km<sup>2</sup> pixel area measurements (see Freeborn *et al.*, 2014). Nevertheless, the performance of the FRP-PIXEL product in this regard is far better than that of the competing products (see Figure 5 for example). The errors of omission reported in the manuscript during the SEVIRI to MODIS regional FRP comparisons (e.g. Table 2) result directly from SEVIRI's inability to see the lowest FRP fire pixels that MODIS can quite often detect. So this bias has been quantified here, and indeed is reported in Table 1 as the "Slope of linear best fit relationship between SEVIRI-to-MODIS Area-based FRP measures".

The LSA SAF FRP-GRID product, discussed in companion manuscript (Wooster *et al.*, 2015), accounts for the average bias introduced by the non-detection of low FRP fires by SEVIRI (in addition to biases resulting from factors such as cloud cover obscuration and MWIR pixel saturation). The approach used in the FRP-GRID product, discussed in Freeborn *et al.* (2009), applies a statistical matching method, developed using MODIS and SEVIRI FRP measurements made at the same time over a grid cell area (e.g. 5° cell size; Figure 20 in the companion paper Wooster *et al.*, 2015), to adjust SEVIRI grid cell total FRP to that which would have been measured by MODIS.

The use of high spatial resolution burned area data, such as EFFIS, to improve FRP-derived emission estimates has been attempted previously (Roberts *et al.*, 2011). The approach is able to harness the benefits of active fire and burned area datasets and the resulting fuel consumption estimates are closer to those found in emissions inventories such as GFED since the fuel consumption delivered by lower-FRP pixels that can remain undetected can be incorporated via the burned area parameter. However, burned area measurements are made one or more days after the fire event and are therefore not appropriate for the sort of near real-time emissions modelling that the FRP-PIXEL product is aimed at, and which the CAMS is designed to deliver. Burned area datasets, such as EFFIS, could be used to determine which

fires are not detected at all by SEVIRI, and it can be expected these are likely to be small and/or low intensity fires. However, it is also the case that prior work by Freeborn *et al.* (2014) indicates that the vast majority of MODIS active fire pixels over the Central African Republic had a SEVIRI active fire pixel located within 3 - 5 km at some point during the wildfires lifetime (just not necessarily at the time of the MODIS overpass). This leads to the conclusion that SEVIRI may detect one or more active fire observations in a very large proportion of burned areas, for example those included in EFFIS, but in some cases these detections may just occur at the times of 'peak' fire intensity. This is not always the case, it depends on the fire behaviour, and for example our study of the Peloponnese fires conducted here does not show a significant undercounting of low intensity fires by SEVIRI since the fire activity was of an extreme magnitude.

Freeborn, P. H., Wooster, M. J., Roberts, G., and Xu, W. D. (2014) Evaluating the SEVIRI fire thermal anomaly detection algorithm across the Central African Republic using the MODIS Active Fire product. *Remote Sens.*, 6, 1890–1917, 2014.

Freeborn, P. H., Wooster, M. J., Roberts, G., Malamud, B. D., and Xu, W. (2009) Development of a virtual active fire product for Africa through a synthesis of geostationary and polar orbiting satellite data. *Remote Sensing of Environment*, 113, 1700–1711. FRP

Roberts, G., Wooster, M., Freeborn, P.H., & Xu, W. (2011). Integration of geostationary FRP and polar-orbiter burned area datasets for an enhanced biomass burning inventory. *Remote Sensing of Environment*, 115, 2047-2061

P15932 116 ther ! the r  
This has been corrected

The authors highlight the uncertainties in the smoke injection height. They could mention briefly that FRP products could be used to refine this parameter as well.

A number of approaches exist to estimate smoke plume injection height such as using direct satellite observations (e.g. MISR or CALIOP) or various forms of plume-rise model. A comprehensive review of these approaches is provided by Paugam *et al.* (2015a). FRP measurements have been used along with other parameters to characterise plume injection height. The following text has been added to the manuscript (section 5.6) to reflect this :

Smoke emissions from the Peloponnese fires were calculated using Equations 3 and 4, along with the emissions factors given in Table 4. The smoke emissions must be injected into the atmosphere at a particular height, or distribution of heights, and such injection height assumptions can have implications for the resulting spatio-temporal distribution of the emitted species. Leung *et al.* (2007) and Guan *et al.* (2008) demonstrated that use of more detailed plume injection height assumptions resulted in a reduction in near surface CO concentrations, since more plumes were assumed to be lofted above the boundary layer. Paugam *et al.* (2015a) provided a recent review of approaches to estimate smoke plume injection height, including the methods of Sofiev *et al.* (2012) and Paugam *et al.* (2015b) that

use FRP measurements to characterise wildfire thermal properties related to plume rise. This research remains at a relatively early stage, but it appears that FRP measures may indeed have a role to play in characterising smoke plume injection height as well as the rate of emission of chemical and aerosol species. Here we retained the commonly used assumption that the calculated smoke emissions are injected into the lowest atmospheric level, since this is generally what has been assumed in the series of MACC projects thus far (Kaiser *et al.*, 2012). The CAMS is anticipated to use injections heights from Paugam *et al.* (2015b) in the future.

Guan, H., Chatfield, R., B., Freitas, S. R., Bergstrom, R. W., Longo, K. M. (2008) Modeling the effect of plume-rise on the transport of carbon monoxide over Africa with NCAR CAM. *Atmospheric Chemistry and Physics*. 8. 6801–6812.

Leung, F-Y, T., Logan, J. A., Park, R., Hyer, E., Kasischke, E., Streets, S and Yurganov, L. (2007) Impacts of enhanced biomass burning in the boreal forests in 1998 on tropospheric chemistry and the sensitivity of model results to the injection height of emissions. *Journal of Geophysical Research*. 112. D10313, doi:10.1029/2006JD008132

Liu, Y., Kahn, R. A., Chaloulakou, A. and Koutrakis, P. (2009) Analysis of the impact of the forest fires in August 2007 on air quality of Athens using multi-sensor aerosol remote sensing data, meteorology and surface observations. *Atmospheric Environment*. 43. 3310-3318.

Paugam, R., Wooster, M., Freitas, S. R. and Val Martin, M. (2015a) A review of approaches to estimate wildfire plume injection height within large scale atmospheric chemical transport models – Part 1. *Atmospheric Chemistry and Physics Discussions*. 15. 9767-9813.

Paugam, R., Wooster, M., Atherton, J., Freitas, S. R., Schultz, M. G. and Kaiser, J. W. (2015b) Development and optimization of a wildfire plume rise model based on remote sensing data inputs – Part 2. *Atmospheric Chemistry and Physics Discussions*. 15. 9815-9895.

Sofiev, M., Ermakova, T., and Vankevich, R. (2012) Evaluation of the smoke-injection height from wild-land fires using remote sensing data. *Atmospheric Chemistry and Physics*. 12. 1995-2006. doi:10.5194/acp-12-1995-2012.

Formatted: Centered

## Minor changes made to manuscript

The manuscript copied below this section contains the changes made to the manuscript. The text in red indicates changes which have been made to correct typographical errors and also from changes in response to the reviewers comments. The blue text also indicates changes made as a result of the review process. These changes are indicated in the reply to the reviewers comments which are provided at the start of this document and which have been uploaded to the ACPD website. Text in purple indicates text which has been moved or rephrased to improve clarity. Most of these changes are related to the movement and rephrasing of text in response to the reviewers comments by one or more of the co-authors.

During the review process we made two additions to the manuscript which was included to extend the product description and to ensure the performance evaluation was as up to date of possible for the benefit of the users. This work was being carried out during the review and author response period. In section 3.2.2 (end of paragraph 2) of the manuscript we described a proposed change to the operational LSA-SAF algorithm which was being implemented during the reprocessing of the SEVIRI archive. The original text from the manuscript is given below :

*"This issue will be addressed in a future FRP-PIXEL product update, balancing the need to minimise active fire errors of commission with the requirement to deliver each new product in a timely fashion soon after image acquisition. This change is scheduled to be implemented prior to summer 2015, and the entire SEVIRI archive will later be re-processed with the optimised algorithm."*

Whilst the manuscript review process was ongoing we were able to include the findings of a study where we compared one month of SEVIRI active fire observations, which contained the algorithm improvements, against spatially and temporally coincident MODIS active fire observations using the same methodology we applied in section 3.2.1. The text in the paragraph now includes the results of this comparison :

*"We have tested these adaptations using one month of data (July, 2015) collected over the same Southern African region used to perform the evaluation reported in Table 2, and have compared the results to those from contemporaneous MODIS overpasses. Results show that with both adaptations applied, the error of commission of the adjusted FTA algorithm compared to MODIS reduce from the current 14% to 12%, whilst the error of omission remains at 70%. These two adaptations are therefore now being implemented in the operational FTA processing chain."*

The 2<sup>nd</sup> addition we made to the manuscript was the inclusion of two further authors (Jiangping, H<sup>2</sup>. and Fisher, D<sup>2</sup>) who contributed to our response to the reviewers comments. The authors list is now :

Roberts, G<sup>1\*</sup>., Wooster, M. J<sup>23</sup>., Xu, W<sup>2</sup>., Freeborn, P. H<sup>6</sup>., Morcrette, J-J<sup>5</sup>., Jones, L<sup>5</sup>, Benedetti, A<sup>5</sup>, Jiangping, H<sup>2</sup>., Fisher, D<sup>2</sup>. and Kaiser, J. W<sup>4</sup>

Formatted: Centered

**LSA SAF Meteosat FRP Products: Part 2 - Evaluation and demonstration of use in the Copernicus Atmosphere Monitoring Service (CAMS)**

~~Meteosat SEVIRI Fire Radiative Power (FRP) Products from the Land Surface Analysis Satellite Applications Facility (LSA SAF): Part 2—Product Evaluation and Demonstration of use within the Copernicus Atmosphere Service~~

Roberts, G<sup>1\*</sup>, Wooster, M. J<sup>23</sup>, Xu, W<sup>2</sup>, Freeborn, P. H<sup>6</sup>, Morcrette, J-J<sup>5</sup>, Jones, L<sup>5</sup>, Benedetti, A<sup>5</sup>, Jiangping, H<sup>2</sup>, Fisher, D<sup>2</sup>, and Kaiser, J. W<sup>45</sup>

\*corresponding author

- 1) Geography and Environment, University of Southampton, Southampton, UK
- 2) Department of Geography, Kings College London, London, UK
- 3) NERC National Centre for Earth Observation, UK
- 4) Max Planck Institute for Chemistry, Mainz, Germany
- 5) European Center for Medium-Range Weather Forecasts, Reading, UK
- 6) Fire Sciences Laboratory, Missoula, USA

**ABSTRACT**

Characterising the dynamics of landscape scale wildfires at very high temporal resolutions is best achieved using observations from Earth Observation (EO) sensors mounted onboard geostationary satellites. As a result, a number of operational active fire products have been developed from the data of such sensors. An example of which are the Fire Radiative Power (FRP) products, the FRP-PIXEL and FRP-GRID products, generated by the Land Surface

**Formatted:** Font: (Default) +Headings CS (Times New Roman), 16 pt, Font color: Auto, Complex Script Font: +Headings CS (Times New Roman), 16 pt

**Formatted:** Font color: Auto

**Formatted:** Font: (Default) +Headings CS (Times New Roman), 16 pt, Font color: Auto, Complex Script Font: +Headings CS (Times New Roman), 16 pt

**Formatted:** Font color: Auto

**Formatted:** Font: (Default) +Headings CS (Times New Roman), 16 pt, Font color: Auto, Complex Script Font: +Headings CS (Times New Roman), 16 pt

**Formatted:** Font: (Default) +Headings CS (Times New Roman), 18 pt, Complex Script Font: +Headings CS (Times New Roman), 18 pt

**Formatted:** Not Superscript/ Subscript

**Formatted:** Not Superscript/ Subscript

**Formatted:** Superscript

**Formatted:** Not Superscript/ Subscript

**Formatted:** Superscript

**Formatted:** Not Superscript/ Subscript

Analysis Satellite Applications Facility (LSA SAF) from imagery collected by the Spinning  
 Enhanced Visible and Infrared Imager (SEVIRI) on-board the Meteosat Second Generation  
 (MSG) series of geostationary EO satellites. The processing chain developed to deliver these  
 FRP products detects SEVIRI pixels containing actively burning fires and characterises their  
 FRP output across four geographic regions covering Europe, part of South America and  
 northern and southern Africa. The FRP-PIXEL product contains the highest spatial and  
 temporal resolution FRP dataset, whilst the FRP-GRID product contains a spatio-temporal  
 summary that includes bias adjustments for cloud cover and the non-detection of low FRP  
 fire pixels. Here we evaluate these two products against active fire data collected by the  
 Moderate Resolution Imaging Spectroradiometer (MODIS), and compare the results to those  
 for three alternative active fire products derived from SEVIRI imagery. The FRP-PIXEL  
 product is shown to detect a substantially greater number of active fire pixels than do  
 alternative SEVIRI-based products, and comparison to MODIS on a per-fire basis indicates a  
 strong agreement and low bias in terms of FRP values. However, low FRP fire pixels remain  
 undetected by SEVIRI, with errors of active fire pixel detection commission and omission  
 compared to MODIS ranging between 9 - 13% and 65 - 77% respectively in Africa. Higher  
 errors of omission result in greater underestimation of regional FRP totals relative to those  
 derived from simultaneously collected MODIS data, ranging from 35% over the Northern  
 Africa region to 89% over the European region. High errors of active fire omission and FRP  
 underestimation are found over Europe and South America, and result from SEVIRI's larger  
 pixel area over these regions. An advantage of using FRP for characterising wildfire  
 emissions is the ability to do so very frequently and in near real time (NRT). To illustrate the  
 potential of this approach, wildfire fuel consumption rates derived from the SEVIRI FRP-  
 PIXEL product are used to characterise smoke emissions of the 2007 'mega fire' event  
focused on Peloponnese (Greece) and used-wildfires within the European Centre for  
 Medium-Range Weather Forecasting (ECMWF) Integrated Forecasting System (IFS), as a  
 demonstration of what can be achieved when using geostationary active fire data within the  
 Copernicus Atmosphere Monitoring System Service (CAMS). Qualitative comparison of the  
 modelled smoke plumes with MODIS optical imagery illustrates that the model captures the  
 temporal and spatial dynamics of the plume very well, and that high temporal resolution  
 emissions estimates such as those available from geostationary orbit are important for  
 capturing the sub-daily variability in smoke plume parameters such as aerosol optical depth  
 (AOD), which are increasingly less well resolved using daily or coarser temporal resolution  
 emissions datasets. Quantitative comparison of modelled AOD with coincident MODIS and

AERONET AOD indicates that the former is overestimated by ~20 - 30%, but captures the observed AOD dynamics with a high degree of fidelity. The case study highlights the potential of using geostationary FRP data to drive fire emissions estimates for use within atmospheric transport models such as those ~~currently~~ implemented ~~as part of~~ the Monitoring Atmospheric Composition and Climate (MACC) ~~series of programme projects~~ ~~for within~~ the ~~CAMS~~ Copernicus atmospheric service.



## 1. INTRODUCTION

### *1.1. Biomass Burning Emissions and Meteosat SEVIRI FRP Products from the LSA SAF*

Biomass burning emissions databases derived from Earth Observation (EO) satellite data, such as the widely used Global Fire Emissions Database (GFED; van der Werf *et al.*, 2006; 2010), typically follow the approach proposed by Seiler and Crutzen (1980) and estimate fire emissions via the multiplication of burned area ( $\text{m}^2$ ), fuel load ( $\text{kg m}^{-2}$ ) and combustion completeness (unitless, 0-1) estimates. Emissions databases developed in this manner have been widely applied to deliver wildfire emissions of trace gases and aerosols for use in atmospheric transport models (Mu *et al.*, 2011; Tsyro *et al.*, 2007). However, whilst excellent for many applications, some limitations of this ‘burned area’ based approach are that it works only after the fire event, cannot be applied in near real-time, and has a relatively low temporal resolution that provides little or no information on the variability of the emissions during the fire itself. All these maybe limitations when modelling certain aspects of fire emissions transport and generally preclude use of the approach in real-time atmospheric monitoring or forecasting systems (Reid *et al.*, 2004). The companion paper to this work, Wooster *et al.* ([this-issue2015](#)) describes the geostationary Meteosat SEVIRI Fire Radiative Power (FRP) products being generated operationally by the EUMETSAT Land Surface Analysis Satellite Applications Facility (LSA SAF; <http://landsaf.meteo.pt/>). This type of geostationary active fire product offers an alternative route to biomass burning emissions estimation based on assessments of the thermal energy being radiated away from fires, and can do so in near real-time with frequent updates whilst the fires are still burning, though there are also some limitations caused mainly by fires having too low a fire radiative power remaining undetectable with the relatively coarse spatial resolution SEVIRI observations (Roberts and Wooster, 2008). Whilst Wooster *et al.* ([this-issue2015](#)) describe the methodologies and algorithms used to produce the LSA SAF Meteosat FRP products, and their information

characteristics, the purpose of the current work is to (i) provide a full evaluation of the product compared to other real-time active fire products derived from the same SEVIRI observations, (ii) to provide a product validation via comparisons to the widely used and higher spatial resolution (albeit lower temporal resolution) MODIS active fire detections, and (iii) to demonstrate how the product can be used as a high temporal resolution biomass burning emissions driver within a case study that exploits components of the prototype CAMS Copernicus Atmosphere Service (<http://www.copernicus-atmosphere.eu/>)

## 1.2. Satellite Earth Observation Active Fire Products

Active fire products that are based on detecting the thermal radiation being emitted by landscape scale fires have been available for over three decades from numerous polar orbiting and geostationary satellites (Prins *et al.*, 1994; Prins *et al.*, 1998; Matson, 1981, Justice *et al.*, 1998; Giglio, 2003b). In addition to simple detection, Dozier (1981) first demonstrated the additional potential to estimate a fire's subpixel effective temperature and fractional area, and this approach has been applied in the Wildfire Automated Biomass Burning Algorithm (WFABBA) to data from the Geostationary Operational Environmental Satellite (GOES) for over two decades (Prins *et al.*, 1994). Building on this idea, the FRP route to characterising active fires and estimate wildfire emissions was first proposed by Kaufman *et al.* (1996). The FRP approach is based on the understanding that the amount of heat produced by burning a fixed mass of biomass is relatively invariant to vegetation type (Jenkins *et al.*, 1998). By measuring the component of this "heat of combustion" that is radiated away from the surface, the amount of vegetation being burned per second can then be estimated (Wooster *et al.*, 2003; Wooster *et al.*, 2005; Freeborn *et al.*, 2008). An advantage of the FRP approach for estimating smoke emissions to the atmosphere is that it is based on a direct remotely sensed observation, and a large number of polar and geostationary satellite instruments have the requisite midwave infrared ~~Infrared~~ (MWIR) waveband required to estimate FRP using the MIR radiance approach of Wooster *et al.* (2003; 2005). The Moderate Resolution Imaging Spectroradiometer (MODIS) instruments onboard the Terra and Aqua satellites have been providing FRP measurements since 2000 and 2002 respectively (Kaufman *et al.*, 1998; Giglio *et al.*, 2003b) and is currently supported by the Visible Infrared Imaging Radiometer Suite (VIIRS) onboard Suomi-NPP (Csiszar *et al.*, 2013) and the soon-to-be-launched Sea and Land Surface Temperature Radiometer (SLSTR) onboard Sentinel-3 (Wooster *et al.*, 2012). Geostationary instruments, such as the Geostationary Operational Environmental Satellite (GOES) imager (Xu *et al.*, 2010), are also providing FRP measurements at much higher

temporal resolution but at lower spatial resolution and coverage, and those from the Meteosat SEVIRI instrument (Wooster *et al.*, [this issue 2015](#)) are the target of the current work.

### **1.3. Wildfire Emissions Datasets from FRP Observations**

Information on the fuel consumption totals required to build wildfire emissions inventories have already been developed using FRP data derived from polar-orbiter (Vermote *et al.*, 2009; Ellicott *et al.*, 2009; Kaiser *et al.*, 2012) and geostationary satellite EO data (Pereira *et al.*, 2011; Roberts *et al.*, 2011). A limitation associated with the former is their intermittent observation of the diurnal fire cycle, which needs to be characterised in order to estimate daily Fire Radiative Energy (FRE; the temporal integration of FRP). MODIS typically provides around four daily observations depending on latitude which, when accumulated over a sufficiently long time period, have been exploited to model the diurnal fire cycle and estimate total emissions over 8-day or longer periods (Vermote *et al.*, 2009; Ellicott *et al.*, 2009). Geostationary FRP datasets provide much higher observation frequencies, and thus unparalleled data on the diurnal fire cycle (e.g. Roberts and Wooster, 2007; Roberts *et al.*, 2009;), and Zhang *et al.* (2012) illustrate one way such data can be used to develop a near global biomass burning emissions dataset at hourly type temporal resolutions. However, a limitation of geostationary data is their coarse spatial resolution, which results biases in regional-scale FRP and FRE due to the omission of small and/or low intensity wildfires (Roberts *et al.*, 2005; Xu *et al.*, 2010). Freeborn *et al.* (2009) addressed this issue by synthesising a ‘virtual’ FRP product via the integration of both geostationary and polar-orbiter FRP data, maintaining the high temporal resolution of geostationary data whilst simultaneously adjusting them for the active fire detection biases using the higher spatial resolution MODIS measurements. Roberts *et al.* (2011) blended geostationary FRP data with MODIS-derived burned area information to meet a similar objective.

Perhaps the most obvious advantage FRP-based biomass burning emissions inventories offer over a burned area based inventory is their near real-time capability, since the thermal radiation being emitted by the active fires is being sensed whilst the fire is actually burning, rather than somewhat after the event. As a result, FRP-derived emissions estimates are being increasingly applied to characterise wildfire emissions for use in near real time atmospheric transport models. Sofiev *et al.* (2009) use MODIS FRP measurements to characterise particulate matter (PM) emissions using the method proposed by Ichoku and Kaufmann (2005), and the dispersion of the resulting emissions are propagated using the System for

Integrated modelling of Atmospheric composition (SILAM) dispersion model. In this approach, the diurnal variation of emissions is specified as being 25% greater than the daily mean during the day, and 25% less than the mean during the night. Kaiser *et al.* (2009a; 2012) developed the Global Fire Assimilation System (GFAS) to prescribe wildfire emissions for use in the ~~CAMSCopernicus Atmosphere Service~~, potentially calculating the FRP density emitted by actively burning fires ( $\text{mW m}^{-2}$ ) using a variety of FRP measurements from different spacecraft. However, in the NRT version of GFAS used currently only FRP measurements from MODIS are used. The FRE density ( $\text{J m}^{-2}$ ) is estimated by temporally integrating the MODIS-derived FRP density using a Kalman ~~smoother~~filter. Most recently, Turquety *et al.* (2014) used SEVIRI FRP measurements from the LSA SAF products to prescribe the fire diurnal cycle for the APIFLAME European fire emissions model, and Baldassarre *et al.* (~~in press~~2015) used both the LSA SAF SEVIRI FRP products and other active fire products to simulate the emissions and emissions transport of a large fire in Turkey.

This manuscript provides a detailed evaluation of the Meteosat SEVIRI FRP products available from the LSA SAF, both the full resolution FRP-PIXEL product and the reduced resolution FRP-GRID product, both available in near real time and in archived form (<http://landsaf.meteo.pt/>), and provides a detailed example of their use in characterising wildfire emissions and its atmospheric transport at high temporal resolution. Section 2 provides a brief product summary, and readers are referred to the companion paper (Wooster *et al.*, ~~this issue~~2015) for a more detailed description of the algorithms used to derive the information from the raw SEVIRI level 1.5 observations. Section 3 describes a detailed inter-comparison of the LSA SAF SEVIRI FRP-PIXEL product with both the MODIS active fire products (Giglio *et al.*, 2003), and three alternative active fire products also derived from SEVIRI observations: namely the WFABBA (Prins *et al.*, 1998), Fire Detection and Monitoring (FDeM; Amraoui *et al.*, 2010) and Active Fire Monitoring (FIR) product (Joro *et al.*, 2008). Section 4 evaluates the specific performance of spatio-temporal summary ‘FRP-GRID’ product available from the LSA SAF, which incorporates statistical adjustments for SEVIRI’s regional FRP biases, whilst Section 5 describes use of the FRP-PIXEL product for parameterising wildfire emissions at high temporal resolution within the ECMWF Integrated Forecasting System (IFS) atmospheric chemistry and transport model that is used to deliver the ~~CAMSCopernicus Atmosphere Service~~ (<http://www.copernicus-atmosphere.eu/>).

## 2. METEOSAT SEVIRI FRP PRODUCTS FROM THE EUMETSAT LSA SAF

The Spinning Enhanced Visible and Infrared Imager (SEVIRI) onboard the Meteosat Second Generation (MSG) series of satellites acquires observations every 15 minutes over the Earth's disk centred on West Africa, including in MWIR and long-wave infrared (LWIR) wavebands. Data collected in these wavebands enables the detection of active fires using the type of algorithms detailed in Li *et al.* (2001), and this has been exploited for the development of a number of geostationary active fire products based on SEVIRI observations. One of these is the Meteosat SEVIRI FRP-PIXEL family of products that has been produced operationally since 2008 by the European Organisation for the Exploitation of Meteorological Satellites (EUMETSAT) LSA SAF (<http://landsaf.meteo.pt>). The LSA SAF Meteosat SEVIRI FRP product suite currently contains two components; (i) the FRP-PIXEL product which records active fire information at the full temporal and spatial resolution of SEVIRI, and (ii) the FRP-GRID product that provides a spatio-temporal summary of the FRP-PIXEL product, along with statistical adjustments for cloud cover and for the regional biases caused by the lowest FRP fires being undetectable with SEVIRI.

### 2.1 FRP-PIXEL Product Summary

The Level 2 FRP-PIXEL product provides information on the spatial location, thermal properties, atmospherically corrected FRP and uncertainty of pixels containing actively burning fires every 15 minutes over Europe, North and South Africa and part of South America (Figure 1), based upon an extended version of the geostationary Fire Thermal Anomaly (FTA) active fire detection algorithm of Roberts and Wooster (2008) and a set of FRP estimation routines that are together fully detailed in Wooster *et al.* ([this issue 2015](#)). The structure of the FRP-PIXEL product is also detailed in Wooster *et al.* ([this issue 2015](#)), and follows the heritage of the MODIS active fire products (Giglio *et al.*, 2003) but separated into two discrete files, (i) the FRP-PIXEL 'Quality Product' file, a 2D dataset that provides information on the status of each SEVIRI pixel in the geographic region under study (e.g. whether it is a cloud, water, or land pixel, whether it has been classed as containing an active fire etc; Wooster *et al.*, [this issue 2015](#)), and (ii) a smaller 'List Product' file that provides detailed information of pixels in which active fires have been detected (e.g. including the pixel MWIR and LWIR brightness temperatures, FRP, FRP uncertainty, latitude and

longitude, and some of the metrics derived during algorithm application such as background window size and estimated MWIR band atmospheric transmissivity).

## 2.2 FRP-GRID Product Summary

The Level 3 FRP-GRID product is a spatio-temporal summary of a series of FRP-PIXEL products. At the regional scale, the FRP-PIXEL product provides a minimum estimate of the FRP being emitted from landscape fires due to (i) the inability of SEVIRI to detect the lowest FRP active fire pixels (Roberts and Wooster, 2008; Freeborn *et al.*, 2014a) and (ii) the fact that the assessment of the highest FRP fires suffer from some effects of pixel saturation and other SEVIRI-specific observation characteristics (Wooster *et al.*, [this-issue2015](#)). In order to try mitigate these impacts on regional FRP estimation, the LSA SAF processing chain generates the Level 3 FRP-GRID product by temporally accumulating active fire pixels and associated information from the maximum of four FRP-PIXEL products obtained each hour, grids this information within 5.0° grid cells, and applies a set of regional bias adjustment factors. Wooster *et al.* ([this-issue2015](#)) describe the procedures in full, and an evaluation of the resulting product performance is presented in Section 4 herein.

## 3. FRP-PIXEL PRODUCT PERFORMANCE EVALUATION

Here we validate the SEVIRI FRP products using MODIS active fire data. The relatively high spatial resolution of MODIS' active fire observations (1 km at nadir), and the high saturation temperature of its MWIR channel (~ 500 K), coupled with its better than daily availability from two platforms (the Terra and Aqua satellites), ensure that the MODIS active fire product (Kaufman *et al.*, 1998; Giglio *et al.* 2003) ~~are-is~~ the standard against which geostationary active fire products are compared when performing product evaluations (Xu *et al.*, 2010; Schroeder *et al.*, 2014; Roberts and Wooster, 2014). Here we use near-simultaneously recorded Collection 5 MODIS active fire detections (MOD14 from Terra and MYD14 from Aqua) as the basis of our LSA SAF SEVIRI FRP Product performance evaluations. For completeness, we also include a series of other SEVIRI active fire products, derived using different algorithms and methods to the LSA SAF FRP products, within the same comparison.

### 3.1 SEVIRI FRP-PIXEL and MODIS Active Fire Product Intercomparison

### 3.1.1 Methodology

The FRP-PIXEL product is generated in separate files for the four LSA SAF geographic regions whose boundaries as shown in Figure 1 (Wooster *et al.*, [this issue2015](#)). We conducted the FRP-PIXEL product performance evaluation using one week of operational FRP-PIXEL data collected by Meteosat-9 in each of the LSA SAF regions, together with the matching MODIS MOD14 and MYD14 products. The FRP-PIXEL products of each region were derived from 672 separate SEVIRI imaging slots taken every 15 minutes over a 168 hour period in 2008, with the timing of the products for each geographic region being that corresponding to its peak fire period; December in Northern hemisphere Africa, and August in the remaining three regions. Freeborn *et al.* (2014a) previously performed an evaluation of the FRP-PIXEL product over the Central African Republic (CAR), finding that the products active fire detection errors of commission reduced greatly (from 24% to 9%) when the MODIS active fire detections being used as the independent data source were limited to a  $\pm 18.6^\circ$  scan angle. This is due to the increasing pixel area of MODIS with increasing scan angle, which results in MODIS itself showing progressively greater active fire errors of omission towards the scan edge (Freeborn *et al.*, 2011). When comparing large-scan angle MODIS data to active fire detections made from SEVIRI, it may well be that MODIS actually misses fires that the SEVIRI FRP-PIXEL product actually correctly detects, but in the absence of any other information a SEVIRI-to-MODIS performance evaluation would record this as a SEVIRI commission error. Therefore, to mitigate against the impact of MODIS' decreasing ability to detect low FRP pixels as MODIS scan angle increases, yet balance this with the need to maintain sufficient data in our intercomparison, MODIS observations are limited to those within  $\pm 30^\circ$  scan angle within which MODIS' pixel area increases up to a maximum of 1.7 km<sup>2</sup> from the nadir 1 km<sup>2</sup> size (Freeborn *et al.*, 2011). For each LSA SAF geographic region we compared the active fire detections made by MODIS within this scan angle limit to the active fire pixels present in the FRP-PIXEL product subsets covering the same area and collected at the closest matching time (generally this will be within ~ 6 minutes of the MODIS overpass). To deal with the differing MODIS and SEVIRI pixel sizes, we remapped the MODIS active fire data to SEVIRI's imaging grid. SEVIRI's per-pixel point spread function (PSF) at the sub-satellite point extends more than 5 km radially from the pixel centre (Wooster *et al.*, [this issue2015](#)), so following the approach of Freeborn *et al.* (2014a) we evaluated active fire detection performance using the presence of



an active fire pixel within a  $3 \times 3$  pixel window centred on the active fire pixel under investigation within this grid as a matched detection. For SEVIRI errors of commission we searched for the presence of a matching MODIS pixel for each SEVIRI active fire pixel studied, whilst the reverse analysis was conducted for SEVIRI errors of omission.

When undertaking the SEVIRI-to-MODIS FRP intercomparison, this was conducted on a 'per fire' basis by clustering the MODIS and SEVIRI per-pixel FRP measurements for the same fire into 'fire pixel clusters' on the basis of spatial closeness (e.g. Zhukov *et al.*, 2006; Roberts and Wooster; 2008; Xu *et al.*, 2011). The MODIS FRP measurements were derived using the same MIR radiance approach to FRP derivation as is used for SEVIRI (Wooster *et al.*, 2005; [this-issue2015](#)), and as will be employed in the forthcoming Collection 6 MODIS Active fire products (L. Giglio, *pers comm.*). We atmospherically corrected these MODIS FRP estimates using the same procedure applied when generating the FRP-PIXEL product, detailed in Wooster *et al.* ([this-issue2015](#)), based on an atmospheric transmission look-up-table (LUT) developed using the MODTRAN5 and RTMOM atmospheric radiative transfer models (Berk *et al.* 2005; Govaerts, 2006) and ECMWF forecasts of total water column vapour (interpolated from an original spatial and temporal resolution of  $0.5^\circ$  and 3 hours). Generally, the adjustment for the MWIR atmospheric transmission made to the SEVIRI FRP data was larger than that for MODIS, because the SEVIRI MWIR spectral band used in FRP derivation is significantly wider than that of MODIS and extends into spectral regions having much lower atmospheric transmission (Wooster *et al.*, [this-issue2015](#)).

### 3.1.2 Results

The results of our SEVIRI-to-MODIS per-fire active fire detection intercomparison are detailed in Table 1, Columns 3 and 4. Taking the north African (NAfr) LSA SAF region as the first example, this is closest region to the Meteosat sub-satellite point and therefore offers the highest degree of SEVIRI spatial detail and smallest pixel area. We find that 65% of MODIS' active fire detections made within this region had no corresponding SEVIRI-detected active fire within the closest matching (in time) FRP-PIXEL product file. This 'active fire error of omission' rate is higher than the 54% found previously by Roberts and Wooster (2008) over the same geographic area, but using the prototype SEVIRI FTA algorithm, a different period satellite (Meteosat-8) and different time period. The reverse analysis showed that 9% of the Meteosat-9 FRP-PIXEL product active fire pixels had no matching MODIS active fire pixel, a very similar commission error to that found by Roberts

and Wooster (2008) for the prototype SEVIRI FTA algorithm over the same North African region.

SEVIRI FRP-PIXEL product active fire detection performance metrics for the other three LSA SAF geographic regions are also shown in Table 1, and indicate a substantially increased active fire omission error in South America and Europe compared to the two African regions. This is in part due to SEVIRI's increased pixel area and greater view zenith angle (and thus greater atmospheric attenuation) over the former two regions which are further from the Meteosat [sub-satellite point](#) (SSP). South America and Europe have a mean view zenith angle of 59° and 54° respectively and this significantly raises the minimum per-pixel FRP detection limit in these areas (Figure 1), meaning a greater proportion of lower FRP landscape-scale fires fail to be detected by SEVIRI in comparison to the African regions.

Figure 2 and Table 1 (Column 5) present the results of the SEVIRI-to-MODIS per-fire FRP intercomparison. Again taking north Africa as an example, on a per-fire basis there is a strong correlation between the FRP measures made by SEVIRI in this region and by MODIS (Figure 2; top left) with over half (53%) of the SEVIRI-to-MODIS matchups having an FRP difference less than 20%. In fact, a strong level of agreement exists for all regions in terms of a low FRP bias between the two datasets, but there is significant scatter. Overall, we find that 57% of the FRP-PIXEL products per-fire FRP measures are within 20% of those of MODIS, and this level of agreement remains consistent even when limiting the comparison to fires with FRP > 50 MW to ensure we focus on the ~~region where~~ [the FRP range where](#) SEVIRI does not clearly underdetect active fires (e.g. Wooster *et al.*, [this issue 2015](#)). This suggests that the degree of variability seen between the near-simultaneous measures of per-fire FRP provided by SEVIRI and MODIS is not driven only by active fire pixel errors of omission (e.g. by SEVIRI failing to detect some of the low FRP fire pixels making up a fire cluster), but maybe impacted by other aspects of the FRP measurement process coming from:

- i) uncertainty in the ambient background signal used to calculate the FRP for each fire pixel with SEVIRI and MODIS data (Wooster *et al.*, 2003; 2005; Zhukov *et al.*, 2006; Wooster *et al.*, [this issue 2015](#));

- ii) the  $\pm 6$  minute time difference between corresponding MODIS and SEVIRI observations of the same fire, during which changes in the active fire characteristics that determine the fires FRP may occur;
- iii) the uncertainties present in the MODIS FRP measures coming from the sub-pixel location of the fire with respect to the sensor instantaneous field of view, recently been characterised by Freeborn *et al.* (2014c), and with SEVIRI also from certain image processing operations conducted during the production of SEVIRI level 1.5 data (Wooster *et al.*, ~~this issue~~2015).
- iv) effects of sensor saturation of SEVIRI's MWIR channel at high FRP fire pixels.

To place the magnitude of the scatter seen in Figure 2 between the SEVIRI FRP-PIXEL product's FRP measures and those from the MODIS MOD14 and MYD14 products into context, during the recent Freeborn *et al.* (2014c) study, multiple MODIS FRP measurements of the same fires made almost simultaneously ( $\ll 1$  sec difference) in consecutive MODIS scans were compared and some large scan-to-scan differences found. An approximately normally distributed ~~%-percentage~~ difference between the two FRP measures, with a mean close to zero but a standard deviation of 26.6% was determined from a large dataset of such matchups (Freeborn *et al.*; 2014c). Further investigation showed that the scan-to-scan differences were largely controlled by the differing sub-pixel location of the fire within the different MODIS scans, a subject previously indicated as potentially significant with regard to FRP observations made by the BIRD Hot Spot Recognition Sensor (HSRS; Zhukov *et al.*, 2006). Freeborn *et al.* (2014c) also showed that the scatter reduced as fire clusters containing increasing numbers of active fire pixels were compared, since the sub-pixel location effects would increasingly cancel out as more pixels were included in the instantaneous scan-to-scan FRP inter-comparison. Nevertheless, given the degree of scatter found between even almost totally simultaneous MODIS FRP observations of the same fire made at the same scan angle and pixel area by Freeborn *et al.* (2014c), it is unsurprising that higher levels of scatter arises when comparing FRP data from different sensors (Figure 2; Table 1), where pixel areas, scan angles and imaging time differences are all somewhat greater. Nevertheless, our results indicate that when the FRP-PIXEL product and the MODIS active fire products both detect the same fire, the FRP reported by the two products show small biases. Over the four LSA SAF regions, 391 individual active fire 'clusters' detected by MODIS and SEVIRI were compared and 76% (298 fire clusters) had an FRP within 30% of that measured by MODIS.

Given the uncertainties on per-fire FRP retrievals, the LSA SAF target accuracy of the FRP-PIXEL product is specified as, on a per-fire basis, 70% of the SEVIRI-retrieved FRP values being within 50% of those simultaneously measured by MODIS. Therefore, the FRP-PIXEL product significantly exceeds this specification, and actually approaches that specified by the LSA SAF 'optimal accuracy' definition (70% of retrieved SEVIRI-retrieved FRP value being within 20% of the MODIS-derived value on a per-fire basis).

Whilst our per-fire FRP inter-comparison has indicated a comparatively low degree of FRP bias between the FRP-PIXEL and MODIS MOD14/MYD14 FRP records of the same successfully detected active fires, there remains a significant degree of regional-scale FRP underestimation by the FRP-PIXEL product due to ~~its-the~~ inability of the coarser SEVIRI observations to detect the lowest FRP component of a regions fire regime (Roberts and Wooster, 2008). Therefore when data from both the MOD14/MYD14 and near-simultaneous matching FRP-PIXEL products covering the same area (i.e. the area covered by MODIS within a  $\pm 30^\circ$  scan angle) are compared, SEVIRI reports a lower cumulative 'regional' FRP than does MODIS (Table 1, Column 6). This effect is directly related to SEVIRI's aforementioned active fire errors of omission, an effect that ~~this-is~~ magnified in geographic regions in which SEVIRI mostly observes at higher view zenith angles. Figure 3 again uses the example of the North African region, where the slope of the linear of best fit to the regional FRP totals recorded near simultaneously in the FRP-PIXEL product and the MODIS active fire products is 0.65. This indicates the relatively small, but certainly not ~~-~~insignificant, impact of the FRP-PIXEL products active fire errors of omission in this region, which is that closest to the Meteosat sub-satellite point (SSP) and thus in which the FRP-PIXEL products active fire errors of omission are lowest (Table 1). Regional FRP underestimation increases away from the SSP, and appears particularly extreme in the European LSA SAF geographic region in our inter-comparison. This is in part a result of a large proportion of active fires being present in Eastern Europe during our inter-comparison period, where the SEVIRI view zenith angle exceeds  $60^\circ$ . With respect to regional FRP characterisation, the performance of the FRP-PIXEL product for southern European fires, which lie relatively close to the Meteosat SSP, is likely to be much closer to that of the North African geographic region. Section 5 includes study of the August 2007 Greek Fires as a case study example of fires in this region.

### 3.2 Inter-comparison of Alternative SEVIRI Active Fire Products

Since the launch of Meteosat Second Generation in 2002, a number of studies have used different algorithms to study active fires with SEVIRI observations (e.g. Calle *et al.*, 2009; Amraoui *et al.*, 2010). This has led to certain other routinely generated SEVIRI active fire products being available, in addition to the LSA SAF FRP-PIXEL product focused upon herein. These alternative SEVIRI-based products include the Wildfire Automated Biomass Burning Algorithm (WFABBA, version 6.5) product (based on the WFABBA fire detection algorithm of Prins *et al.*, 1998), the Fire Detection and Monitoring (FDeM) product (Amraoui *et al.*, 2010), and the Active Fire Monitoring (FIR) product (Joro *et al.*, 2008), each of which essentially generate active fire pixel detections from SEVIRI level 1.5 data as does the FTA algorithm used within the FRP-PIXEL product processing chain (Wooster *et al.*, [this issue2015](#)).

### 3.2.1 Methodology

We assessed the active fire detection performance of the FRP-PIXEL product in comparison to the three main alternative SEVIRI active fire products, and to the MODIS MOD14/MYD14 active fire products using the SEVIRI-to-MODIS intercomparison methodology detailed in Section 3.1. The inter-comparison was conducted using all available FRP-PIXEL products collected over the southern African LSA SAF geographic region in August 2014 (a total of 2959), a month when fires are highly prevalent in southern Africa. For comparison we collected all the available files from the alternative SEVIRI active fire data products, a total of 2949 for WFABBA (Prins *et al.*, 1998), 2963 for FDeM product (Amraoui *et al.*, 2010), and 2914 for FIR (Joro *et al.*, 2008). Due to various data collection and processing issues, not all products were available for all SEVIRI source scenes, as is evident from the slightly different (max 1.5%) number of products in each case. Also, each product has different classes of output, and the FIR product for example classifies fire pixels as either active fires or potential active fires. In this comparison we focus on only [confirmed active](#) fire [pixelsdetections](#). Similarly, the WFABBA product 'filters' active fire pixels detected only once in a 24 hour period and classes them less likely to be fires, aiming to reduce the number of false alarms detected and minimise effects due to sunglint. [In our analysis of the WFABBA active fire product we therefore include four variations of the WFABBA dataset. These are the inclusion of all fire detections, all the WFABBA 'filtered' detections \(where pixels only detected once during 24 hrs are removed\) and the WFABBA 'filtered' detections keeping only 1\) the high probability fires \(WFABBA flags 0 to 3\) and 2\)](#)

~~high and medium probability fires (WFABBA flags 0 to 4). We are therefore careful to conduct our comparison with the various classes of WFABB detection data.~~

For comparison to the SEVIRI-derived active fire products we used 544 Collection 5 MODIS MOD14/MYD14 active fire products, acquired over southern hemisphere Africa. To facilitate comparison with the SEVIRI products, we subset the SEVIRI products to cover the same area as the MODIS products and selected the set of temporally coincident MODIS active fire pixels that matched with SEVIRI active fire products in time ( $\pm 6$  minutes). The MODIS active fire pixels were remapped to SEVIRI's imaging grid and had their FRP atmospherically corrected using the same approach as detailed in Section 3.1 to match the methodology used to generate the FRP values within the FRP-PIXEL product. SEVIRI's per-pixel point spread function (PSF) at the sub-satellite point extends more than 5 km radially from the pixel centre (Wooster *et al.*, [this issue 2015](#)), so following the approach of Freeborn *et al.* (2014a) we evaluated the SEVIRI-derived active fire detection performances against the presence of MODIS active fire pixels within a  $3 \times 3$  pixel window centred on the SEVIRI active fire pixel under investigation. Again, as with Section 3.1 the comparison was restricted to MODIS active fire detections made within a  $\pm 30^\circ$  scan angle (Freeborn *et al.*, 2014a).

### 3.2.2 Results

The MOD14/MYD14 products contained 286,000 active fire detections during August 2014 over the southern African LSA SAF geographic region, and once remapped onto the SEVIRI imaging grid, this equated to 112,576 pixels. Within the specified  $\pm 6$  minute MODIS to SEVIRI imaging time limit, the FRP-PIXEL product detects 33,414 active fire pixels and 29,037 of these are also detected by the remapped MOD14/MYD14 data. This corresponds to a SEVIRI active fire pixel detection commission error of 13%. Using the same SEVIRI level 1.5 data, the WFABBA, FDeM and FIR active fire products detect 13,008, 7664 and 7151 active fire pixels respectively, and of these, 12,284, 7260 and 6730 are coincident with a MODIS active fire detection respectively. Hence, the active fire pixel errors of commission are 5.5%, 5.2% and 5.8% respectively for these three SEVIRI-derived products, active fire errors of commission rates around half those of the FRP-PIXEL product. - The WFABBA filtered dataset also stratifies active fire detections according to their detection confidence. We analysed the fire detection performance of the WFABBA filtered dataset by just including medium and high probability fires (flags 0-4) and only high probability fires (flags

1034 0-3). These filtered WFABBA datasets detect 9736 (flags 0-4) and 8832 (flags 0-3) active  
1035 fires and of which 9369 and 8496 are coincident with MODIS active fire pixels. This equates  
1036 to a reduced commission rate of 4 % for both whilst the omission rate increases to 87% and  
1037 88% respectively.

1038  
1039 A summary of the SEVIRI active fire product intercomparison results is given in Table 2.  
1040 The ~13% active fire error of commission rate for the FRP-PIXEL product found here and by  
1041 Freeborn *et al.* (2014a) is higher than the ~8% found by Roberts and Wooster (2008, 2014)  
1042 using the FTA algorithm prototype. The disparity is in part due to the differing way in which  
1043 the operational FTA algorithm applies a high-pass spatial filter to screen out certain false  
1044 alarms from the potential fire pixel set (Roberts and Wooster, 2008). As discussed in the  
1045 companion paper that describes the fire thermal anomaly (FTA) algorithm in detail (Wooster  
1046 *et al.*, 2015), the current LSA SAF implementation of the FTA algorithm (whose  
1047 performance results are reported in Table 2) has some characteristics that are open to being  
1048 updated, namely whether dynamic or static thresholds are used in the spatial filter applied at  
1049 the end of the potential fire pixel (PFP) stage, and whether application of the cloud-edge  
1050 mask is really necessary (see Wooster *et al.*, 2015 for details). We have tested these  
1051 adaptations using one month of data (July, 2015) collected over the same Southern African  
1052 region used to perform the evaluation reported in Table 2, and have compared the results to  
1053 those from contemporaneous MODIS overpasses. Results show that with both adaptations  
1054 applied, the error of commission of the adjusted FTA algorithm compared to MODIS reduce  
1055 from the current 14% to 12%, whilst the error of omission remains at 70%. These two  
1056 adaptations are therefore now being implemented in the operational FTA processing chain.  
1057 ). As detailed in Wooster *et al.* (this issue) whilst the prototype FTA algorithm applies a  
1058 dynamic threshold derived for each SEVIRI imaging slot at this stage (Roberts and Wooster,  
1059 2008), the operational version used to generate the FRP-PIXEL product uses a set of static  
1060 thresholds to speed up data processing (since this stage was by far the most computationally  
1061 intensive part of the algorithm and each slot has to be processed rapidly). It has since been  
1062 found that this change results in the removal of fewer areas of 'solar heated warm ground'  
1063 than did the prototype implementation, meaning a much larger number of potential fires  
1064 pixels that are false alarms passing through the early stage of the FRP-PIXEL product  
1065 processing chain, and some of these may end up being classed as 'true' fires. This issue will  
1066 be addressed in a future FRP-PIXEL product update, balancing the need to minimise active

**Formatted:** Font: (Default) +Headings CS (Times New Roman), Complex Script Font: +Headings CS (Times New Roman)

**Formatted:** Font: (Default) +Headings CS (Times New Roman), 12 pt, Complex Script Font: +Headings CS (Times New Roman), 12 pt

**Formatted:** Font: (Default) +Headings CS (Times New Roman), 12 pt, Italic, Complex Script Font: +Headings CS (Times New Roman), 12 pt, Italic

**Formatted:** Font: Italic, Complex Script Font: Italic

**Formatted:** Font: (Default) +Headings CS (Times New Roman), 12 pt, Complex Script Font: +Headings CS (Times New Roman), 12 pt

**Formatted:** Font: (Default) +Headings CS (Times New Roman), 12 pt, Complex Script Font: +Headings CS (Times New Roman), 12 pt

**Formatted:** Font: (Default) +Headings CS (Times New Roman), 12 pt, Italic, Complex Script Font: +Headings CS (Times New Roman), 12 pt, Italic

**Formatted:** Font: (Default) +Headings CS (Times New Roman), 12 pt, Complex Script Font: +Headings CS (Times New Roman), 12 pt

**Formatted:** Font: (Default) +Headings CS (Times New Roman), 12 pt, Complex Script Font: +Headings CS (Times New Roman), 12 pt

**Formatted:** Font: (Default) +Headings CS (Times New Roman), 12 pt, Complex Script Font: +Headings CS (Times New Roman), 12 pt

**Formatted:** Font: (Default) +Headings CS (Times New Roman), 12 pt, Complex Script Font: +Headings CS (Times New Roman), 12 pt

**Formatted:** Font: (Default) +Headings CS (Times New Roman), 12 pt, Complex Script Font: +Headings CS (Times New Roman), 12 pt

**Formatted:** Font: (Default) +Headings CS (Times New Roman), 12 pt, Complex Script Font: +Headings CS (Times New Roman), 12 pt



~~fire errors of commission with the requirement to deliver each new product in a timely fashion soon after image acquisition.~~

The minimum FRP detection limit of an active fire detection algorithm is directly proportional to the pixel area (Roberts and Wooster, 2008; Wooster *et al.*, [this issue 2015](#)). If the active fire detection algorithm of Giglio *et al.* (2003) used to generate the Collection 5 MOD14/MYD14 MODIS active fire products were applied to SEVIRI level 1.5 imagery, the minimum FRP detection limit at the Meteosat SSP would be 70 - 80 MW, around 10× the minimum FRP detection limit of the MOD14/MYD14 active fire products due to SEVIRI's ~ 10× larger nadir view pixel area. By contrast, the design of the FRP-PIXEL product attempts to lower the minimum FRP detection limit significantly below this by detecting active fire pixels whose radiometric signals in the MWIR, LWIR and MWIR-LWIR are raised even quite minimally above that of the ambient background (Roberts and Wooster, 2008). By exploiting a variety of spectral and spatial thresholds and contextual processing methods, the FTA algorithm is sometimes capable of detecting SEVIRI active fire pixels having an FRP down to ~ 20 MW at the Meteosat SSP. Nevertheless, statistics show that for active fire pixels below ~ 50 MW the active fire pixel count is underestimated more by SEVIRI compared to the performance above this threshold (Freeborn *et al.*, 2009). However, by restricting our comparison of the FRP-PIXEL product to active fire pixels having FRP ≥ 50 MW the active fire pixel error of commission of the FRP-PIXEL product fell only slightly to 12%, indicating that false alarms are not necessarily dominated by these low FRP fire pixels.

Whilst our analysis has shown somewhat higher active fire errors of commission for the FRP-PIXEL product compared to the WFABBA, FIR and FDeM products, we find the latter have much higher active fire errors of omission. Figure 4 illustrates the variation seen in active fire pixel detection performance between the different SEVIRI products for one imaging slot (21<sup>st</sup> August, 2014, 13:15 UTC). In this example, the FRP-PIXEL, WFABBA, FDeM and FIR [products](#) detect 1249, 686, 346 and 312 active fire pixels respectively, illustrating a substantial degree of difference. Furthermore, the fire diurnal cycle retrieved using the four products from a single [say-day](#) of data shown in Figure 5 highlights the fact that these differences are maintained over the course of the day, leading to very large variations in the total count of active fires detected on a daily basis.

1100 When compared to the matching MODIS active fire pixel detections, the WFABBA, FDeM  
1101 and FIR products contain active fire pixel detections that match 16%, 8% and 5%  
1102 respectively of the MODIS active fire pixels, whereas the figure for the LSA SAF FRP-  
1103 PIXEL product is substantially higher at 23%. Georgiev and Stoyanova (2013) previously  
1104 undertook a limited study of the FRP-PIXEL product performance in south-east Europe, and  
1105 determined that it provided a marginally higher active fire detection efficiency than did the  
1106 FIR product. Using a wider area of a region with many more fires covering a wide FRP range  
1107 we find much larger differences, and indeed the FIR product appears to provide the worst  
1108 performance of all the four SEVIRI products in terms of its ability to detect active fire pixels.  
1109 Restricting the FRP-PIXEL active fire detections to those pixels  $\geq 50$  MW, the FRP-PIXEL  
1110 product still detects 9896, 14864, 15896 more active fire pixels that are coincident with  
1111 MODIS than do the WFABBA, FDeM and FIR products respectively. This corresponds to  
1112 active fire pixel count differences in excess of  $\sim 175\%$ , even when limiting the detection  
1113 regime to an FRP level-range where all the SEVIRI-derived products should in theory be able  
1114 to show a reasonably strong performance.

1115  
1116 Our analysis of the operational FTA algorithm's performance has shown an active fire pixel  
1117 error of omission rate of 77% when comparing the FRP-PIXEL product to simultaneously  
1118 collected MODIS active fire pixels. This omission error is similar to that previously found by  
1119 Roberts and Wooster (2014) and Freeborn *et al.* (2014a) for the FTA algorithm, and primarily  
1120 results from the  $\sim 10\times$  larger nadir pixel area of SEVIRI than MODIS. In comparison, the  
1121 errors of omission for the WFABBA, FDeM and FIR products are significantly greater, at  
1122 84%, 92% and 95% respectively. Restricting the comparison to those FRP-PIXEL product  
1123 pixels having a SEVIRI-retrieved FRP  $\geq 50$  MW, which SEVIRI-based algorithms should be  
1124 able to detect quite readily, reduces the FRP-PIXEL product active fire pixel error of  
1125 omission to  $\sim 50\%$  in comparison to MODIS.

1126  
1127 In terms of FRP measurements, the ratio between the total cumulative FRP measured within  
1128 the same southern African geographic region covered by the near-simultaneous FRP-PIXEL  
1129 and MODIS active fire products is 0.48. This represents a lower underestimate of FRP than  
1130 might be expected from the FRP-PIXEL omission error rate, and the reason is that the  
1131 unidentified active fire pixels are predominantly those having low FRP values ( $\ll 50$  MW).  
1132 Restricting the analysis to only those active fires that are correctly identified by both products  
1133 provides a cumulative FRP ratio of 0.96, showing an excellent agreement in the regional FRP

assessment when only active fires successfully detected by both sensors are taken into account. This agrees with the strong-performance in terms of per-pixel FRP assessment seen in Section 3.1.

Certain previous studies evaluating the FTA algorithm or prototype FRP-PIXEL datasets (e.g. Roberts and Wooster, 2008; Xu *et al.*, 2010; Roberts *et al.*, 2014) have applied an alternative approach when comparing these to MODIS active fire datasets. Rather than the per-pixel approach to inter-comparison applied above, Freeborn *et al.* (2014a) grouped active fire pixels into contiguous clusters based on their spatial closeness to other active fire pixels in the same manner as that described in Section 3.1 for the per-fire FRP intercomparison. To strengthen the link between this work and these previous findings, active fire pixels within each of the active fire products tested were also clustered into spatially contiguous groupings, and the active fire detection errors of commission and omission calculated based on a ‘fire cluster’ basis instead of for the individual fire pixels. We used a similar strategy for this inter-comparison as used at the pixel scale, specifically searching the surrounding  $3 \times 3$  pixels for matching active fires in the products to be compared. Using this ‘clustering’ approach, we found the error rates of the FRP-PIXEL product to be higher than those determined using the per-pixel approach, with errors of commission and omission of 19% and 85% respectively when compared to the matching MOD14/MYD14 products. Again, if only those fire clusters having an FRP  $\geq 50$  MW are included, these reduce to 18% and 57% respectively, demonstrating in particular a high success of active fire detection in this region of the FRP regime. Using the same approach with the alternative SEVIRI active fire products, we find that the WFABBA products also show slightly higher errors of omission and commission than when examined at the fire cluster scale, now being 7% (commission) and 90% (omission) respectively in comparison to the MODIS product. The error rates for FDeM and FIR products are, however, very similar when examined on a fire cluster basis to the results on a per fire pixel basis, with a commission rate of 6% for both and an omission rate of 96% and 95% for FDeM and FIR respectively.

## **4. FRP GRIDDED Product Evaluation**

### **4.1 Method**

Section 2.2 detailed how the LSA SAF SEVIRI FRP-GRID product uses a series of regionally-specific bias adjustment factors ( $\alpha$ ) to upwardly adjust regional FRP estimates for e.g. the impact of undetected low FRP fire pixels. The aim is to produce an hourly, regional FRP estimate that has minimal bias compared to if MODIS had been able to view the same area at the same time. Full details of the FRP-GRID processing chain are included in Wooster *et al.* ([this issue 2015](#)). We evaluated the performance of the applied bias adjustments using a validation dataset composed of coincident SEVIRI and MODIS observations collected between May 2008 and May 2009 in each of the four LSA SAF geographic regions. Boundaries of the relevant MODIS level 2 swath products were used to identify all MODIS granules that intersected each region during the year-long study period, and fire pixels subset from the full MODIS ‘MOD14’ and ‘MYD14’ products using six, non-overlapping 5.0° grid cells arranged in the centre of each MODIS granule (Figure 6). Active fire pixels detected by MODIS outside of this region of interest were discarded and not used during the analysis. The sampling design ensured complete coverage of the 5.0° grid cells regardless of the MODIS ground track, and also mitigated the effects of image distortion at the edge of the MODIS swath. All MODIS granules collected during the year-long study period were matched to the most concurrent SEVIRI image, always within  $\pm 6$  minutes of each other. The same 5.0° grid cells inscribed within the MODIS granule were then used to clip SEVIRI fire pixels from both (i) the most coincident SEVIRI timeslot, and (ii) the three SEVIRI timeslots immediately preceding the MODIS overpass. Again, active fire pixels detected by SEVIRI outside of this region of interest were not included in the analysis. Entire grid cells were also discarded if three consecutive SEVIRI imaging timeslots could not be retrieved prior to the SEVIRI timeslot concurrent with the MODIS overpass (i.e., if four imaging timeslots were not available). This sampling design not only permitted a genuine comparison of coincident SEVIRI and MODIS observations of FRP, but also mimicked the hourly temporal resolution of the gridded FRP product.

After the SEVIRI and MODIS fire pixels were spatially and temporally accumulated, half of the concurrent and collocated 5.0° grid cells in each region were used to generate the validation dataset. Relationships between the atmospherically corrected FRP observed by SEVIRI and MODIS were directly compared among the 5.0° grid cells contained within this dataset. Rather than using the instantaneous FRP observed by SEVIRI at the timeslot most concurrent with the MODIS overpass however, the mean FRP generated from the SEVIRI

data available over the preceding hour was used instead to correspond more appropriately with the hourly resolution of the FRP-GRID product.

## 4.2 Results

A complete summary of the FRP-GRID product validation results derived from the methodology detailed in Section 3.1 is provided in Table 3. Application of the weighted least squares (WLS) coefficients in northern and southern Africa to the validation dataset yielded unbiased estimates of the instantaneous FRP that would have been measured by MODIS at 5.0° spatial resolution (e.g., Figure 7a, Table 3). As expected, however, the region-specific coefficients for South America (Same) and Europe (Euro) geographic regions did not perform as well. Although the adjustment procedure provides an unbiased estimate of the FRP that MODIS would have measured in South America, the coefficient of determination ( $r^2$ ) indicates that confidence in the predictive capability of the model is limited at this spatial and temporal resolution. As a caveat, however, the validation results in South America and Europe are influenced by observations when SEVIRI did not detect a single active fire pixel within a 5.0° grid cell during the hour. After removing 5.0° grid cells that only contained an active fire pixel detected by a single sensor (i.e., thereby forcing a comparison between observations in which both SEVIRI and MODIS viewed a fire) the  $r^2$  improved to 0.43 in the South America region. Furthermore, by removing a lone outlier improved the correlation coefficient slightly further to 0.55. Likewise for Europe, only including observations in which SEVIRI and MODIS simultaneously detected an active fire pixel yielded an  $r^2$  of 0.31.

Of course, the linear bias adjustments applied in the FRP-GRID product only capture the underlying macroscopic features of the sensor-to-sensor relationships, and do not account for any temporal variability in the SEVIRI-to-MODIS ratios of FRP induced by diurnal or seasonal fluctuations in fire activity (e.g. as seen in Freeborn *et al.*, 2009). By deriving different regression coefficients for each of the four LSA SAF regions, however, the FRP-GRID algorithm does account for broad spatial differences in the sensor-to-sensor relationships that potentially arise from (i) differences in fire regimes, and (ii) differences in SEVIRI view zenith angles.

To assess the predictive capability of the bias adjustment factors at broader spatial and temporal scales than simply the hourly/5° spatio-temporal resolution of the FRP-GRID product, the SEVIRI and MODIS validation data were accumulated over weekly intervals

and comparisons were performed at scale of the LSA SAF geographic regions. Figure 7b illustrates that in southern Africa, the bias adjustment factors used to generate the FRP-GRID product consistently underestimate the weekly sum of FRP measured by MODIS across this region, and that these results are typical of all four regions (Table 3). Again, this systematic underestimation is partly attributed to the challenge of performing a bias adjustment when SEVIRI does not detect a fire pixel (i.e. the linear bias adjustment coefficient is then applied to an FRP of zero). Nevertheless, the weekly/regional biases shown in Table 3 could in turn be used to adjust the SEVIRI FRP-GRID product measurements to deliver unbiased estimates of the FRP that would have been measured by MODIS at the regional/weekly scale.

## 5. EXAMPLE APPLICATION OF THE LSA SAF METEOSAT SEVIRI FRP PRODUCTS IN THE COPERNICUS ATMOSPHERE MONITORING SERVICE (CAMS)

### 5.1 Introduction to FRP-PIXEL Product use in Atmospheric Transport Models

From the FRP-PIXEL product evaluation and inter-comparison conducted in Section 3 it is apparent that the FRP-PIXEL product detects a larger proportion of the ‘true’ landscape-scale fire activity than do alternative SEVIRI-derived active fire products, albeit with a higher commission rate. That evaluation also highlighted the failure of the FRP-PIXEL product to detect many of the actively burning fires that MODIS would detect, particularly the lower FRP fires, resulting in an overall omission rate of 77% over the four geographic regions (Table 1). The degree of difference between geostationary and polar-orbiting active fire products does, however, vary with factors such as geographic location, season and time of day (which all influence the type of fire regime and its subcomponents being sampled), sensor viewing geometry, land cover heterogeneity, fire detection algorithm and the quality of ancillary data such as cloud masks (Freeborn *et al.*, 2014a; Schroeder *et al.*, 2008; Roberts and Wooster, 2014; Xu *et al.*, 2010). Indeed, under some conditions, geostationary active fire datasets compare rather favourably against those derived from polar-orbiting sensors. Georgiev and Stoyanova (2013) analysed a series of short-lived wildfires in south-eastern Europe with the FRP-PIXEL product, and found the higher temporal resolution of SEVIRI resulted in a 50% lower active fire omission rate than did the use of MODIS. Wooster *et al.* (~~this issue~~2015) also demonstrate that, taking the Central African Republic as an example, most fires detected by the MODIS are detected by the SEVIRI FTA algorithm, just not

necessarily at the same time as the fire is detected by MODIS. Indeed, the high temporal frequencies offered by geostationary observations can enable the diurnal fire cycle and related short-term changes in fire activity to be far better characterised than with polar-orbiting data, and this ability is starting to be exploited to parameterise wildfire emissions in atmospheric transport models.

One such example is provided by Baldassarre *et al.* (~~in press~~2015), who used the FRP-PIXEL products (Wooster *et al.*, ~~this issue~~2015) and the WFABBA SEVIRI products (Zhang *et al.*, 2012), along with MODIS-derived information from the Global Fire Assimilation System (GFAS) inventory of Kaiser *et al.* (2012), to derived biomass burning emissions inputs for simulations of emissions from a large fire in Turkey (Antalya, 2008). The FRP-PIXEL product provided by far the most accurate description of the emissions, both with regard to their spatio-temporal variation and their absolute magnitude. Unlike the MODIS-derived GFAS inventory, the SEVIRI FRP-PIXEL product was able to capture the fires complete life cycle, including the time of peak emissions intensity. And compared to the WFABBA product, the FRP-PIXEL product produced information more consistent with that from MODIS when both SEVIRI and MODIS viewed the Antalya region simultaneously. The simulated smoke plume produced by ingesting the FRP-PIXEL data into the Community Multi-scale Air Quality (CMAQ) atmospheric chemistry model compared far better with observations of MODIS-derived aerosol optical depth (AOD), and with carbon monoxide and ammonia column totals provided by the Infrared Atmospheric Sounding Interferometer (IASI), in particular in relation to the diurnal variability of the fire emissions and the spatial distribution and peak concentrations of the smoke. Please refer to Baldassarre *et al.* (~~in press~~2015) in this Monitoring Atmospheric Composition and Climate (MACC) special issue for further information on the simulation and inter-comparison. Here we provide a second European demonstration of the value of geostationary FRP data in the parameterising of wildfire emissions for use in atmospheric transport models, building on a previous more limited study ~~carried-conducted out~~ by Kaiser *et al.* (2009b).

## 5.2 Methodology for ~~Modelling-modelling~~ emissions and transport of smoke from the for-the-2007 Peloponnese-Greek 'mega fires' event

We use the FRP-PIXEL product as the basis for ~~parameterising-calculating~~the smoke emissions to the atmosphere from a catastrophic from a series of large-'mega fire' event that



occurred around the Mediterranean, in particular focused on the Greek island of Peloponnese, wildfires that occurred in August and September 2007. We use these emissions on the island of Peloponnese in Greece, using these within components of the CAMS Copernicus Atmosphere Service modelling systems to simulate the transport and fate of the emitted smoke, ultimately estimating the level of human exposure to high levels of particulate matter (PM<sub>2.5</sub>). These Peloponnese catastrophic wildfires occurred after a period of prolonged drought (Gitas *et al.*, 2008), and during a heatwave (Theoharatos *et al.*, 2010). The MODIS burned area product (Roy *et al.*, 2005) indicates ~~a they~~ burned across an area of around 1847 km<sup>2</sup> (Figure 8), a figure in good agreement with burned area reports provided by the local Hellenic fire brigade (1899 km<sup>2</sup>). The Peloponnese fires predominantly occurred in forested land, both occurred in areas of e~~c~~oniferous and broadleaved forest, though some areas of shrublands, grasslands and olive groves were also affected, although they predominantly occurred in forested land (Veraverbeke *et al.*, 2010; Koutsias *et al.*, 2012). Such was their severity that 0.32 Tg (or 40 %) of the estimated mean annual carbon monoxide (CO) emissions for the entire country of Greece overall were ~~are~~ estimated to have been released by these fires alone (Turquety *et al.*, 2009). The fires contributed greatly to reductions in local air quality, with PM<sub>10</sub> values in Athens reaching almost 100 µg m<sup>-3</sup>, double that of the European Union Ambient Air Quality Standard for daily PM<sub>10</sub> (50 µg m<sup>-3</sup>). Outside Athens at a background non-urban site, on 24-25<sup>th</sup> August the PM<sub>10</sub> concentration rose to 49 µg m<sup>-3</sup>, and their average contribution to the 3 day record of PM<sub>10</sub> measured in Athens was 28 µg m<sup>-3</sup>, which is 67% significantly up from greater than the background concentration (the 19 µg m<sup>-3</sup>) measured a few the days before previously (Liu *et al.*, 2009). Marlier *et al.* (2014) and Reid *et al.* (2009) have already highlighted the potential improvements that such high temporal resolution source information can have on the modelling of biomass burning emissions transport, and the These exceptional and strongly varying intensity of the characteristics of the Peloponnese wildfires, which showed strongly varying intensities over their lifecycle, provides an excellent opportunity to demonstrate the value of the high temporal frequency FRP observations provided by SEVIRI this further using SEVIRI-derived FRP observations. Marlier *et al.* (2014) and Reid *et al.* (2009) already highlight the potential improvements that such high temporal resolution source information can have on the modelling of biomass burning emissions transport.

Formatted: Font: Not Bold, Complex Script Font: Not Bold

Formatted: Superscript

### 5.2.1 Derivation of SEVIRI-derived FRP smoke emissions fields from FRP-PIXEL data for the Peloponnese wildfires

Formatted: Font: Italic

FRP-PIXEL data of the European LSA SAF geographic region collected between the 1<sup>st</sup> August and 13<sup>th</sup> September 2007 was examined for signals of the ~~Peloponnese fires~~ that occurred around the Mediterranean during July - Aug 2007. Clear FRP signals were apparent from these fires, particularly those on Peloponnese, but it was also evident that the adjusted version of Cloud Mask (CMa) of Derrien and Le Gleau (2005) delivered by the Nowcasting and Very Short Range Forecasting SAF (NWC SAF; [www.nwcsaf.org](http://www.nwcsaf.org)) and used within the FRP-PIXEL product processing chain (Wooster *et al.*, ~~this issue~~2015) was identifying some of the extremely thick smoke emitted by these fires as cloud. This is ~~not a problem~~appropriate for studies requiring clear sky observations, but the sensitivity of the algorithm for detecting cloud or smoke contaminated pixels can occasionally result in the omission of fire activity. Since cloud masking is one of the first things conducted within the FRP-PIXEL product processing chain (Wooster *et al.*, ~~this issue~~2015), misidentification of very thick smoke as cloud prevents fires being identified in these pixels using the FTA algorithm, even though we know that active fires can be quite reliably detected through even quite thick smoke (Petitcolin and Vermote, 2002). This is because smoke particles have a diameter typically much smaller than the wavelength of the MWIR band and so do not act as strong scatterers of the fire-emitted radiation, unlike meteorological cloud (Kaufman and Remer, 1994). Analysis of the raw SEVIRI level 1.5 data, along with the EUMETSAT Meteorological Product Extraction Facility (MPEF) cloud mask (Tjemkes and Schmetz, 1997), confirmed the identification of some areas of thick smoke as cloud by the CMa cloud mask, and also confirmed that the true median percentage cloud cover over Peloponnese was low over the period of the mega fires event (13%). To prevent the masking out of smoke covered fires, which also then impacts surrounding pixels due to the single pixel wide mask that is applied around cloud and water pixels (Wooster *et al.*, this issue), for this particular application we decided to turn off the use of the adjusted CMa cloud mask, and simply relied on the basic cloud masking tests used within the FTA algorithm itself (Wooster *et al.*, ~~this issue~~2015). Currently investigations are ongoing to make the cloud masking within the FRP-PIXEL product less sensitive to thin cloud and other atmospheric phenomena through which fires can still be identified, including very thick smoke (Wooster *et al.*, ~~this issue~~2015).

~~The~~ We then gridded the FRP data from within the FRP-PIXEL products ~~was gridded within~~ to 0.1° grid cells and ~~used to calculate~~calculated the mean FRP for each cell at an hourly temporal resolution. As with the operational version of the Global Fire Assimilation System

(GFAS; Kaiser *et al.*, 2012), the FRP density ( $\tilde{q}_j$ ,  $\text{Wm}^{-2}$ ) for each cell was then calculated by normalising the measured FRP by the grid cell area ( $a_j$ ,  $\text{m}^2$ ):

$$\tilde{q}_j(d, h) = \frac{1}{a_j} \frac{1}{4} \sum_{k=0,15,30,45} \sum_{i_k \in j} F_{ik}(d, h) \quad (1)$$

where  $d, h$  and  $k$  are the date, hour and minute of the SEVIRI observations respectively,  $\sum F_{ik}$  is the summation of all FRP measurements within grid cell  $j$ .

The rate of dry matter (DM) fuel consumption ( $\varphi$  [ $\text{kg s}^{-1} \text{m}^{-2}$ ]) was derived from the FRP density measures of each grid cell ( $\tilde{q}$ ,  $\text{Wm}^{-2}$ ) following the method described in Wooster *et al.* (2005), but with the land cover dependent adjustments that are designed to related the FRP-derived fuel consumption estimates from GFAS to those from GFEDv3 (Kaiser *et al.*, 2012):

$$\varphi(d, h) = c \times \tilde{q}(d, h) \times \beta_l \quad (2)$$

where  $d$  is the day,  $h$  is the hour and  $c$  is the conversion factor that relates fuel consumption to FRP and which is  $0.368 \pm 0.015$  ( $\text{kg MJ}^{-1}$ ; Wooster *et al.*, 2005) and where  $\beta_l$  is the adjustment factor for land cover type  $l$  taken from GFAS (Kaiser *et al.*, 2012). The approach was further developed with land cover dependent adjustments by Kaiser *et al.* (2012). However, we maintain the original fuel consumption estimation and adjust the emission fluxes at the level of the emission factors, see below section 5.2.2. is the approach to biomass burning fuel consumption estimation currently used within the GFAS component of the CAMS Copernicus Atmosphere Service.

### 5.2.2 FRP-derived aerosol emissions and atmospheric modelling

Ichoku and Kaufmann (2005) first developed an approach to estimate aerosol emissions using FRP and aerosol optical depth (AOD) measurements using ‘coefficients of emission’ that related FRP to total particulate matter (TPM) as a function of land cover type. The approach implemented by Kaiser *et al.* (2012) for GFAS and used again herein calculates emissions using the DM fuel consumption rate ( $\varphi$ ,  $\text{kg s}^{-1} \text{m}^{-2}$ ):

$$\Phi_s(d, h) = \eta_s \times \varphi(d, h) \quad (3)$$

where  $\Phi_s$  is the emission flux density ( $\text{kg s}^{-1} \text{m}^{-2}$ ) of species  $s$ ,  $d$  is the day,  $h$  is the hour and  $\eta$  is the emissions factor ( $\text{kg kg}^{-1}$ ) given by :

$$\eta_s = \alpha(s) \times \kappa_l(s) \quad (4)$$

~~$$\eta_s = \alpha_t(s) \times \kappa_t(s) \quad (4)$$~~

where  $\kappa_l$  is the land cover ( $l$ ) specific emissions factor for species  $s$  and  $\alpha$  is a constant which is used to adjust bottom-up aerosol emissions estimates to those observed in top-down inventories. A regionally varying bias occurs between bottom-up derived aerosol emissions and MODIS AOD measurements, requiring the former to be adjusted when being used in air quality or climate model simulations (Peterenko *et al.*, 2012). ~~Kaiser *et al.* (2012) recommend a global enhancement by a factor of 3.4 as first order correction.~~ Yang *et al.* (2011) also found smoke emissions ( $\text{PM}_{2.5}$ ) derived using the bottom-up approach was underestimated by a factor of three when compared to MODIS AOD ~~measurements retrievals.~~ Kaiser *et al.* (2012) recommend a global aerosol enhancement by a factor of 3.4 as first-order correction. These values are also broadly consistent with differences of up to a factor of three found by Ichoku and Kaufmann (2005) using satellite observations of FRP and AOD compared to measurements of  $c \times \kappa_l(s)$  derived from laboratory measurements. ~~Kaiser *et al.* (2012) recommend a global enhancement by a factor of 3.4 as first order correction.~~ Here, we estimate emissions of organic matter and black carbon in exact agreement with Ichoku and Kaufmann (2005) by enhancing their emission factors for Andreae and Merlet (2001) with a factor of 3.1, ~~which we deploy here in Equation (4) for our aerosol emissions calculation.~~ According to the GFEDv3 land cover dataset, also used for our calculations in GFAS (Kaiser *et al.*, 2012), the fire affected region of Greece is classed as extratropical forest and the emitted species and relevant emissions factors are given in Table 4.

~~first order correction and, in this case study,  $\alpha$  is also defined as 3.4 for aerosol emissions and 1  $\alpha$  is 1 for gaseous smoke constituents.~~ According to the GFEDv3 land cover dataset, Greece is extratropical forest and the species and their emissions factors are given in Table 4.

The atmospheric aerosol model (Morcrette *et al.*, 2008) used within the ECMWF Integrated Forecasting System (IFS) represents smoke aerosols as black carbon (BC) and organic matter

Formatted: Font color: Auto

Formatted: Font color: Auto

Formatted: Font color: Auto

Formatted: Font: Italic, Font color: Auto

Formatted: Font color: Auto

Formatted: Font color: Auto

(OM), ~~in of~~ both hydrophilic and hydrophobic types. Emissions of the latter are approximated by scaling organic carbon (OC) emissions estimates by a factor of 1.5. Other aerosols included in the modelling are sea salt, dust and sulphate aerosols, ~~and, The model simulates~~ advection, convection, diffusion, dry and wet deposition and chemical conversion of these aerosols ~~are simulated~~, with meteorology nudged to the operational ECMWF analysis every 12 hours. The aerosol abundance however, is based solely on source and sink processes and the atmospheric transport. In this study the IFS model was run with a horizontal resolution of 25 km (T799) and with 91 vertical levels up to 0.01 hPa. ~~Smoke emissions were calculated using Equations 3 and 4, along with the emissions factors given in Table 4~~

~~Smoke emissions from the Peloponnese fires were calculated using Equations 3 and 4, along with the emissions factors given in Table 4, and were released into the lowest atmospheric level. In this case study, smoke emissions were injected into the lowest atmospheric level. The smoke emissions must be injected into the atmosphere at a particular height, or distribution of heights, and such injection height assumptions can have which has implications for modelling the resulting their spatio-temporal distribution of the emitted species. Leung et al. (2007) and Guan et al. (2008) found demonstrated that that the inclusion of use of more detailed plume injection height information assumptions in atmospheric transport models resulted in a reduction in near surface CO concentrations, since more plumes were assumed to be lofted above the boundary layer since a greater proportion of emissions are lofted above the planetary boundary layer. Paugam et al. (2015a) provided a recent review of There are a number of approaches for to estimate determining smoke plume injection height, including which are reviewed by Paugam et al. (2015a). Once such approach is that proposed by the methods of Sofiev et al. (2012) and Paugam et al. (2015b) who discuss methods that that use FRP measurements to characterise the wildfire thermal properties related to required to simulate smoke plume injection height within plume rise models. Sofiev et al. (2012) found ~70% of estimated plume injection heights were within 500m of the plume heights measured by the Multi angle Imaging SpectroRadiometer (MISR) whilst Paugam et al. (2015b) found very good agreement between the modelled and measured plume injection layer over a small (n=38) number of wildfire events. Although This research remains at a relatively early stage, but it appears that this is an active area of research, these studies suggest that EO fire thermal measurements, such as FRP, measures may indeed have a role to play in have a role in characterising smoke plume injection height as well as the rate of emission of chemical and aerosol species. Here we retained the commonly used assumption that the calculated smoke~~

emissions are injected into the lowest atmospheric level, since this is generally what has been assumed in the Copernicus Atmosphere Service series of MACC projects modelling of fire emissions thus far (Kaiser *et al.*, 2012). The CAMS is anticipated to use injections heights from Paugam *et al.* (2015b) in the future.

## 5.3 Results

### 5.3.1 Fuel consumption during the Peloponnese Wildfires

Figure 9a illustrates the temporal dynamics of total fire FRP (MW) and the equivalent rate of fuel consumption ( $\text{tonnes s}^{-1}$ ), calculated from the MODIS and SEVIRI FRP measurements at their native temporal resolutions. The period of greatest fire activity occurs between the 23<sup>rd</sup> and 27<sup>th</sup> August, where the initial active fire detections made by ~~from~~ SEVIRI and MODIS occur at 07:57 and 09:00 (UTC) respectively (23<sup>rd</sup> August). At their most intense, the Peloponnese fires consumed over 15  $\text{tonnes s}^{-1}$  of biomass, and such was their intensity that large quantities of fuel ( $> 3 \text{ tonnes s}^{-1}$ ) were consumed even during the night, a period when more landscape typically fires ~~when typical fires~~ die down quite considerably due to less fire-conducive ambient conditions (Roberts and Wooster, 2007; Roberts *et al.*, 2009). The temporally intermittent MODIS Terra and Aqua FRP measurements broadly capture the pattern seen in the much more frequent SEVIRI data, and are typically much higher in magnitude. On the 25<sup>th</sup> August, MODIS Aqua (12:05 UTC) detects a total FRP exceeding 180 GW, with the SEVIRI FRP (12:12 UTC) very much lower (38 GW). The large difference mainly derives from the fact that whilst 10% (31) of the MODIS active fire pixels have an FRP  $> 1600 \text{ MW}$  and 5%  $> 3000 \text{ MW}$ , 23% of the 100 active fire pixels detected by the FRP-PIXEL product SEVIRI are in fact saturated in their SEVIRI MWIR channel from which the FRP is estimated. Between the 24<sup>th</sup> and 26<sup>th</sup> August, when the wildfires were most intense, MODIS made 13 overpasses and the unadjusted SEVIRI observations measured 39% of the total FRP measured by MODIS-measured FRP. This demonstrates the massive scale and intensity of these fires, particularly given that the SEVIRI-ss pixel area ~~over~~ at this location is the region is ~~around~~  $14 \text{ km}^2$ .

Temporal integration of the SEVIRI FRP measurements between the 23<sup>rd</sup> August and 3<sup>rd</sup> September indicates an energy release of 4.73 PJ which, following Equation 2, equates to

**Formatted:** Automatically adjust right indent when grid is defined, Adjust space between Latin and Asian text, Adjust space between Asian text and numbers

1.74 Tg of combusted fuel, predominantly consumed on 23 - 27 August (Figure 9b). Various burned area estimates exist for ~~these the Peloponnese wildfires~~, including 1773 km<sup>2</sup> (Gitas *et al.*, 2008), 1628 km<sup>2</sup> (European Forest Fires Information System, EFFIS; European Commission, 2010) and 1847 km<sup>2</sup> (Roy *et al.*, 2005; Figure 8). Dividing the SEVIRI-FRP derived fuel consumption with these burned areas provides mean dry matter (DM) fuel consumptions of 0.98 kg m<sup>-2</sup>, 1.07 kg m<sup>-2</sup> and 0.94 kg m<sup>-2</sup> respectively. Aleppo pine forests occupy around 370,000 ha in Greece and are abundant on Peloponnese (Verroios and Georgiadis, 2011). Mitsopoulos and Dimitrakopoulos (2013) assessed 40 stands in this fuel type and found canopy fuel loads to range between 0.63 and 1.82 kg m<sup>-2</sup>, estimating a mean of 1.08 kg m<sup>-2</sup>. Using the maximum fuel load (1.82 kg m<sup>-2</sup>), the three burned area estimates (1773 km<sup>2</sup>, 1628km<sup>2</sup> and 1847km<sup>2</sup>), and assuming a combustion completeness value for forest of 0.6 (van der Werf *et al.*, 2006) we calculated a fuel consumption for these fires of 1.94 Tg, 1.77 Tg and 2.01 Tg respectively using the standard burned area based approach (Seiler and Crutzen, 1980), ~~which is similarsimilar~~ to our SEVIRI-derived estimate of 1.74 Tg. Turquety *et al.* (2009) estimates that 0.32 Tg of CO was emitted during the ~~Peloponnese fires, fire events~~ which, using the emissions factors given in Table 4, results in a ~~larger top-down derived~~ fuel consumption ~~estimate of 3.0 Tg (with a stated~~ uncertainty of ~30%). ~~Whilst these alternative, independently derived fuel consumption estimates are not too dissimilar to the SEVIRI FRP derived values, the fuel load assumption made does not include the combustion of surface litter and/or organic soils, which would increase the burned area based estimates somewhat. Furthermore, d~~Due to the ~~aforementioned~~ SEVIRI MWIR channel saturation, the SEVIRI FRP-derived fuel consumption estimate ~~will beis considered~~ a minimum estimate.

### 5.3.2 Smoke Plume Evolution

The Peloponnese wildfires produced huge volumes of smoke that affected regional air quality in the Eastern Mediterranean (Poupkou *et al.* 2014). Figure 10a shows a true colour composite image derived from MODIS Terra imagery acquired on the 26<sup>th</sup> August 2007 (09:35 UTC). ~~These~~ mirrored 'S' shaped plume present over the Mediterranean extends across to Tunisia at this time. Figure 10b shows a snapshot of the modelled smoke emissions derived from our use of the FRP-PIXEL product dataset to derive the wildfire emissions, and the use of these within the IFS model (Section 5.2). The modelled smoke emission transport captures the spatial structure of the advected smoke plumes very well, consisting of a series



of ‘pulses’ of increased AOD that result from the particularly intense emissions during the peak of each diurnal fire cycle. The large region of particularly high AOD on the coast of Libya (L on Figure 10b, and shown in Figure 11a ~~and~~ 11b) results from the intense fire emissions on the 25<sup>th</sup> August, where more than 18 tonnes s<sup>-1</sup> of biomass were apparently being consumed at the peak intensity. To the west of the main smoke plume, a thinner plume with a lower AOD is evident emanating from fires in Albania. To the east, a smaller plume resulting from ~~the~~ wildfires in Turkey is also captured.

It is evident from Figure 10 that the modelled smoke plumes are offset slightly compared to the actual plumes observed by MODIS, and this is most evident over the Libyan coast. The difference is believed to result from injecting the smoke plume into the lowest atmospheric level, which ~~maybe is~~ an oversimplification as stated earlier since MISR-derived smoke plume heights acquired on 26<sup>th</sup> August indicated that the plume closest to the wildfires had a height of 2.5 km (Lui *et al.*, 2009) and CALIPSO lidar observations have detected the plumes at altitudes of 2-3 km on 25<sup>th</sup> and 26<sup>th</sup> August (Turquety *et al.* 2009). In contrast, the simulated plumes are located predominantly below 1 km (not shown). Global analysis of MISR data indicates that a large proportion wildfire smoke plume heights remain beneath the boundary layer, although particularly intense fires can inject smoke into the free troposphere (Val Martin *et al.*, 2010; Dirksen *et al.*, 2009; Fromm *et al.*, 2000). ~~The~~ Our modelled plume is typically also broader than that observed by MODIS, and covers a larger spatial extent. ~~This, which~~ may result from the ~~models~~ relatively coarse spatial resolution used in the model, ~~and~~ ~~We made~~ comparisons between our simulation and our model output and the MODIS AOD estimates made on the 26<sup>th</sup> August (DOY 238, Figure 11a and b). ~~These~~ indicate that, whilst the broad magnitude of the modelled smoke emission ‘pulses’ are in good agreement with observations, ~~the model typically~~ the simulated plumes AOD appears ~~overestimated~~ AOD compared to MODIS. This suggests some inaccuracies remain in the aerosol source modelling, and for example Garcia-Menendez *et al.* (2014) found modelled PM<sub>2.5</sub> concentrations are more sensitive to the injection height parameterisation rather than to the emissions vertical distribution, due to the diurnal evolution of the planetary boundary layer and local meteorological conditions.

✧

#### 5.4. Impact of Emissions Fields Temporal Resolution

Formatted: Superscript

Formatted: Superscript

A number of studies (e.g. Chen *et al.*, 2009; Marlier *et al.*, 2014; Reid *et al.*, 2009; Garcia-Menendez *et al.*, 2014) have found that resolving the diurnal variability of fire emissions has important implications when modelling ~~their-the emissions~~ atmospheric transport. We used our study of the Peloponnese fires to address this issue by reducing the temporal resolution of the SEVIRI FRP-derived emissions density fields, from the original 1-hour to 1-day and then 1-week, the latter two being more representative of the global emissions inventories developed using only observations from polar orbiting instruments (van der Werf *et al.*, 2010; Kaiser *et al.*, 2012; Sofiev *et al.*, 2009). The ~~resulting influence of source sensitivity to~~ temporal resolution is illustrated in Figure 12a and b, which show modelled AOD (at 550nm) on the 26<sup>th</sup> August (09:35 UTC) using the emissions prescribed at a daily and weekly temporal resolution. In both cases, the shape of the modelled Peloponnese smoke plume remains broadly consistent with the hourly simulation of Figure 10a, although smoke emissions from neighbouring countries are much less pronounced. The Albanian plume is progressively shorter in Figure 12a and 12b, whilst some plumes (e.g. those from Turkey to Crete) are missing altogether. Source emissions at weekly temporal resolution (Figure 12b) remove the daily variability, resulting in lower aerosol amounts at both the source region and over the entire plume. It is also evident that emissions are being generated at incorrect times when using in these reduced temporal resolution ~~instances~~ source data. For example, the daily and weekly simulations have plumes emanating from southern Italy too early, since fires are in fact in reality just developing in the source region (Figure 12b). Baldassarre et al. (2015) provide further evidence of the importance of the high temporal resolution provided by the SEVIRI FRP-PIXEL dataset when modelling smoke transport from individual large fire events.

## 5.5 Comparison of *in-situ* and modelled aerosol optical depth

Section 5.4 has indicated that model simulations using hourly smoke emissions fields improves the representation of both the spatial and temporal evolution of the ~~Peloponnese~~ smoke plumes from the main Mediterranean mega-fires of August 2007. However, qualitative comparison to MODIS AOD estimates (Figure 11 a,b) indicated that the plumes modelled AOD was somewhat higher than ~~the~~ satellite derived AOD estimates. Over the same time period as the Peloponnese fires, a series of fires occurred on the Algerian coast (Figure 13a) whose plumes were detected by the AERONET (Holben *et al.*, 2001) site at Lecce (Italy; 40.35°N, 18.16°E). Figure 13b and c show the modelled smoke and dust AOD

1598 respectively on the 31<sup>st</sup> August (00:00 UTC) where the former illustrates the smoke plume  
 1599 extension over the AERONET site (yellow star symbol). Figure 13d is a temporal profile of  
 1600 AOD recorded (at 500 nm) over Lecce from AERONET observations of total (red circles)  
 1601 and fine mode (orange circles) AOD, daily averaged MODIS AOD (550 nm) observations  
 1602 (black triangles) and model simulations of total AOD (blue line). Modelled AOD  
 1603 contributions of smoke (purple line) and dust (green line) to the total AOD are also shown.  
 1604 The MODIS AOD estimates are derived through averaging all observations within the model  
 1605 grid cell. The smoke AOD displays greater short term variability than does the dust AOD,  
 1606 since the wildfires represent significantly more localised sources than do the regions of dust  
 1607 uplift. The smoke AOD displays an increase in magnitude from 0.6 to 1.3 between the 31<sup>st</sup>  
 1608 August and 1<sup>st</sup> September, which occurs 23 hours prior to the peak FRP (63 GW) of the  
 1609 Algerian fires. However, between the 27<sup>th</sup> and 31<sup>st</sup> August, MODIS detected 330 active fires  
 1610 in southern Italy (Figure 14) which were greatest in number on the 27<sup>th</sup> (114) and 31<sup>st</sup> (110)  
 1611 August and which are likely to have contributed to the Algerian smoke plume but which may  
 1612 not all be included in our modelling since the majority (63%) had an FRP <30 MW and so  
 1613 may not be detected by SEVIRI.

1614  
 1615 Compared to the daily averaged MODIS AOD, our modelled total AOD is typically  
 1616 overestimated by ~20% during the overpass of the smoke plume (31<sup>st</sup> August), but the model  
 1617 does capture the temporal trend of the observed AOD rather well. The AERONET AOD data  
 1618 provides a more complete temporal profile than do ~~the~~ MODIS' AOD observations, and our  
 1619 modelled total AOD typically captures these dynamics. However, the onset of increased  
 1620 AOD due to the Algerian fires (30<sup>th</sup> August) is captured 8 hours earlier by AERONET than  
 1621 by ~~the-our~~ modelled AOD, whilst the descending limb is temporally coincident between  
 1622 datasets. The former may result from assumptions made regarding the smoke plume injection  
 1623 heights, or to shortcomings in the simulations due to increased cloud cover over Algeria on  
 1624 the 29<sup>th</sup> August. It is also possible that, given the rapid rise in AOD in a three hour period,  
 1625 this is a localised effect due small, undetected fires in the vicinity of the AERONET station  
 1626 and which are not represented in ~~the-model-our simulation~~. Between the 28<sup>th</sup> and 29<sup>th</sup> August,  
 1627 MODIS ~~detects-detected~~ 96 active fires (Figure 13, red symbols) to the south-west of Lecce  
 1628 and in close proximity to the smoke plume emitted by the Algerian fires, and these most  
 1629 likely to contribute to the elevated AOD at this time (Figure 11a and b). In general, the AOD  
 1630 resulting from the use of the SEVIRI FRP-PIXEL product data and the IFS model is  
 1631 overestimated compared to AERONET observations by 10 - 40% during the biomass burning

plume overpass, and with a discrepancy of 8 hours at the onset of the plume overpass. Clearly we will in future aim to further refine the fire emissions parameterisation, which appears currently to be positively biased relative to the observations. Nevertheless, this case study has demonstrated the clear value of the high temporal frequency SEVIRI-derived FRP observations for large, rapidly varying wildfires such as this.

## 5.6 Air quality assessment

The 2007 Mediterranean 'mega fire' event significantly impacted regional air quality, and fires worldwide are known to have severe health implications for those badly affected by their emissions. Jacobson (2014) estimated that ~~the~~ average annual ~~number of~~ premature mortalities due to biomass burning emissions of PM<sub>2.5</sub> and ozone are of the order of 20,000 (10,000-30,000) and 230,000 (63,000-405,000) respectively, equating to. ~~This equates to between 5- and 10% of the~~ global mortality due to indoor and outdoor air pollution. One of the primary uses of the ~~CAMS Copernicus Atmospheric Service~~ is to ~~be able to~~ forecast regional air quality across Europe, including impacts from wildfires, providing rapid and reliable information directly relevant to ~~such~~ human health issues, and this includes the consequences of wildfire emissions (Hollingsworth *et al.*, 2008). It is therefore pertinent to assess the significance of our modelled impacts of our the Peloponnese fires smoke emissions transports simulations in relation to ~~in relation to such~~ air quality ~~impact~~ and human health ~~impacts~~, potentially since Mitsakis *et al.* (2014) already estimated that over 2000 people were admitted to hospitals and medical centres as a direct result of the Peloponnese fire event, and of these 1100 were due to cardio-vascular and respiratory problems. The World Health Organisation (WHO) air quality guidelines (WHO, 2006) in particular set a limit of 25 µg m<sup>-3</sup> for the concentration of fine mode particulate matter (PM<sub>2.5</sub>) averaged over a 24 hour period. We In the model, we estimated ~~the~~ concentrations of PM<sub>2.5</sub> using ~~the our~~ simulated OM and BC concentrations in the lowest modelled atmospheric layer, and calculated the 24-hour running average for comparison to this WHO threshold.

Figure 15 shows the distribution of 24-hour mean PM<sub>2.5</sub> concentrations modelled between 23<sup>rd</sup> August and 3<sup>rd</sup> September (when the Peloponnese wildfires were at their most intense; Figure 9a). It is clear that the impacts of the Peloponnese wildfires extend well beyond Greece's national borders, and indeed ~~that they~~ resulted in large parts of the Mediterranean region exceeding the WHO 25 µg m<sup>-3</sup> PM<sub>2.5</sub> concentration threshold by large significant margins. In fact, analysis of the spatial distribution of these data with respect to population

Formatted: Justified, Line spacing: 1.5 lines

density (CIESIN and CIAT, 2005) indicated that, for the region shown in Figure 15, ~~around up to 404~~ million people ~~were~~ may have been subject to PM<sub>2.5</sub> concentrations exceeding the WHO guidelines. However, it should be stressed that this is an upper limit for the exposure, because our study ~~almost certainly~~ significantly over-estimates near-surface smoke concentrations due to the assumed ~~near surface~~ boundary-layer injection of the emissions. ~~In~~ particular, surface PM<sub>2.5</sub> concentrations in regions reasonably close to the source that are well above 100 µg m<sup>-3</sup> are ~~very very~~ likely to be spurious, and Liu et al. (2009) report elevated non-urban values closer to 49- µg m<sup>-3</sup>, albeit still at some distance from source. Nonetheless, the spatial range of the affected area, and the considerable human health impacts that these type of large wildfire events can have, ~~and their potential to extend over large regions,~~ highlights the necessity of modelling their smoke emissions and forecasting their atmospheric transport in the manner demonstrated here. Through such work, the ~~CAMS Copernicus Atmospheric Service~~ and its downstream services aim at improving emergency preparedness through air quality forecasts. Geostationary FRP data are likely to be an important component of this system, particularly so as their high temporal resolution FRP data provides a unique view of the type of individual large "mega fire" ~~fire~~ event studied here, that can impact regional air quality so dramatically over short timescales. ~~In this case study, smoke emissions were injected into the lowest atmospheric level which has implications for modelling their spatio-temporal distribution. Leung et al. (2007) and Guan et al. (2008) found that the inclusion of plume injection height information in atmospheric transport models resulted in a reduction in near surface CO concentration since a greater proportion of emissions are lofted above the planetary boundary layer. There are a number of approaches for determining smoke plume injection height which are reviewed by Paugam et al. (2015a). Once such approach is that proposed by Sofiev et al. (2012) and Paugam et al. (2015b) who discuss methods that use FRP measurements to characterise the wildfire thermal properties required to simulate smoke plume injection height within plume rise models. Sofiev et al. (2012) found 70% of estimated plume injection heights were within 500m of the plume heights measured by the Multi-angle Imaging SpectroRadiometer (MISR) whilst Paugam et al. (2015b) found very good agreement between the modelled and measured plume injection layer over a small (n=38) number of wildfire events. Although this is an active area of research, these studies suggest that EO fire thermal measurements, such as FRP, may have a role in characterising smoke plume injection height.~~ In this case study, the smoke emissions were injected into the lowest atmospheric level which has implications for modelling their spatio-temporal distribution. Leung et al. (2007)

Formatted: Font: Not Italic

Formatted: Font color: Text 1

Formatted: Line spacing: 1.5 lines

Formatted: Font color: Text 1, English (U.K.)

and Gaum *et al.* (2008) found that the inclusion of plume injection height information in atmospheric transport models resulted a reduction in near surface CO concentration since a greater proportion of emissions are lofted above the planetary boundary layer. There are a number of approaches for determining smoke plume injection height which are reviewed by Paugam *et al.* (2015a). Once such approach is that proposed by Sofiev *et al.* (2012) and Paugam *et al.* (2015b) who discuss methods that make use of FRP measurements to characterise the wildfire thermal properties required to simulate smoke plume injection height within plume rise models. Using FRP measurements, Sofiev *et al.* (2012) found ~70% of estimated plume injection heights were within 500m of the plume heights measured by the Multi angle Imaging SpectroRadiometer (MISR). Using a different approach, Paugam *et al.* (2015b) found very good agreement between the modelled and measured plume injection layer over a small (n=38) number of wildfire events. Whilst this is still an active area of research, the studies by Sofiev *et al.* (2012) and Paugam *et al.* (2015b) suggest FRP measurements could have a role in characterising smoke plume injection height.

Formatted: Font color: Text 1

## 6.0 SUMMARY AND CONCLUSIONS

This work has provided a detailed performance evaluation of the Meteosat SEVIRI FRP products available from the LSA SAF, both the full resolution FRP-PIXEL product and the reduced resolution FRP-GRID product, both available in near real time and in archived form (<http://landsaf.meteo.pt/>). It has also provided a detailed example of use of the former product in characterising the smoke emissions from a large European wildfire event whose smoke significantly affected the Mediterranean region as a whole, and for which we have demonstrated in modelling their an ability to simulate the atmospheric transport and human health impacts at high temporal resolution.

Formatted: Left, Automatically adjust right indent when grid is defined, Adjust space between Latin and Asian text, Adjust space between Asian text and numbers

When evaluated against the MODIS MOD14 and MYD14 active fire products, the active fire pixel detection error of commission of the FRP-PIXEL product is found to be 9% in the North African LSA SAF geographic region, and increases to higher values particularly in Europe and South America. The basis of this variation is the combination of SEVIRI's increasing pixel area with view zenith angle away from the sub-satellite point, and the relative proportion of lower intensity and/or smaller fires in the various LSA SAF geographic regions (i.e. their fire regimes). Area-based comparisons indicate that the FRP-PIXEL product underestimates compared to simultaneously collected MODIS FRP of a region by

between 35 and 89%, with the variation being again dependent upon the above factors. Underestimation is typically maximised at regions extending towards the edge of the viewing disk, furthest away from the SEVIRI sub-satellite point. However, comparison of the FRP of individual fires successfully detected almost simultaneously by both SEVIRI and MODIS indicates a strong agreement between the two FRP measurements, with the FRP-PIXEL product meeting its Target Accuracy requirements. We find that 76% of the examined simultaneously detected fire clusters had an FRP from SEVIRI within 30% of that measured by MODIS, which given the recent quantification of MODIS' FRP uncertainty (Freeborn *et al.*, 2014c) indicates good performance from the FRP-PIXEL product. Overall, minimal bias is seen between the per-fire FRP observations made by the two sensors.

When compared against that of other active fire products derived from the same Meteosat SEVIRI observations, the performance of the operational geostationary fire thermal anomaly (FTA) algorithm used within the FRP-PIXEL product (Wooster *et al.*, ~~this issue~~2015) compares favourably. During our comparison to MODIS, the SEVIRI WFABBA, FDeM and FIR products from Prins *et al.* (1998), Amraoui *et al.* (2010) and Joro *et al.* (2008) respectively have higher active fire errors of omission, varying between 84 and 95%, as compared to the 77% of the FRP-PIXEL product. However, these alternative SEVIRI-derived active fire products do have lower errors of commission than the FRP-PIXEL product when compared to MODIS, ranging between 5 and 6% (the FRP-PIXEL product has a 13% commission error). The FTA errors of commission are currently being reduced by re-inclusion of the dynamic spatial thresholding parameters described in Section 3.2.2 that were removed from the operational FTA algorithm for computational speed, but included in the original Roberts and Wooster (2008) prototype.

The Level-3 FRP-GRID product accumulates a series of FRP-PIXEL products and provides regional estimates of mean FRP at an hourly temporal resolution and a 5.0° spatial resolution. These estimates come already adjusted for cloud cover, and for the impact of the low spatial resolution detection bias that results in SEVIRI failing to detect the lower FRP active fire pixels. Our evaluation indicates good performance of these bias corrections at the hourly, 5.0° product resolution, but evaluation of accumulated data against summed weekly MODIS FRP over the four LSA SAF geographic regions indicates that the FRP-GRID product underestimates total FRP at this scale. This largely results from the difficulty in accounting for situations where MODIS detects fire activity in a grid cell whilst SEVIRI does not, and so



the bias corrections ~~are~~ remain inactive. We provide herein some additional adjustment factors for those wishing to use the SEVIRI FRP-GRID datasets at this type of scale.

Despite their coarse spatial resolution limitations, the FRP products available from geostationary satellites offer an unprecedented high temporal resolution for studying wildfire emissions. This is a key advantage when using such data to parameterise wildfire smoke emissions within atmospheric transport models (Reid *et al.*, 2009). Here we use a version of the FRP-PIXEL product, ~~adjusted to remove the impacts of cloud masking~~, to characterise the smoke emissions from the August 2007 Peloponnese wildfires. The resulting emissions fields are used within ECMWF's Integrated Forecast System (IFS) to model the smoke emissions transport, and in particular the black carbon and organic carbon aerosols and the resulting aerosol optical depth and PM<sub>2.5</sub> surface concentrations. Our results support the findings of other recent studies (e.g. Garcia-Menendez *et al.*, 2014; Marlier *et al.*, 2014) in that higher temporal resolution smoke emissions estimates provide increased fidelity in the resulting smoke plume aerial distribution and optical thickness metrics than do simulations conducted using daily ~~(e.g. from MODIS FRP)~~ or weekly ~~(e.g. from burned area estimates)~~ temporal resolution data. Visual assessment of the modelled plumes spatial distribution against simultaneous MODIS optical imagery shows good agreement, but the modelled plume is slightly offset from the observations which is believed to result from injecting the plume into the lowest atmospheric layer (whereas in reality it would have been lofted to higher altitudes). Quantitative comparisons between our modelled AOD and the coincident MODIS- and AERONET-derived AOD values indicate that modelled AODs are overestimated by ~ 20 - 30%. Further research into model parameterisation (e.g. injection height) and the aerosol emission factors used is required to investigate this bias, ~~particularly~~ so as it is likely that we underestimate fuel consumption due to ~~many SEVIRI FRP pixels being affected by~~ SEVIRI -MWIR channel saturation during this extreme wildfire event. The European Union (EU) has recently signed a delegation agreement with ECMWF to provide the services implemented in MACC, including the FRP-based Global Fire Assimilation System (GFAS; Kaiser *et al.*, 2012), in an operational manner until at least 2020. This includes on-going developments of GFAS which aim at providing emission estimates with an hourly temporal resolution by combining FRP observations from both polar orbiting and geostationary satellites. Key pre-requisites are the implementation of a model for the diurnal cycle of FRP (Andela *et al.* ~~this issue~~2015) and a suitable bias correction for

1801 geostationary FRP products to account for the omission of low intensity fires, building on the  
1802 simple linear bias corrections applied currently in the FRP-GRID products.

1803  
1804

## 1805 **7.0 Acknowledgements**

1806 Funding for this work came from the UK NERC National Centre for Earth Observation  
1807 (NCEO), from the LSA SAF project, from EUMETSAT and the EU H2020 project MACC-  
1808 III (contract no. 633080). SEVIRI data were kindly provided under an ESA/EUMETSAT  
1809 AO, the MODIS data were provided by the NASA EDC DAACS and the European Forest  
1810 Fire Information System (EFFIS; <http://effis.jrc.ec.europa.eu>) of the European Commission  
1811 Joint Research Centre provided burned area data. The GOES ~~WFABABA~~<sup>SEVIRI</sup> data were  
1812 kindly provided by the Cooperative Institute for Meteorological Satellite Studies (CIMSS)  
1813 within the Space Science and Engineering Center (SSEC) at University of Wisconsin (UW-  
1814 Madison) as a collaborative effort between NOAA / NESDIS / STAR and UW-CIMSS  
1815 personnel. The SEVIRI FRP product ~~and FDeM product~~ were provided by the LSA SAF  
1816 (<http://landsaf.meteo.pt/>), the FDeM product was provided by Carlos C. DaCamara and Sofia  
1817 Ermida at Universidade de Lisboa (<http://www.fc.ul.pt/>). The FIR fire products were obtained  
1818 from EUMETSAT EO portal (<https://eoportal.eumetsat.int/>). The authors would also like to  
1819 thank ~~Jiangping He (Kings College London)~~, Alessio Lattanzio (EUMETSAT), Isabel Trigo  
1820 (LSA-SAF) and Yves Govaerts (Rayference) for the assistance and advice provided during  
1821 this study.

1822  
1823  
1824  
1825  
1826  
1827  
1828  
1829  
1830  
1831  
1832  
1833  
1834

1835  
1836  
1837  
1838  
1839  
1840  
1841 **8.0 References**  
1842  
1843  
1844 Aminou, D. M. A., Jacquet, B. and Pasternak, F. (1997) Characteristics of the Meteosat  
1845 Second Generation Radiometer/Imager: SEVIRI, *Proceedings of SPIE, Europto series*, Vol.  
1846 3221 pages 19-31.  
1847  
1848 Amraoui, M., DaCamara, C. C. and Pereira, J. M. C. (2010) Detection and monitoring of  
1849 African vegetation fires using MSG-SEVIRI imagery. *Remote Sensing of Environment*. 114.  
1850 1038-1052.  
1851  
1852 Andela, N., Kaiser, J.K, van der Werf, G., Wooster, M.J. (submitted) New fire diurnal cycle  
1853 characterizations to improve Fire Radiative Energy assessments made from low-Earth orbit  
1854 satellites sampling, *Atmos. Chem. Phys.*, 15(15):8831–8846.~~*Atmos. Chem. Phys. Discuss.*,~~  
1855 ~~submitted~~  
1856  
1857 Baldassarre, G., Pozzoli, L., Schmidt, C. C., Unal, A., Kindap, T., Menzel, W. P., Whitburn,  
1858 S., Coheur, P.-F., Kavgaci, A., and Kaiser, J. W. (2015). Using SEVIRI fire observations to  
1859 drive smoke plumes in the CMAQ air quality model: a case study over Antalya in 2008.  
1860 *Atmospheric Chemistry and Physics*, 15(14):8539–8558.  
1861  
1862 Andreae, M. O., and P. Merlet (2001) Emission of trace gases and aerosols from biomass  
1863 burning. *Global Biogeochemical Cycles*, 15. 4. 995-966.  
1864  
1865 Berk, A., Anderson, G.P., Acharya, P.K., Bernstein, L.S., Muratov, L., Lee, J., Fox, M.,  
1866 Adler-Golden, S.M., Chetwynd, J.H., Hoke, M.L., Lockwood, R.B., Gardner, J.A., Cooley,  
1867 T.W., Borel, C.C., & Lewis, P.E. (2005). MODTRAN (TM) 5, a reformulated atmospheric  
1868 band model with auxiliary species and practical multiple scattering options: Update.

**Formatted:** Font: (Default) +Headings CS (Times New Roman), Complex Script Font: +Headings CS (Times New Roman)

**Formatted:** Left, Automatically adjust right indent when grid is defined, Snap to grid

**Formatted:** Font: Italic

**Formatted:** Font: Italic

1869 *Algorithms and Technologies for Multispectral, Hyperspectral, and Ultraspectral Imagery*  
1870 *XI*, 5806, 662-667  
1871  
1872 Calle, A., Casanova, J-L. and Gonzales-Alonso, F. (2009) Impact of point spread function of  
1873 MSG SEVIRI on active fire detections. *International Journal of Remote Sensing*. 30. 17.  
1874 4567-4579.  
1875  
1876 Center for International Earth Science Information Network (CIESIN) and Centro  
1877 Internacional de Agricultura Tropical (CIAT) Gridded Population of the World Version 3  
1878 (GPWv3). Palisades, NY. CIESIN Columbia University.  
1879 <http://sedac.ciesin.columbia.edu/gpw/index.jsp>.  
1880  
1881 Chen, Y., Li, Q., Randerson, J. T., Lyons, E. A., Kahn, R. A., Nelson, D. L. and Diner, D. J.  
1882 (2009) The sensitivity of CO and aerosol transport to the temporal and vertical distribution of  
1883 North American boreal fire emissions. *Atmospheric Chemistry and Physics*. 9. 6559-6580.  
1884  
1885 Csizar, I., Schroeder, W., Giglio, L., Ellicott, E., Vadrevu, K. P., Justice, C. O. and Wind, B.  
1886 (2014) Active fires from Suomi NPP Visible Infrared Imaging Radiometer Suite : Product  
1887 status and fire evaluation results. *Journal of Geophysical Research : Atmospheres*. 119. 2.  
1888 803-816.  
1889  
1890 DaCamara, C.C. (2006) The Land Surface Analysis SAF: one year of pre-operational  
1891 activity. *The 2006 EUMETSAT Meteorological Satellite Conference*. Helsinki. Finland. 12<sup>th</sup>-  
1892 16<sup>th</sup> June 2006. EUMETSAT P.48, ISBN 92-9110-076-5, 8pp.  
1893  
1894 Derrien, M. and Le Gleau, H. (2005) MSG/SEVIRI cloud mask and type from SAFNWC.  
1895 *International Journal of Remote Sensing*. 26. 21. 4707-4732.  
1896  
1897 EUMETSAT (2007) Active Fire Monitoring with MSG. *Algorithm Theoretical Basis*  
1898 *Document*. EUM/MET/REP/07/0170. Darmstadt. Germany.  
1899  
1900 European Commission (2010) Forest Fires in Europe 2009. EUR 24502 EN. Office for  
1901 Official Publications of the European Communities. Luxembourg. p. 81.  
1902

Field Code Changed

Formatted: English (U.K.)

1903 Freeborn, P. H., Wooster, M. J., Hao, W. M., Ryan, C. A., Nordgren, B. L., Baker, S. P. and  
 1904 Ichoku, C. (2008) Relationships between energy release, fuel mass loss, and trace gas and  
 1905 aerosol emissions during laboratory biomass fires. *Journal of Geophysical Research*. 113.  
 1906 D01301. doi:10.1029/2007JD008679  
 1907  
 1908 Freeborn, P. H., Wooster, M. J., Roberts, G., Malamud, B. D. and Xu, W. (2009)  
 1909 Development of a virtual active fire product for Africa through a synthesis of geostationary  
 1910 and polar orbiting satellite data. *Remote Sensing of Environment*. 113. 1700-1711.  
 1911  
 1912 Freeborn, P. H., Wooster, M. J., Roberts, G. (2011) Addressing the spatiotemporal sampling  
 1913 design of MODIS to provide estimates of the fire radiative energy emitted from Africa.  
 1914 *Remote Sensing of Environment*. 115. 2. 475 – 489  
 1915  
 1916 Freeborn, P. H., Wooster, M. J., Roberts, G. and Xu, W. (2014a) Evaluating the SEVIRI Fire  
 1917 Thermal Anomaly Detection Algorithm across the Central African Republic Using the  
 1918 MODIS Active Fire Product. *Remote Sensing*. 6. 1890-1917. Doi:10.3390/rs6031890.  
 1919  
 1920 Freeborn, P. H., Cochrane, M. A. and Wooster, M. J. (2014b) A decade long, multi-scale map  
 1921 comparison of fire regime parameters derived from three publically available satellite-based  
 1922 fire products : a case study in the Central African Republic. *Remote Sensing*. 6. 5. 4061-4089.  
 1923  
 1924 Freeborn, P.H., Wooster, M.J., Roy, D.P., & Cochrane, M.A. (2014c). Quantification of  
 1925 MODIS fire radiative power ( FRP) measurement uncertainty for use in satellite- based active  
 1926 fire characterization and biomass burning estimation. *Geophysical Research Letters*, 41,  
 1927 1988-1994  
 1928  
 1929 Fromm, M., Jerome, A., Hoppel, K., Hornstein, J., Bevilacqua, R., Shettle, E., Servranckx,  
 1930 R., Zhanqing, L., and Stocks, B. (2000) Observations of boreal forest fire smoke in the  
 1931 stratosphere by POAM III, SAGE II, and lidar in 1998. *Geophysical Research Letters*. 27.  
 1932 1407–1410. doi:10.1029/1999GL011200.  
 1933  
 1934 Garcia-Meenedez, F., Hu, Y. and Odman, M. T. (2014) Simulating smoke transport from  
 1935 wildland fires with a regional-scale air quality model : Sensitivity to spatiotemporal  
 1936 allocation of fire emissions. *Science of the Total Environment*. 493. 544-553.

1937

1938 Georgiev, C.G., Stoyanova, J.S. (2013) Parallel use of SEVIRI LSA SAF FRP and MPEF

1939 FIR products for fire detection and monitoring. *2013 EUMETSAT Meteorological Satellite*

1940 *Conference. 19<sup>th</sup> American Meteorological Society. AMS Satellite Meteorology,*

1941 *Oceanography and Climatology Conference. 16<sup>th</sup>-20<sup>th</sup> September. 2013. Vienna. Austria.*

1942 ISSN 1011-3932

1943

1944 Giglio, L., Descloitres, J., Justice, C. O., and Kaufman, Y. J., (2003) An enhanced contextual

1945 fire detection algorithm for MODIS. *Remote Sensing of Environment*. 87. 2-3. 273-282.

1946

1947 Gitas, I. Z., Polychronaki, A., Katagis, T and Mallinis, G. (2008) Contribution of remote

1948 sensing to disaster management activities : A case study of the large fires in the Peloponnese,

1949 Greece. *International Journal of Remote Sensing*. 29. 6. 1847-1853. Doi:

1950 10.1080/01431160701874553

1951

1952 Govaerts, Y., (2006) RTMOM V0B.10 Evaluation report, report EUM/MET/DOC/06/0502,

1953 EUMETSAT. 2006. 2226.

1954

1955 Govaerts, Y.M., M.Wooster, Freeborn, P., A.Lattanzio and G.Roberts (2010). Algorithm

1956 Theoretical Basis Document for MSG SEVIRI Fire Radiative Power (FRP) Characterisation.

1957 EUM/MET/SPE/06/0398. EUMETSAT.

1958

1959 [Guan, H., Chatfield, R., B., Freitas, S. R., Bergstrom, R. W., Longo, K. M. \(2008\) Modeling the](#)

1960 [effect of plume-rise on the transport of carbon monoxide over Africa with NCAR CAM.](#)

1961 [Atmospheric Chemistry and Physics. 8. 6801–6812.](#)

1962

1963 Heil, A., Kaiser, J. W., van der Werf, G. R., Wooster, M. J., Schultz, M. J. and Dernier, van

1964 der Gron, H. (~~2012~~2010) Assessment of the real-time fire emissions (GFAS) by MACC. Tech

1965 Memo. 628. ECMWF. Reading. UK

1966

1967 Holben, B. N., Smirnov, A., Eck, T. F., Slutsker, I., Abuhassan, N., Newcomb, W. W.,

1968 Schafer, J. S., Tanre, D., Chatenet, B., and Lavenue, F. (2001) An emerging ground-based

Formatted: Line spacing: 1.5 lines

1969 aerosol climatology: Aerosol optical depth from AERONET. *Journal of Geophysical*  
1970 *Research: Atmospheres*. 106. 12 067–12 097. doi: 10.1029/2001JD900014  
1971  
1972 Hollingsworth, A., Engelen, R. J., Benedetti, A., Dethof, A., Flemming, J., Kaiser, J. W.,  
1973 Morcrette, J.-J., Simmons, A. J., Textor, C., Boucher, O., Chevallier, F., Rayner, P., Elbern,  
1974 H., Eskes, H., Granier, C., Peuch, V.-H., Rouil, L., and Schultz, M. G. (2008) Toward a  
1975 Monitoring and Forecasting System For Atmospheric Composition: The GEMS Project.  
1976 *Bulletin of the American Meteorological Society*. 89. 1147–1164. doi:  
1977 <http://dx.doi.org/10.1175/2008BAMS2355.1>  
1978  
1979 Ichoku, C. and Kaufman, Y. J. (2005) A method to derive smoke emission rates from MODIS  
1980 fire radiative energy measurements, *IEEE Transactions on Geoscience and Remote Sensing*.  
1981 43. 2636–2649.  
1982  
1983 Jacobson, M. Z. (2014) Effects of biomass burning on climate, accounting for heat and  
1984 moisture fluxes, black and brown carbon, and cloud absorption effects. *Journal of*  
1985 *Geophysical Research : Atmospheres*. 119. 8980-9002. Doi:10.1002/2014JD021861.  
1986  
1987 Jenkins, B. M., Baxter, L. L., Miles Jr, T. R., and Miles, T. R. (1998) Combustion properties  
1988 of biomass. *Fuel Processing Technology*. 54. 17 – 46.  
1989  
1990 Joro, S., Samain, O., Yildirim, A., van de Berg, L. and Lutz, H. J. (2008) Towards an  
1991 improved active fire monitoring product for MSG satellites.  
1992 [www.eumetsat.int/cs/idcplg?IdcService=GET\\_FILE&dDocName=pdf\\_conf\\_p\\_s8\\_47\\_joro\\_v](http://www.eumetsat.int/cs/idcplg?IdcService=GET_FILE&dDocName=pdf_conf_p_s8_47_joro_v&allowInterrupt=1&noSaveAs=1&RevisionSelectionMethod=LatestReleased)  
1993 [&allowInterrupt=1&noSaveAs=1&RevisionSelectionMethod=LatestReleased](http://www.eumetsat.int/cs/idcplg?IdcService=GET_FILE&dDocName=pdf_conf_p_s8_47_joro_v&allowInterrupt=1&noSaveAs=1&RevisionSelectionMethod=LatestReleased)  
1994  
1995 Kaiser, J. W., Heil, A., Andrae, M. O., Benedetti, A., Chubarova, N., Jones, L., Morcrette, J.-  
1996 J., Razinger, M., Schultz, M. G., Suttie, M. and van der Werf, G., R. (2012) Biomass burning  
1997 emissions estimates with a global fire assimilation system based on observed fire radiative  
1998 power. *Biogeosciences*. 9. 5125-5142. doi:10.5194/bg-9-5125-2012  
1999  
2000 Kaiser, J. W., Suttie, M., Flemming, J., Morcrette, J.-J., Boucher, O. and Schultz, M. G.  
2001 (2009a). Global real-time fire emission estimates based on space-borne fire radiative power  
2002 observations. *AIP Conference Proceedings*, 1100:645–648.

Formatted: Line spacing: 1.5 lines



2003

2004 Kaiser, J. W., Boucher, O., Doutriaux-Boucher, M., Flemming, J., Govaerts, Y. M., Gulliver,

2005 J., Heil, A., Jones, L., Lattanzio, A., Morcrette, J.-J., Perrone, M. R., Razinger, M., Roberts,

2006 G., Schultz, M. G., Simmons, A. J., Suttie, M., and Wooster, M. J. (2009b). Smoke in the air.

2007 *ECMWF Newsletter*, 119. 9–15. European Centre for Medium-range Weather Forecasts.

2008

2009 Kaufman, Y. J. and Remer, L. A. (1994) Detection of forests using Mid-IR reflectance : An

2010 application for aerosol studies. *IEEE Transactions on Geoscience and Remote Sensing*. 32. 3.

2011 672-683.

2012

2013 Koutsias, N., Arianmoutsou, M., Kallimanis, A. S., Mallinis, G., Halley, J. M., and

2014 Dimopoulos, P. (2012) Where did the fires burn in Peloponnese, Greece the summer of 2007?

2015 Evidence for a synergy of fuel and weather. *Agricultural and Forest Meteorology*. 156. 41-

2016 53.

2017

2018 Leung, F-Y, T., Logan, J. A., Park, R., Hyer, E., Kasischke, E., Streets, S and Yurganov, L.

2019 (2007) Impacts of enhanced biomass burning in the boreal forests in 1998 on tropospheric

2020 chemistry and the sensitivity of model results to the injection height of emissions. *Journal of*

2021 *Geophysical Research*, 112. D10313, doi:10.1029/2006JD008132

2022

2023 Li, Z, Kaufman, Y. J., Ichoku, C., Fraser, R., Trishchenko, A., Giglio, L. and Yu, X. (2001) A

2024 review of AVHRR-based active fire detection algorithms: Principles, limitations, and

2025 recommendations. *Global and regional vegetation fire monitoring from space, planning and*

2026 *coordinated international effort*. Academic Publishing. The Hague. 199-225pp

2027

2028 Liu, Y., Kahn, R. A., Chaloulakou, A. and Koutrakis, P. (2009) Analysis of the impact of the

2029 forest fires in August 2007 on air quality of Athens using multi-sensor aerosol remote sensing

2030 data, meteorology and surface observations. *Atmospheric Environment*. 43. 3310-3318.

2031

2032 Mallinis, G., Mitsopoulos, I., Stournara, P., Patias, P. and Dimitrakopoulos, A. (2013)

2033 Canopy fuel load mapping of Mediterranean pine sites based on individual tree crown

2034 delineation. *Remote Sensing*. 5. 6461-6480. Doi:10.3390/rs5126461.

2035

**Formatted:** Font: (Default) +Headings CS (Times New Roman), Complex Script Font: +Headings CS (Times New Roman)

**Formatted:** Line spacing: 1.5 lines

**Formatted:** Font: (Default) +Headings CS (Times New Roman), Italic, Complex Script Font: +Headings CS (Times New Roman), Italic

**Formatted:** Font: (Default) +Headings CS (Times New Roman), Complex Script Font: +Headings CS (Times New Roman)

2036 Marlier, M.E., Voulgarakis, A., Shindell, D.T., Faluvegi, G., Henry, C.L. and Randerson, J.T.  
 2037 (2014) The role of temporal evolution in modeling atmospheric emissions from tropical fires.  
 2038 *Atmospheric Environment*. 89. 158-168. doi:10.1016/j.atmosenv.2014.02.039.  
 2039  
 2040 MeteoFrance (2010). Algorithm theoretical basis document for cloud products. Technical  
 2041 Report. SAF/NWC/CDOP/MFL/SCI/ATBD/01,MeteoFrance.  
 2042  
 2043 Mistakis, E, Stamos, I., Panakinolaou, A., Aifadopoulou, G. and Kontoes, H (2014)  
 2044 Assessment of extreme weather events on transport networks : case study of the 2007  
 2045 wildfires in Peloponnesus. *Natural Hazards*. 72. 87-107. Doi:10.1007/s11069-013-0896-3.  
 2046  
 2047 Mitsopoulos, I. D. and Dimitrakopoulos, A. P. (2013) Estimation of canopy fuel characteristics  
 2048 of Aleppo pine (*Pinus halepensis* Mill.) forests in Greece based on common stand parameters.  
 2049 *European Journal of Forest Research*. 133:73-79, Doi:10.1007/s10342-013-0740-z.  
 2050  
 2051 Morcrette, J.-J., L. Jones, J.W. Kaiser, A. Benedetti, O. Boucher (2008) Toward a forecast of  
 2052 aerosols with the ECMWF Integrated Forecast System. *ECMWF Newsletter*. No. 114.  
 2053 ECMWF. Reading. UK.  
 2054  
 2055 Paugam, R., Wooster, M., Freitas, S. R. and Val Martin, M. (2015a) A review of approaches  
 2056 to estimate wildfire plume injection height within large scale atmospheric chemical transport  
 2057 models – Part 1. *Atmospheric Chemistry and Physics Discussions*. 15. 9767-9813.  
 2058  
 2059 Paugam, R., Wooster, M., Atherton, J., Freitas, S. R., Schultz, M. G. and Kaiser, J. W.  
 2060 (2015b) Development and optimization of a wildfire plume rise model based on remote  
 2061 sensing data inputs – Part 2. *Atmospheric Chemistry and Physics Discussions*. 15. 9815-9895.  
 2062  
 2063 Petrenko, M., Kahn, R., Chin, M., Soja, A., Kucsera, T., and Harshvardhan (2012). The use  
 2064 of satellite-measured aerosol optical depth to constrain biomass burning emissions source  
 2065 strength in the global model GOCART. *Journal of Geophysical Research*. 117(D18):D22204.  
 2066 doi:10.1029/2012JD017870  
 2067

Formatted: Line spacing: 1.5 lines

2068 Pereira, G., Shimabukuro, Y. E., Moraes, E. C., Freitas, S. R., Cardozo, F., S., and Longo, K.  
 2069 M. (2011) Monitoring the transport of biomass burning emission in South America.  
 2070 *Atmospheric Pollution Research*. 3. 247-254.  
 2071  
 2072 Petitcolin, F. and Vermote, E. (2002) Land surface reflectance, emissivity and temperature  
 2073 from MODIS middle and thermal infrared data. *Remote Sensing of Environment*. 82. 112-  
 2074 134.  
 2075  
 2076 Prins, E. M., and Menzel, W. P., (1994) Trends in South American biomass burning with the  
 2077 GOES visible infrared spin scan radiometer atmospheric sounder from 1983 to 1991. *Journal*  
 2078 *of Geophysical Research*. 99. 16719-16735.  
 2079  
 2080 Prins, E. M., Felts, J. M., Menzel, W. P., Ward, D. E. (1998) An overview of GOES-8 diurnal  
 2081 fire and smoke results for SCAR-B and 1995 fire season in South America. *Journal of*  
 2082 *Geophysical Research*. 103. 31821-31835.  
 2083  
 2084 Poupkou, A., Markakis, K., N.Liora, Giannaros, T. M., Zanis, P., Im, U., Daskalakis, N.,  
 2085 Myriokefalitakis, S., Kaiser, J. W., Melas, D., Kanakidou, M., Karacostas, T., and Zerefos, C.  
 2086 (2014). A modeling study of the impact of the 2007 Greek forest fires on the gaseous  
 2087 pollutant levels in the Eastern Mediterranean. *Atmospheric Environment*. 148. 1–17.  
 2088  
 2089 Reid, J. S., Hyer, E. J., Prins, E. M., Westphal, D. L., Zhang, J., Wang, J., Christopher, S. A.,  
 2090 Curtis, C. A., Schmidt, C. C., Eleuterio, D. P., Richardson, K. A. and Hoffman, J. P. (2009)  
 2091 Global monitoring and forecasting of biomass-burning smoke : description of and lessons  
 2092 from the Fire Locating and Modeling of Burning Emissions (FLAMBE) program. *IEEE*  
 2093 *Journal of Selected Topics in Applied Earth Observations and Remote Sensing*. 2. 3. 144 -  
 2094 162.  
 2095  
 2096 Roberts, G., Wooster, M. J., Perry, G. L. W. , Drake, N., Rebelo, L.-M., Dipotso, F. (2005),  
 2097 Retrieval of biomass combustion rates and totals from fire radiative power observations:  
 2098 Application to southern Africa using geostationary SEVIRI imagery, *Journal of Geophysical*  
 2099 *Research*. 110. D21111. doi:10.1029/2005JD006018.  
 2100

2101 Roberts, G. and Wooster, M. J. (2007) New perspectives on Africa biomass burning  
 2102 dynamics. *EOS. Transactions American Geophysical Union*. 88. 38. 369-370.  
 2103  
 2104 Roberts, G. and Wooster, M. J. (2008) Fire Detection and Fire Characterization over Africa  
 2105 using Meteosat SEVIRI. *IEEE Transactions on Geoscience and Remote Sensing*. 48. 4. 1200-  
 2106 1219  
 2107  
 2108 Roberts, G. and Wooster, M. J. (2014) Development of a multi-temporal Kalman filter  
 2109 approach to geostationary active fire detection and fire radiative power (FRP) estimation.  
 2110 *Remote Sensing of Environment*. 152. 392-412. DOI: 10.1016/j.rse.2014.06.020  
 2111  
 2112 Roberts, G., Wooster, M. J., and Lagoudakis, E. (2009). Annual and diurnal ~~african~~-African  
 2113 biomass burning temporal dynamics. *Biogeosciences*, 6, 849-866.  
 2114  
 2115 Roy, D.P. and Boschetti, L. (2009) Southern Africa Validation of the MODIS, L3JRC and  
 2116 GLOBCARBON Burned Area Products. *IEEE Transactions on Geoscience and Remote*  
 2117 *Sensing*. 47. 4. 1032-1044. doi:10.1109/TGRS.2008.2009000.  
 2118  
 2119 Schroeder, W., Prins, E., Giglio, L., Csiszar, I., Schmidt, C., Morisette, and Morton, D.  
 2120 (2008) Validation of GOES and MODIS active fire detection products using ASTER and  
 2121 ETM+ data. *Remote Sensing of Environment*. 112. 2711-2726.  
 2122  
 2123 Seiler, W., and Crutzen, P. J. (1980). Estimates of gross and net fluxes of carbon between the  
 2124 biosphere and the atmosphere from biomass burning. *Climatic Change*, 2(3), 207-247.  
 2125  
 2126 Sofiev, M., Vankevich, R., Lotjonen, M., Prank, M., Petukhov, V., Ermakova, T., Koskinen,  
 2127 J., and Kukkonen, J. (2009) An operational system for the assimilation of the satellite  
 2128 information on wild-land fires for needs of air quality modelling and forecasting.  
 2129 *Atmospheric Chemistry and Physics*. 9. 6833 – 6847.  
 2130  
 2131 Sofiev, M., Ermakova, T., and Vankevich, R. (2012) Evaluation of the smoke-injection  
 2132 height from wild-land fires using remote sensing data. *Atmospheric Chemistry and Physics*.  
 2133 12. 1995-2006. doi:10.5194/acp-12-1995-2012.  
 2134

Formatted: Line spacing: 1.5 lines

2135 Tjemkes, S. A., and Scmetz, J. (1997) Synthetic satellite radiances using the radiance  
 2136 sampling method. *Journal of Geophysical Research*. 102. 1807 – 1818  
 2137

2138 Theoharatos, G., Pantavou, K., Mavrakis, A., Spanou, A., Katavoutas, G., Efstathiou, P.,  
 2139 Mpekas, P., and Asimakopoulos, D (2010) Heat waves observed in 2007 in Athens, Greece:  
 2140 Synoptic conditions, bioclimatological assessment, air quality levels and health effects.  
 2141 *Environmental Research*. 110. 152–161.  
 2142

2143 Tsyro, S., Simpson, D., Tarrason, L., Klimont, Z., Kupianen, K., Pio, C. and Yttri, K. E.  
 2144 (2007) Modeling of elemental carbon over Europe. *Journal of Geophysical Research :*  
 2145 *Atmospheres*. 112. ~~D23S19D23~~. 16. DOI: 10.1029/2006JD008164  
 2146

2147 Turquety, S., Hurtmans, D., Hadji-Lazaro, J., Coheur, P., Clerbaux, C., Josset, D. and  
 2148 Tsamalis, C. (2009) Tracking the emission and transport of pollution from wildfires using the  
 2149 IASI CO retrievals: analysis of the summer 2007 Greek fires. *Atmospheric Chemistry*  
 2150 *Physics*. 9. 4897–4913.  
 2151

2152 Turquety, S., Menut, L., Bessagnet, B., Anav, A., Viovy, N., Maignan, F., & Wooster, M.  
 2153 (2014). APIFLAME v1.0: high resolution fire emission model and application to the Euro-  
 2154 Mediterranean region. *Geoscientific Model Development*. 7, 587-612, doi:10.5194/gmd-7-  
 2155 587-2014.  
 2156

2157 Val Martin, M., Logan, J. A., Kahn, R. A., Leung, F-Y., Nelson, D. L., and Diner, D. J.  
 2158 (2010) Smoke injection heights from fires in North America : analysis of 5 years of satellite  
 2159 observations. *Atmospheric Chemistry and Physics*. 10. 1491-1510.  
 2160

2161 Val Martin, M., Kahn, R. A., Logan, J. A., Paugam, R., Wooster, M. and Ichoku, C. (2012)  
 2162 Space-based observational constraints for 1-D fire smoke plume-rise models. *Journal of*  
 2163 *Geophysical Research: Atmospheres*. 117. ~~D22~~. D22204. Doi: 10.1029/2012JD018370  
 2164

2165 van der Werf, G. R., Randerson, J. T., Giglio, L., Collatz, G. J., Mu, M., Kasib- hatla, P. S.,  
 2166 Morton, D. C., DeFries, R. S., Jin, Y., and van Leeuwen, T. T. (2010). Global fire emissions  
 2167 and the contribution of deforestation, savanna, forest, agricultural, and peat fires (1997–  
 2168 2009). *Atmospheric Chemistry Physics*. 10. 11707–11735.

**Formatted:** Font: (Default) +Headings CS (Times New Roman), 12 pt, Complex Script Font: +Headings CS (Times New Roman), 12 pt

**Formatted:** Font: (Default) +Headings CS (Times New Roman), Complex Script Font: +Headings CS (Times New Roman)

**Formatted:** English (U.K.)

2169

2170 | ~~Van~~-van der Werf, G. R., Randerson, J. T., Giglio, L., Collatz, G. J., Kasibhatla, P. S. and  
 2171 Arellano Jr, A. F. (2006) Interannual variability of global biomass burning emissions from  
 2172 1997-2004. *Atmospheric Chemistry and Physics*. 6. 3423-3441.

2173

2174 Veraverbeke, S., Lhermitte, S., Verstraeten, W. W. and Goossens, R. (2010) The temporal  
 2175 dimension of differenced Normalised Burn Ratio (dNBR) fire/burn severity studies : The case  
 2176 of the large 2007 Peloponnese wildfires in Greece. *Remote Sensing of Environment*. 114. 11.  
 2177 2548-2563. Doi: 10.1016/j.rse.2010.05.029

2178

2179 Verroios, G and Georgiadis, T. (2011) Aleppo pine forests of northern and western  
 2180 Peloponnisos (southern Greece) : Plant communities and diversity. *Plant Biosystems*. 145. 3.  
 2181 606-619.

2182

2183 World Health Organisation (2006) Air quality guidelines for particulate matter, ozone,  
 2184 nitrogen dioxide and sulphur dioxide. WHO/SDE/PHE/OEH/06.02. *World Health*  
 2185 *Organization*. WHO Press. Geneva. Switzerland

2186

2187 Wooster, M. J., Zhukov, B., and Oertel, D., (2003) Fire radiative energy for quantitative  
 2188 study of biomass burning: derivation from the BIRD experimental satellite and comparison to  
 2189 MODIS fire products. *Remote Sensing of Environment*. 86. 83-107.

2190

2191 Wooster, M. J., Roberts, G., Perry, G. L. W. and Kaufman, Y. J. (2005) Retrieval of biomass  
 2192 combustion rates and totals from fire radiative power observations: FRP derivation and  
 2193 calibration relationships between biomass consumption and fire radiative energy release.  
 2194 *Journal of Geophysical Research*. 110, D24311. doi:10.1029/2005JD006318

2195

2196 Wooster, M. J., Xu, W., and Nightingale, T (2012) Sentinel-3 SLSTR active fire detection  
 2197 and FRP product: Pre-launch algorithm development and performance evaluation using  
 2198 MODIS and ASTER datasets. *Remote Sensing of Environment*. 120. 236–254.

2199

2200 Xu, W., Wooster, M. J., Roberts, G. and Freeborn, P. (2010) New GOES imager algorithms  
 2201 for cloud and active fire detection and fire radiative power assessment across North, South  
 2202 and Central America. *Remote Sensing of Environment*. 114. 9. 1876-1895.

2203

2204 Yang, E.-S., Christopher, S. A., Kondragunta, S., and Zhang, X (2011) Use of hourly

2205 Geostationary Operational Environmental Satellite (GOES) fire emissions in a Community

2206 Multiscale Air Quality (CMAQ) model for improving surface particulate matter predictions.

2207 | *Journal of Geophysical Research : Atmospheres*. 116. [D04303](#). Doi: 10.1029/2010JD014482.

2208

2209 | Zhang, X., Kondragunta, S., Ram, J., Schmidt, C. and Hung, H-C. (2012) Near-real-time

2210 global biomass burning emissions product from geostationary satellite constellation. *Journal*

2211 | *of Geophysical Research : Atmospheres*. 117. [D14201](#). doi:10.1029/2012JD017459.

2212

2213 Zhukov, B., Lorenz, E., Oertel, D., Wooster, M. and Roberts, G. (2006) Spaceborne detection

2214 and characterisation of fires during the bi-spectral infrared detection (BIRD) experimental

2215 small satellite mission (2001-2004). *Remote Sensing of Environment*. 100. 29-51.

2216 doi:10.1016/j.rse.2005.09.019

2217

2218

2219

2220

2221

2222

2223

2224

2225

2226

2227

2228

2229

2230

2231

2232

Formatted: English (U.K.)



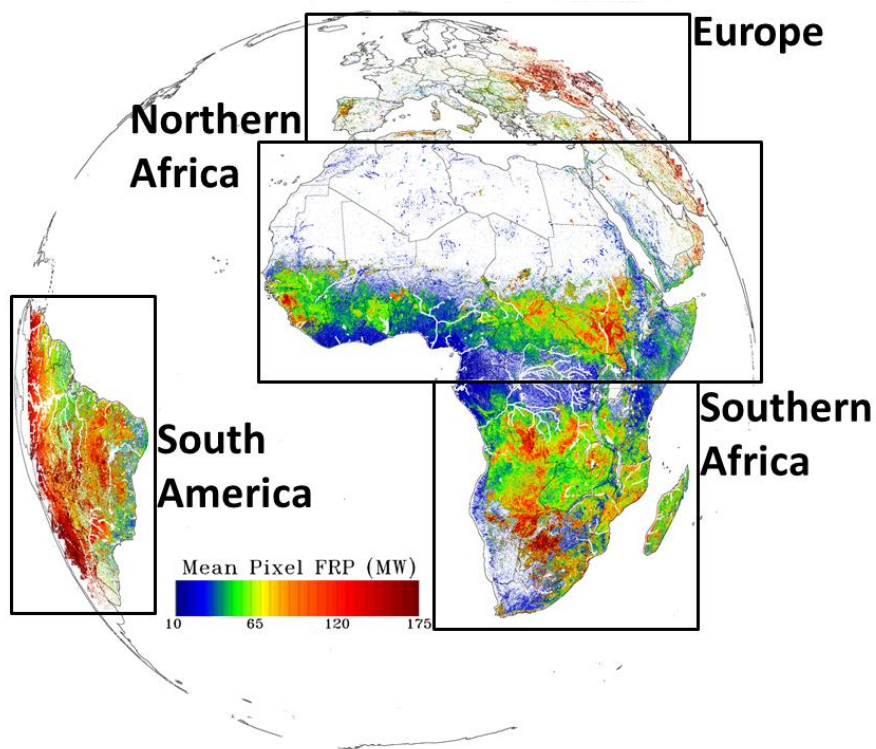


**Figure 1:** SEVIRI's imaging disk showing the mean per-pixel FRP (MW) seen in each SEVIRI pixel, calculated using all FRP-PIXEL products available between 2008-2013. Also indicated are the four geographic regions that LSA-SAF SEVIRI products are subset to.

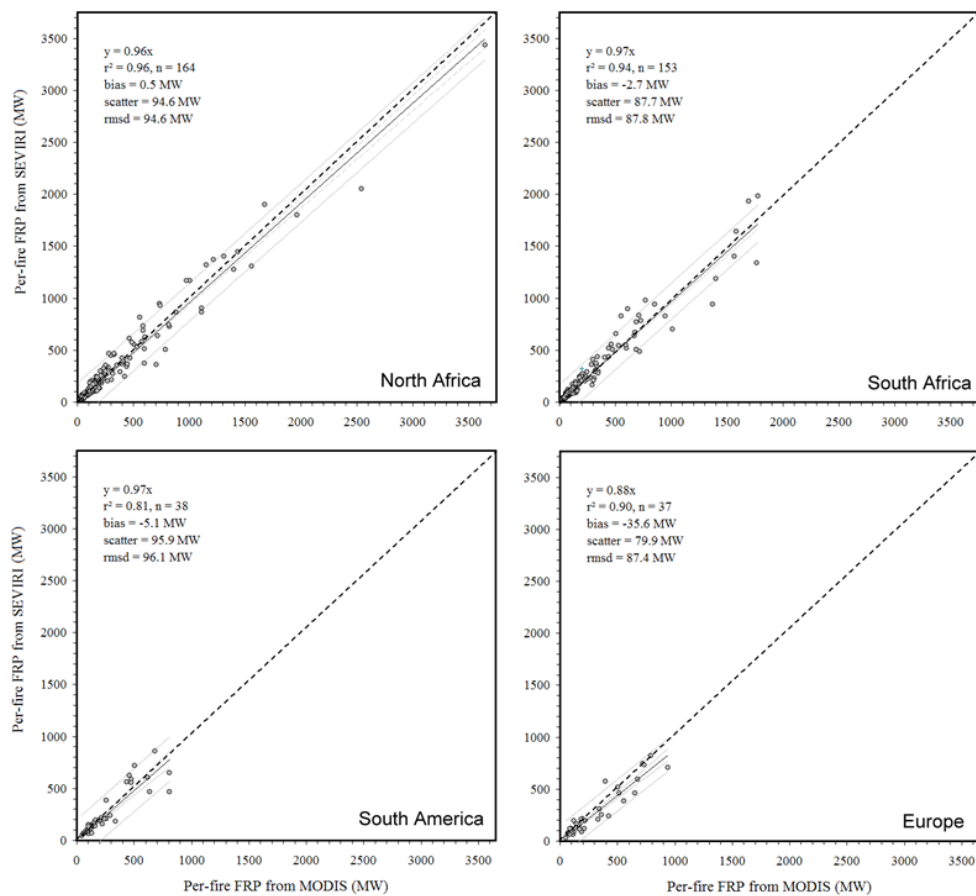


**Figure 2:** A comparison of per-fire FRP derived from SEVIRI and MODIS observations of fires observed near-simultaneously by each sensor during one week in each LSA SAF geographic region (Figure 1). Fires are designated as contiguous clusters of active fire pixels. SEVIRI FRP were taken from the LSA SAF FRP-PIXEL product in each case and MODIS FRP is taken from the MOD14 product (Collection 5; Giglio *et al.*, 2003). The most radiant fires were detected in the northern Africa region (top left), and all regions are displayed on the same x- and y-axis scales for ease of comparison.

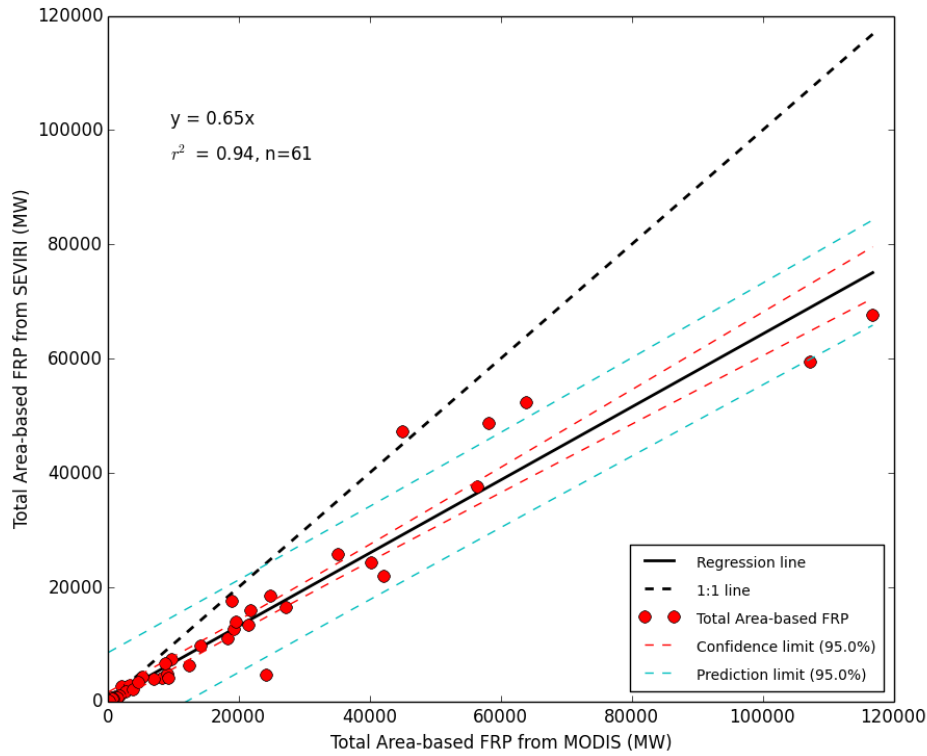


**Figure 3:** Relationship between regional-scale inter-scene FRP derived from all spatially matched, contemporaneous SEVIRI and MODIS FRP-PIXEL observations for the northern Africa region (1-7 December, 2009). The MODIS swath is taken as the observation area. The least squares linear best-fit passing through the origin is shown (bold line), along with the 95% confidence intervals on the mean (light dotted line) and on the prediction of y from x (outermost lines). The 1:1 line is also shown (dashed). SEVIRI tends to generally underestimate regional-scale FRP, primarily due to the non-detection of the lowest FRP fire pixels, many of which MODIS can detect. However, the degree of underestimation is relatively small as described by the slope of the linear best fit to the data.

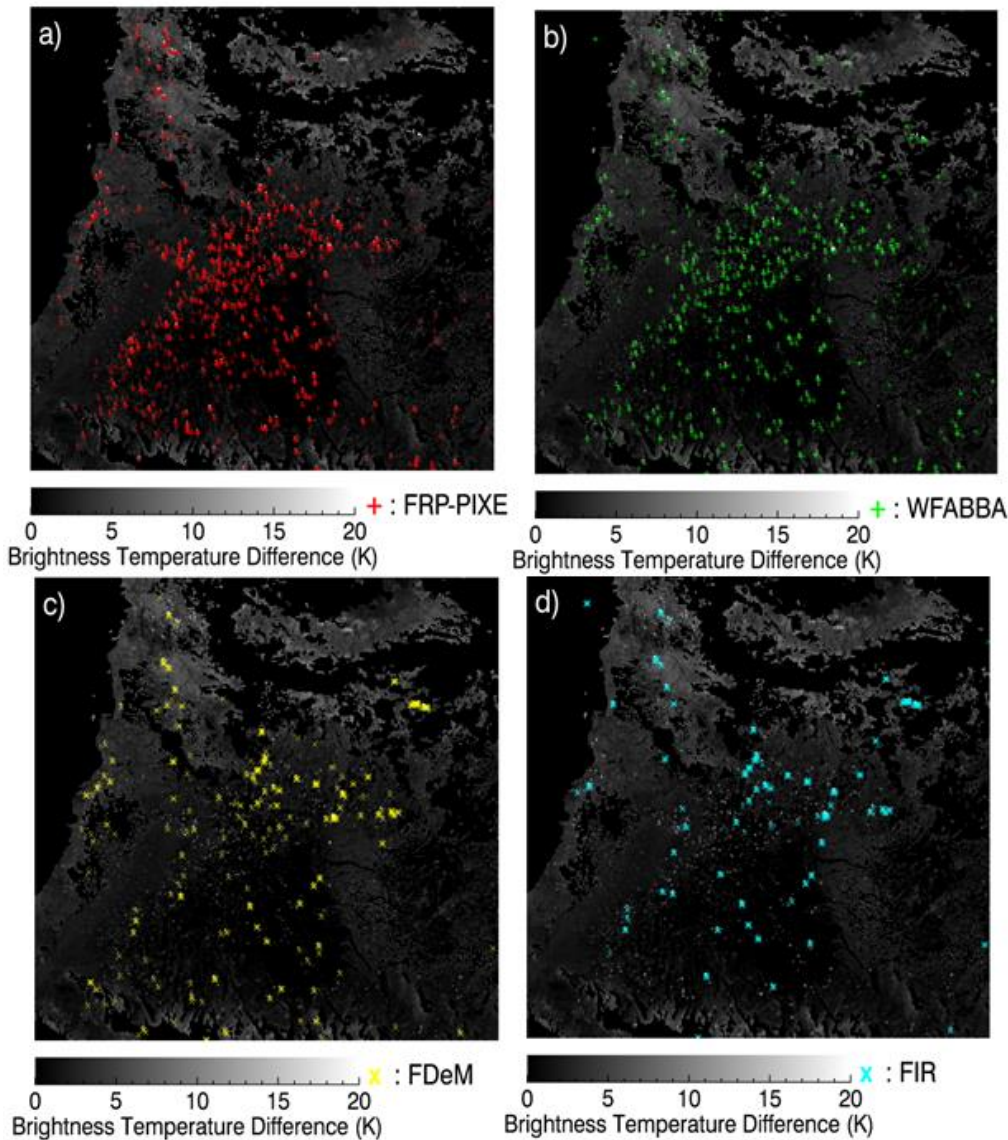
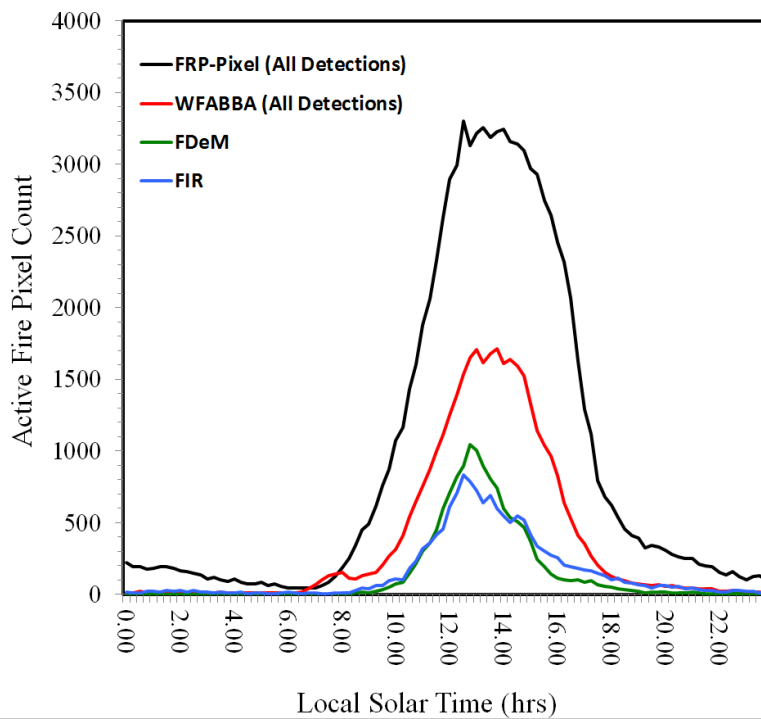


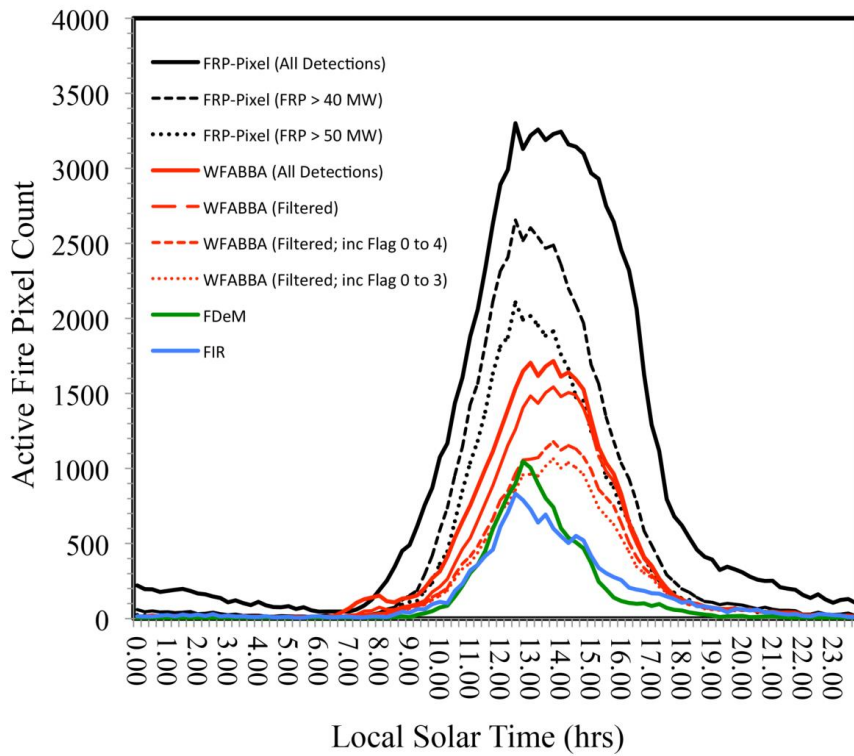
**Figure 4** : Example of the active fire pixel detections contained within the four SEVIRI-derived active fire detection products studied herein (LSA SAF FRP-PIXEL product; Wooster *et al.*, [this issue 2015](#), WF-ABBA; Prins *et al.*, 1998, Fire Detection and Monitoring - FDeM; Amraoui *et al.*, 2010, and FIR Active Fire Monitoring; Joro *et al.*, 2008). The images are produced from a single SEVIRI time slot (13:15 UTC on 21<sup>st</sup> August 2014) and show the active fire detections made in (a) FRP-PIXEL (1249 active fire pixel detections), (b) WFABBA (filtered version; 686 detections made), (c) FDeM (346 detections) and (d) FIR (312 detections). The underlying greyscale image is the SEVIRI brightness temperature difference image (3.9 $\mu$ m - 10.8 $\mu$ m channels) from the same imaging slot. Water bodies and clouds have been masked out (black). The region shown is that over Angola in the southern African LSA SAF geographic region (Figure 1). It is clear that whilst all the products tend to detect a reasonable number of fires that are comprised on multiple SEVIRI active fire pixels,

2295 it is the FRP-PIXEL and WF-ABBA products that detect more of the single pixel fires, with  
2296 the FRP-PIXEL product dominating in this regard.  
2297  
2298

2299



2300  
2301



Formatted: Font: 15 pt, Complex  
Script Font: 15 pt

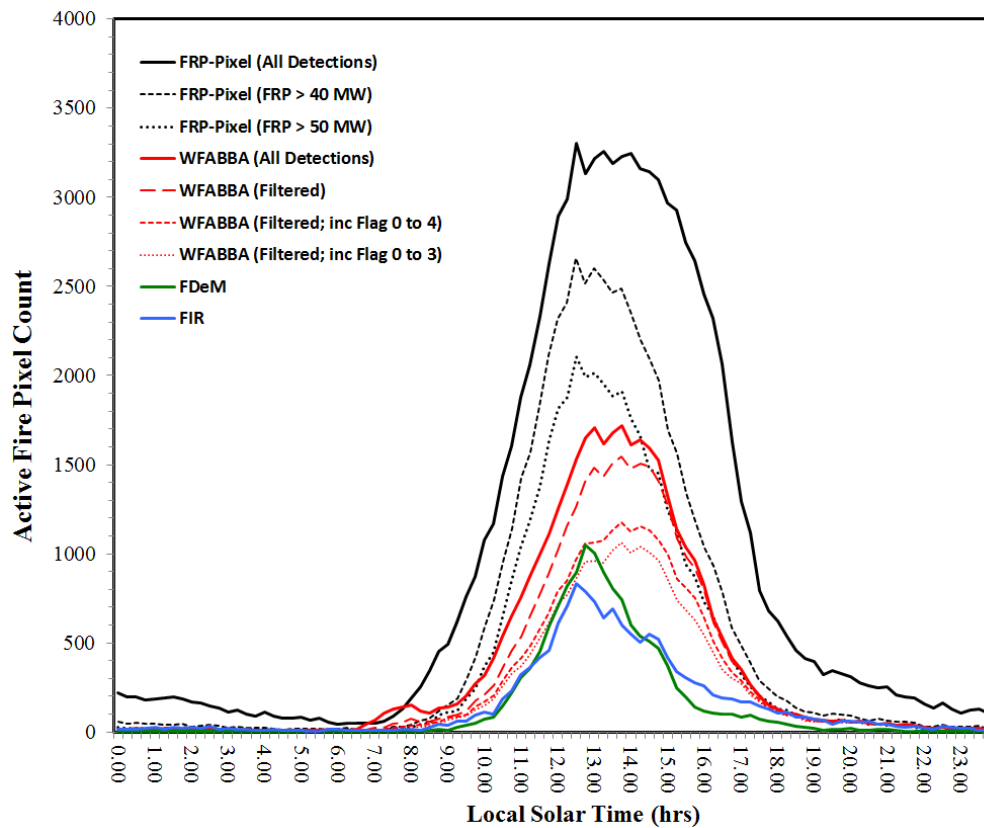


**Figure 5:** Diurnal cycle of active fire detections made by the four SEVIRI-derived active fire products discussed herein over the LSA SAF southern Africa geographic region (Figure 1) on a single day (30<sup>th</sup> August 2014). The products are the LSA SAF FRP-PIXEL product (Wooster *et al.*, 2015), Wildfire-ABBA (WFABBA; Prins *et al.*, 1998), Fire Detection and Monitoring (FDeM; Amraoui *et al.*, 2010) and Active Fire Monitoring (FIR; Joro *et al.*, 2008). All confirmed active fire detections made in each product are included here for completeness, and results are shown in terms of the local solar time of detection. For the FRP-PIXEL product, three active fire time-series are shown; 1) all detections, and those only those detections from fire pixels with FRP magnitudes 2) >40 MW and 3) >50 MW since it is known that increasing undercounting of active fire pixels occurs around these limits (Roberts and Wooster, 2008; and companion paper in this issue). For the WFABBA active fire detections, all four versions of the dataset are included 1) all active fire detections, 2) the WFABBA 'filtered' detections where active fire pixels only detected once during 24 hrs are removed; and the WFABBA filtered detections keeping only 3) the high probability fires (flags 0 to 3) and 4) high and medium probability fires (flags 0 to 4). The LSA SAF FRP-PIXEL product detects a total of 89781 active fire pixels over this day, which reduces to 53561 and 39461 when restricted to fire pixels with FRP magnitudes >40 MW and >50 MW respectively. For the WFABBA detections, the total number of active fire detections is 35759, the WFABBA and the filtered dataset contains 35759 detections which reduces to 30751 and 23957 when WFABBA low and medium probability fire detections are removed. The FDeM and FIR detect only 13477 and 14645 active fire pixels respectively.

**Figure 5:** Diurnal cycle of active fire detections made by the four SEVIRI active fire products discussed herein over the LSA SAF southern Africa geographic region (Figure 1) on

Formatted: Font color: Auto



2326 a single day (30<sup>th</sup> August 2014). The products are the LSA SAF FRP PIXEL product  
 2327 (Wooster *et al.*, 2015), Wildfire ABBA (WFABBA; Prins *et al.*, 1998), Fire Detection and  
 2328 Monitoring (FDeM; Amraoui *et al.*, 2010) and Active Fire Monitoring (FIR; Joro *et al.*,  
 2329 2008). All confirmed active fire detections made in each product are included here for  
 2330 completeness, and results are shown in terms of the local solar time of detection. For the  
 2331 FRP PIXEL product, three active fire time series are shown; 1) all detections, and those only  
 2332 from fire pixels with FRP 2) >40 MW and 3) >50 MW since it is known that significant  
 2333 undercounting of active fire pixels occurs around these limits. For the WFABBA active fire  
 2334 detections, four versions of the dataset are included 1) all active fire detections, 2) the  
 2335 WFABBA 'filtered' detections where pixels only detected as an active fire once during 24 hrs  
 2336 are removed; and the filtered detections keeping only 3) the higher possibility fires  
 2337 (WFABBA flags 0 to 3) and 4) high and medium possibility fires (WFABBA flags 0 to 4).  
 2338 The LSA SAF FRP PIXEL product detects a total of 89781 active fire pixels over the day  
 2339 which reduces to 53561 and 39461 when restricted to >40 MW and >50 MW respectively.  
 2340 For the WFABBA detections, the total number of all active fire detection is 35759, the  
 2341 filtered dataset contains 35759 detections which reduces to 30751 and 23957 when low and  
 2342 medium possibility classed fire detections are removed. The FDeM and FIR detect only  
 2343 13477 and 14645 active fire pixels respectively.  
 2344 **Figure 5:** Diurnal cycle of active fire detections made by the four SEVIRI active fire  
 2345 products discussed herein over the LSA SAF southern African geographic region (Figure 1)  
 2346 on a single day (30<sup>th</sup> August 2014). The products are the LSA SAF FRP PIXEL product  
 2347 (Wooster *et al.*, 2015), Wildfire ABBA (WFABBA; Prins *et al.*, 1998), Fire Detection and  
 2348 Monitoring (FDeM; Amraoui *et al.*, 2010) and Active Fire Monitoring (FIR; Joro *et al.*,  
 2349 2008). All confirmed active fire detections made in each product are included here for  
 2350 completeness, and results are shown in terms of the local solar time of detection. For the  
 2351 FRP PIXEL product, three active fire time series are shown, all detections; and those only  
 2352 from fire pixels with FRP >40 MW and >50 MW since it is known that significant  
 2353 undercounting of active fire pixels occurs around these limits. For the WFABBA active fire  
 2354 detections, four versions of the dataset are included, all active fire detections; the WF ABBA  
 2355 'filtered' detections where pixels only detected as an active fire once during 24 hrs are  
 2356 removed; and the filtered detections keeping only the higher possibility fires (WF ABBA  
 2357 flags 0 to 3) and high and medium possibility fires (WF ABBA flags 0 to 4). The LSA SAF  
 2358 FRP PIXEL product detects a total of 89781 active fire pixels over the day which reduces to  
 2359 53561 and 39461 when restricted to >40 MW and >50 MW respectively. For the WFABBA  
 2360 detections, the total number of all active fire detection is 35759, the filtered dataset contains  
 2361 35759 detections which reduces to 30751 and 23957 when low and medium possibility  
 2362 classed fire detections are removed. The FDeM and FIR detect only 13477 and 14645 active  
 2363 fire pixels respectively.  
 2364 **Figure 5:** Diurnal cycle of active fire detections made by the four SEVIRI active fire  
 2365 products discussed herein over the LSA SAF southern African geographic region (Figure 1)  
 2366 on a single day 30<sup>th</sup> August 2014. The products are the LSA SAF FRP PIXEL product  
 2367 (Wooster *et al.*, this issue), Wildfire ABBA (WFABBA; Prins *et al.*, 1998), Fire Detection  
 2368 and Monitoring (FDeM; Amraoui *et al.*, 2010) and Active Fire Monitoring (FIR; Joro *et al.*,  
 2369 2008). All confirmed active fire detections made in each product are included here for  
 2370 completeness, and results are shown in terms of the local solar time of detection. The LSA  
 2371 SAF FRP PIXEL product detects a total of 89781 active fire pixels over this day, whilst  
 2372 WFABBA, FDeM and FIR detect 35759, 13477 and 14645 active fire pixels respectively.

Formatted: Font color: Auto

Formatted: Font color: Auto

Formatted: Font color: Auto

Formatted: Font color: Auto

2373  
2374

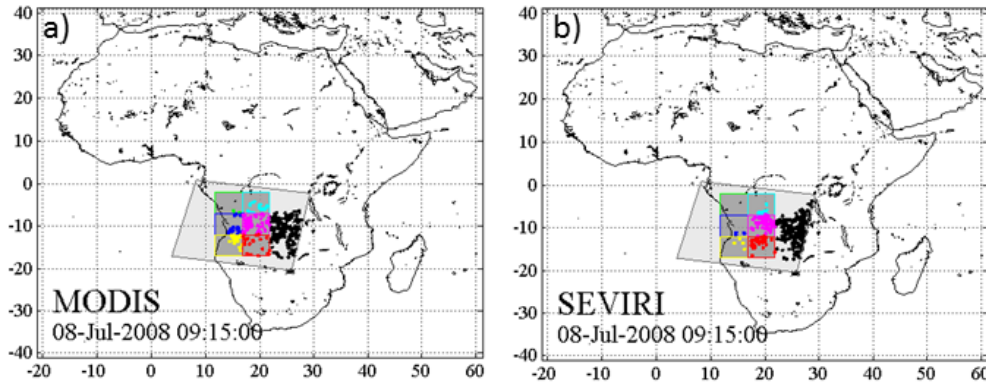


**Figure 6:** Graphical representation of the procedure used to generate the dataset for use in evaluating the bias adjustment factors used within the FRP-GRID product. Fire pixels were subset from the MOD14 and MYD14 MODIS Active Fire products available between May 2008 and April 2009 using six 5.0° grid cells centred on the MODIS swath, as illustrated in (a). These same grid cells were then used in (b) to subset fire pixels from the SEVIRI full Earth disk images acquired at times coincident with the MODIS overpass, as well as from the three previous SEVIRI imaging timeslots collected prior to the MODIS overpass.

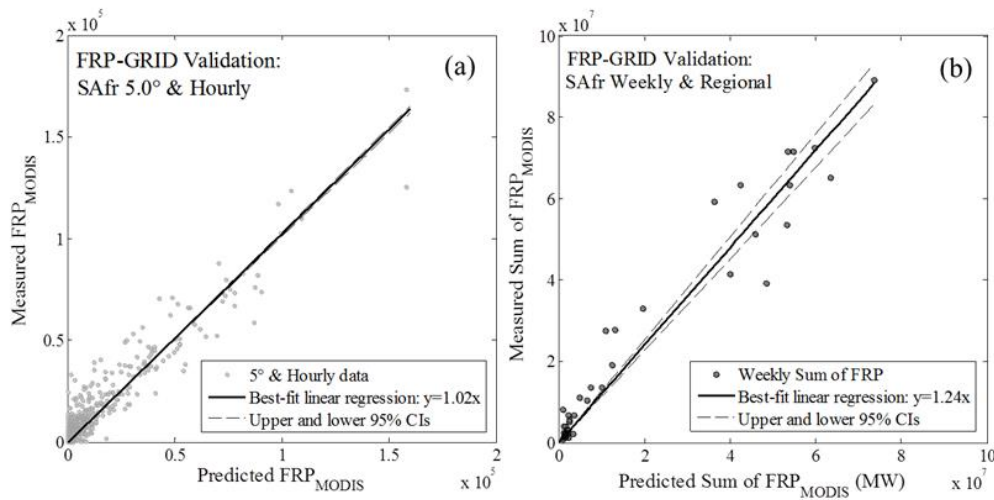


**Figure 7:** Evaluation of the bias adjustment factors used in the SEVIRI FRP-GRID product. Results are based on coincident SEVIRI and MODIS observations taken between May 2008 and May 2009, collected and matched as shown in Figure 6. The nearly 1:1 relationship between the predicted and measured values of MODIS FRP demonstrates the unbiased nature of the adjustment factor applied at (a) 5.0° grid cell resolution and hourly temporal resolution in the FRP-GRID product, in this case for 5.0° grid cells in southern Africa. In (b) the effect of accumulating observations over weekly intervals and over the entire southern Africa LSA SAF geographic region demonstrates that the FRP-GRID product tends to still deliver a result that underestimates the sum of FRP measured by MODIS at this broader spatiotemporal scale, owing primarily to the numerous observations in which SEVIRI failed to detect at least one active fire pixel in a 5.0° grid cell in which MODIS did successfully detect a fire. Full results of the evaluation exercise for all four geographic regions are presented in Table 3.

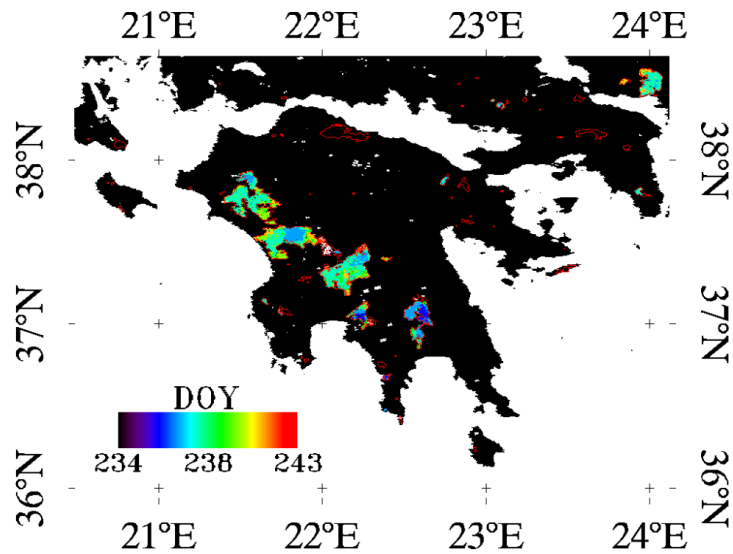
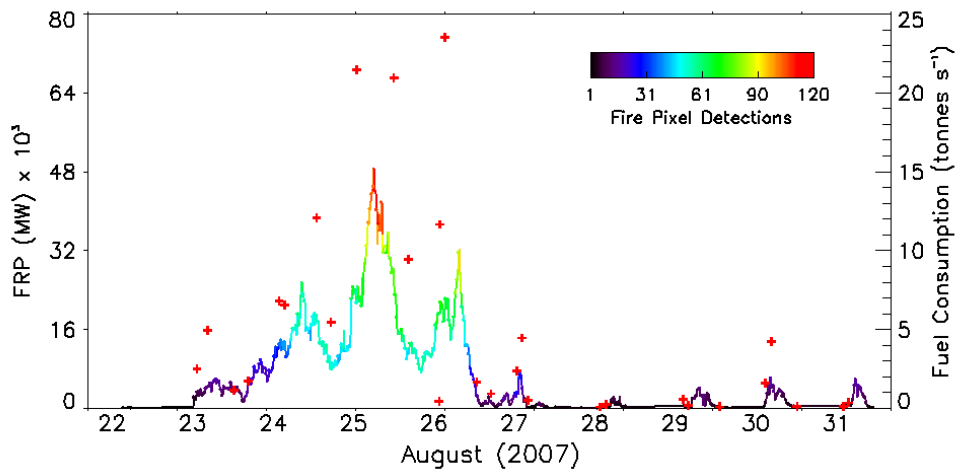
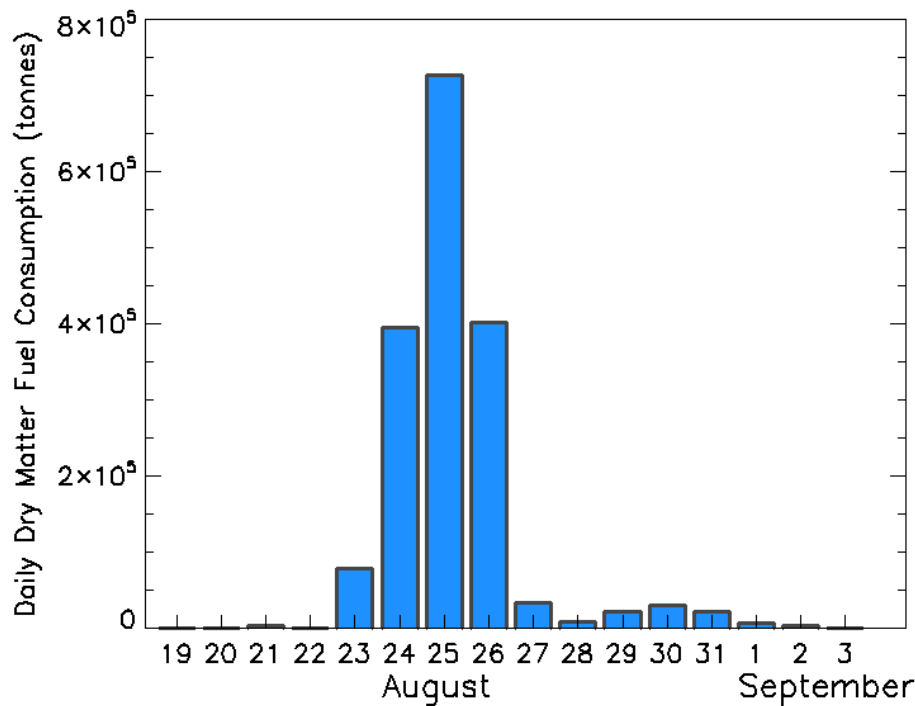


**Figure 8:** The Peloponnese wildfires as viewed by the MODIS 500m burned area of Roy *et al.* (2005) collected in August and September 2007 and coloured by day of the year they were detected (DOY). The fires occurred in areas forest, shrublands and olive groves and affected 1847 km<sup>2</sup> according to these data. Also shown as a red outline are the 2007 burned area perimeters extracted from the European Forest Fire Information System (EFFIS; European Commission, 2010) that encompass 1628 km<sup>2</sup>.

2437  
2438 a)



2439  
2440 b)



2441 **Figure 9:** (a) Time series of atmospherically corrected SEVIRI FRP measures (MW, left  
2442 axis) and equivalent fuel consumption rate ( $\text{tonnes s}^{-1}$ ) for the Peloponnese wildfires, as  
2443 measured between 22<sup>nd</sup> and 31<sup>st</sup> August 2007 using the LSA SAF SEVIRI FRP-PIXEL  
2444 product. Also shown are the atmospherically corrected MODIS FRP data collected over the  
2445 same time period (red crosses). Note that for clarity of presentation the MODIS FRP measure  
2446 recorded on 25<sup>th</sup> August (12:05 UTC) is not shown as this exceeds 180 GW, and SEVIRI  
2447

2448 reaches a far lower value due to strong prevalence of SEVIRI MWIR channel pixel saturation  
2449 at this time. (b) Daily total dry matter fuel consumption estimated using the time-integrated  
2450 SEVIRI FRP data. We estimate 1.74Tg of fuel was consumed in these fires, the bulk of  
2451 which was burned between 24-26<sup>th</sup> August.  
2452

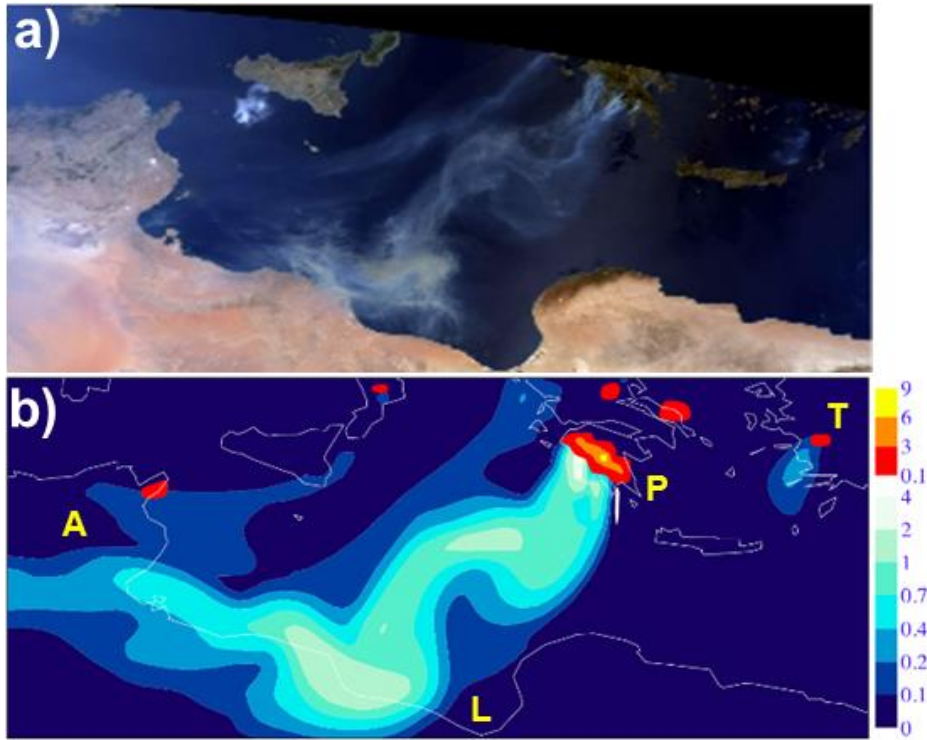
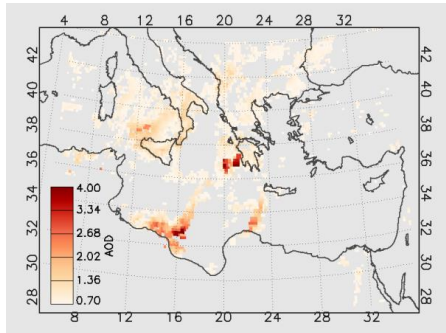


**Figure 10:** (a) MODIS Terra 'true' colour composite derived for August 26<sup>th</sup> (09:35 UTC) and (b) fire-emitted smoke aerosol optical depth at 550 nm derived using the modelling scheme detailed in Section 5.2 (blue scale) along with SEVIRI-derived FRP-density observations derived from the FRP-PIXEL product [ $\text{W m}^{-2}$ , top, red scale] and interpolated to the atmospheric model grid. The FRP-PIXEL observations indicate the smoke plume sources and highlight the strength of the Peloponnese fires at this time. The Peloponnese (P), Libya (L), Algeria (A) and Turkey (T) are identified. MODIS data source in (a): <http://rapidfire.sci.gsfc.nasa.gov>.



a)



b)

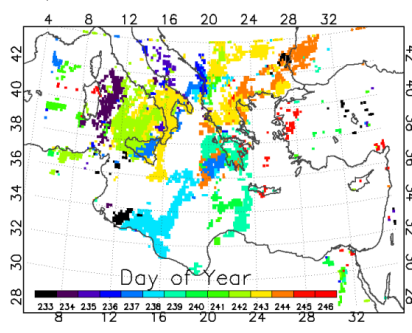
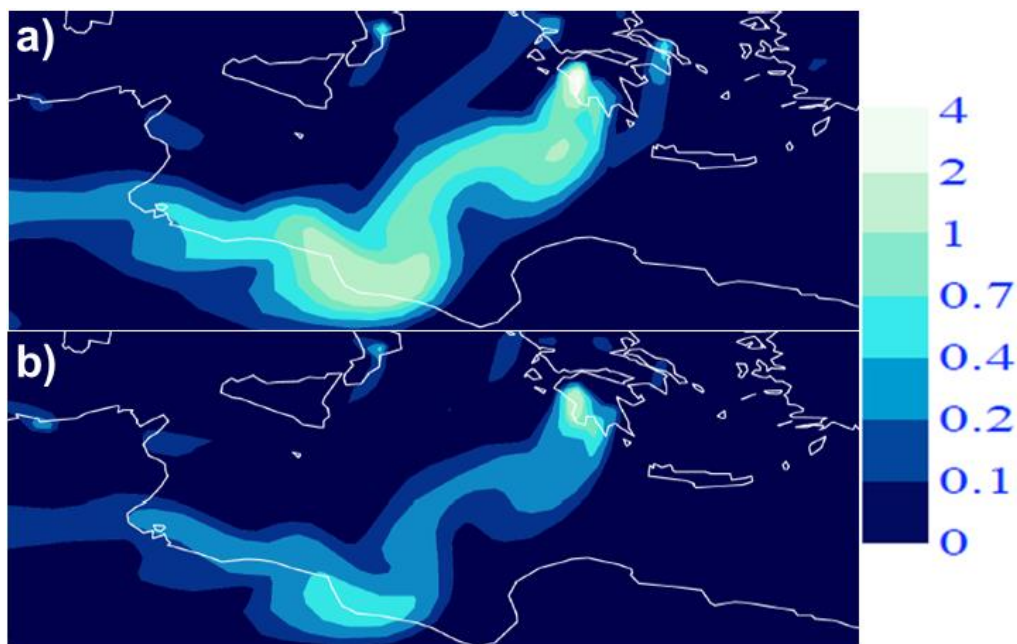


**Figure 11 :** Data extracted for the 2007 Mediterranean 'mega-fire' event from Terra and Aqua MODIS Aerosol Optical Depth (AOD) products (a) Maximum value composite of atmospheric Aerosol Optical Depth (AOD) developed using Terra and Aqua MODIS observations (MOD04 and MYD04 products) acquired between the 21<sup>st</sup> August and 3<sup>rd</sup> September 2007. Only pixels with an AOD value in excess of 0.7 are shown. (b) Day of the year (DOY) of the highest AOD value shown in (a).

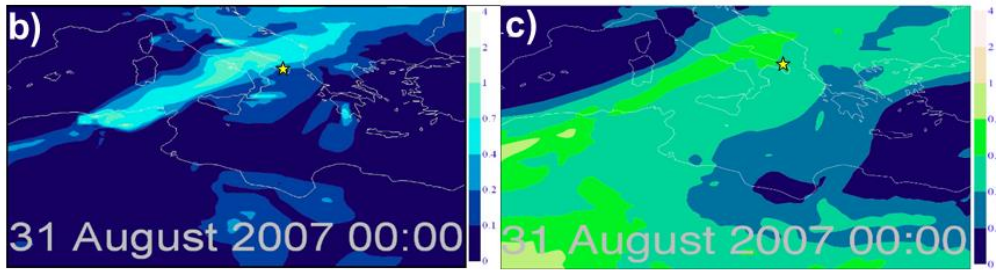
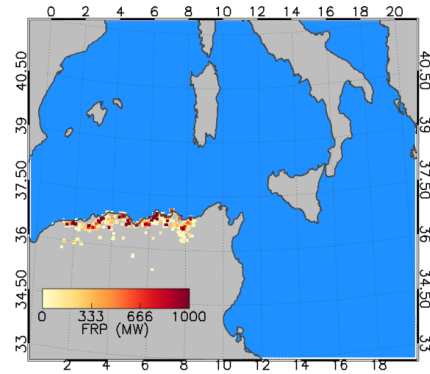
2520  
2521



2522  
2523  
2524  
2525  
2526  
2527  
2528  
2529  
2530  
2531  
2532  
2533  
2534  
2535  
2536  
2537  
2538  
2539  
2540  
2541  
2542  
2543  
2544  
2545  
2546  
2547  
2548  
2549

**Figure 12:** Modelled smoke plume on the 26<sup>th</sup> August (09:35 UTC) calculated using (a) daily, and (b) weekly temporal resolution FRP-derived smoke source emissions as described in Section 5.4. The blue scale indicates variations in the modelled smoke aerosol optical depth (AOD) at 550nm. The corresponding modelled AOD obtained using hourly FRP-derived source emissions is shown in Figure 10b.

a)



Comparison of model (eyvo) & MODIS AOT at 550nm and L1.5 Aeronet AOT at 500nm  
FC Total FC Dust FC BC+OM Aeronet Total Aeronet Fine MODIS Total

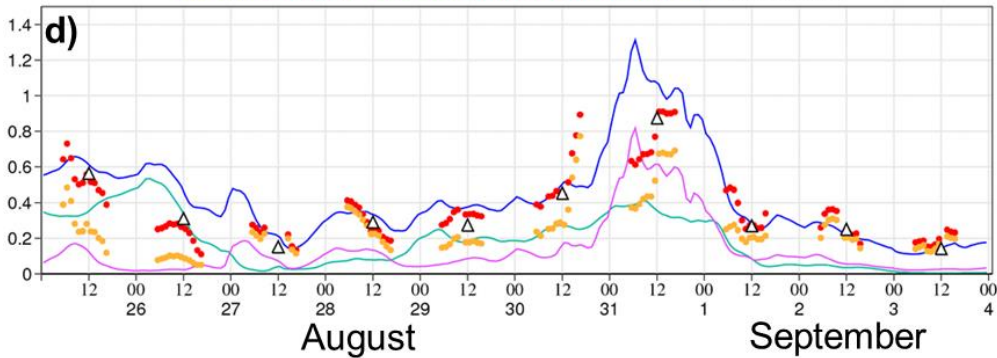
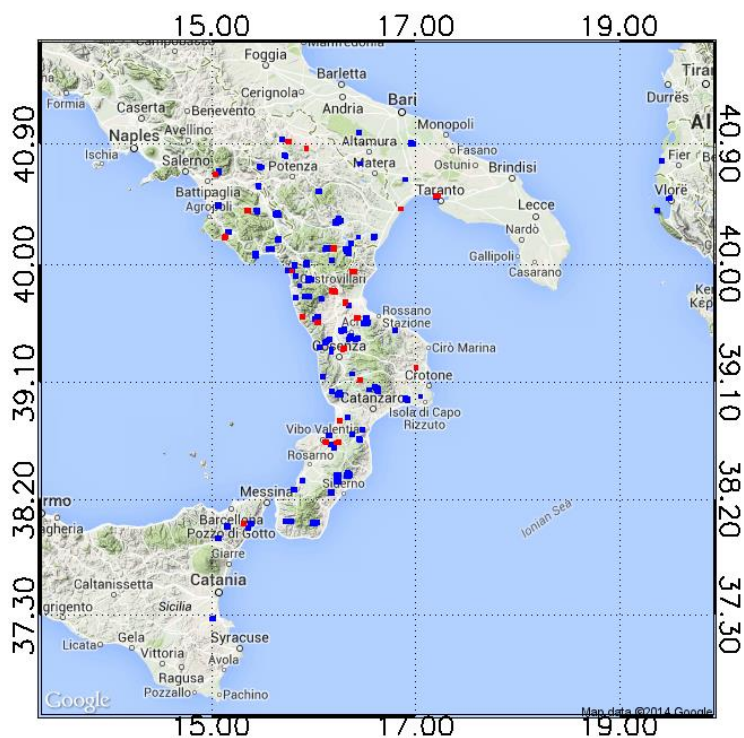


**Figure 13:** MODIS FRP from the Algerian wildfires (a) between the 26<sup>th</sup> August and 4<sup>th</sup> September (2007), (b) modelled smoke, and (c) modelled dust aerosol optical depth (AOD) at 550 nm on August 31<sup>st</sup> 2007 (00:00 UTC). (d) time series of daily averaged MODIS total AOD observations (open black triangles), the AERONET observations of total (red circles) and fine mode AOD (orange circles), modelled total AOD (blue line), and its contributions due to smoke (purple line) and dust (green line). Data sources: MODIS (<http://disc1.sci.gsfc.nasa.gov>) and AERONET (<http://aeronet.gsfc.nasa.gov>)

2566  
2567

2568  
2569



2570  
2571  
2572  
2573  
2574  
2575  
2576  
2577  
2578  
2579  
2580  
2581  
2582  
2583  
2584  
2585  
2586  
2587  
2588  
2589  
2590  
2591  
2592  
2593

**Figure 14** : MODIS active fire detections occurring between the 27 and 31<sup>st</sup> August (blue symbols) and 28 and 29<sup>th</sup> August (red symbols). These fires typically occur downwind of the Algerian smoke plume seen in Figure 13, and therefore are likely to have contributed to elevated AOD values detected at the Lecce AERONET site.

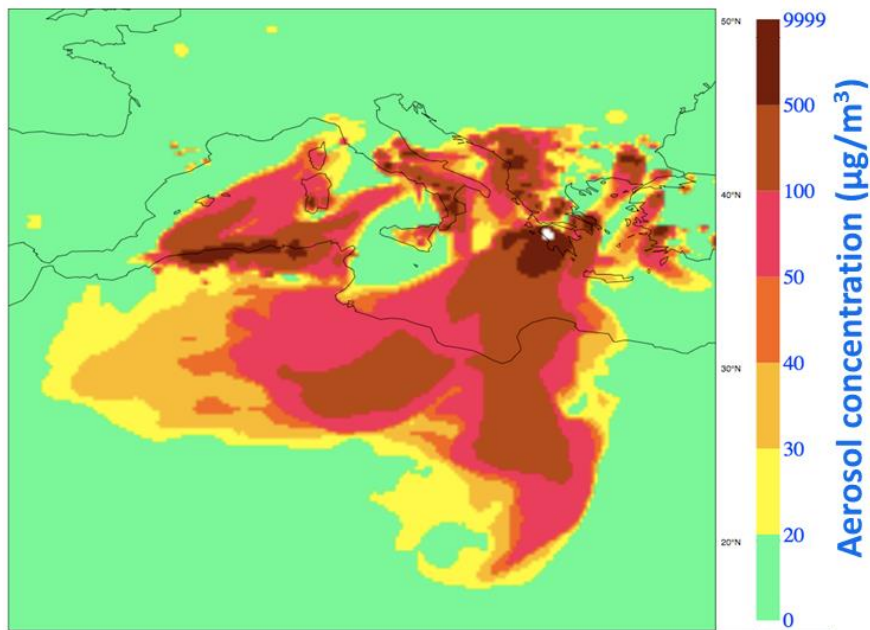


**Figure 15:** Simulated maximum 24-hour running mean smoke aerosol concentration [ $\mu\text{g m}^{-3}$ ] recorded at the surface between the 23<sup>rd</sup> August and 3<sup>rd</sup> September (2007), based on the methodology outlined in Section 5.6. [The values are an upper limit due to unrealistically low smoke injection height into the atmosphere.](#) The World Health Organisation (WHO) air quality guidelines (WHO, 2006) set a limit of  $25 \mu\text{g m}^{-3}$  for the surface concentration of fine mode particulate matter (PM<sub>2.5</sub>) averaged over a 24 hour period.

**Table 1:** Performance characteristics of the LSA SAF Meteosat SEVIRI FRP-PIXEL product in the four LSA SAF geographical regions, as compared to MODIS active fire product (Collection 5 MOD14 and MYD14) collected over the same area and at the same time. Errors of omission and commission with respect to MODIS were calculated on a per fire pixel basis as described in Section 3.1.1. The per-fire basis results (Column 5) were obtained when comparing the total FRP retrieved from MODIS and SEVIRI for fires (defined as a spatially contiguous set of active fire pixels) detected by both sensors. The area-based results (column 6) were derived from comparison of the total FRP measured by all detected fires in a matching MODIS and SEVIRI image area, and thus include the influence of non-detected low FRP fires by SEVIRI whilst the per-fire comparison results (Column 5) do not.

LSA SAF Geographic Region	Image Dates (2008)	Active Fire Pixel Detection Omission Error (%)	Active Fire Pixel Detection Commission Error (%)	Slope of linear best fit relationship between SEVIRI-to-MODIS per-fire-based FRP measures	Slope of linear best fit relationship between SEVIRI-to-MODIS Area-based FRP measures
northern Africa	1-8 Dec	65	9	0.96	0.65
southern Africa	19-24 Aug	77	13	0.97	0.53
South America	14-24 Aug	91	39	0.97	0.22
Europe	9-17 Aug	97	30	0.88	0.11

2655 | **Table 2** : Summary of active fire pixel detection errors of omission and commission ~~of~~ for  
 2656 | the four SEVIRI-derived active fire products explored herein (LSA SAF FRP-PIXEL  
 2657 | product; Wooster *et al.*, ~~this issue~~ 2015, WF-ABBA; Prins *et al.*, 1998, Fire Detection and  
 2658 | Monitoring - FDeM; Amraoui *et al.*, 2010, and FIR Active Fire Monitoring; Joro *et al.*,  
 2659 | 2008). Data were collected over the LSA SAF southern Africa geographic region during  
 2660 | August 2014, when fire activity is widespread in this area. The MODIS active fire products  
 2661 | (MOD14 and MYD14; Giglio *et al.*, 2003) acted as the independent data source for the  
 2662 | comparison.  
 2663 |

	<b>FRP-PIXEL</b>	<b>WFABBA</b>	<b>FDeM</b>	<b>FIR</b>
SEVIRI fire pixels at coincident MODIS overpasses	33414	13008	7664	7151
SEVIRI fire pixels detected by MODIS	29037	12284	7260	6730
Commission error (percent)	13	6	5	6
Omission error (percent)	77	83	92	95

2664 |

	<b>FRP-PIXEL</b>	<b>WFABBA</b>	<b>WFABBA</b>	<b>WFABBA</b>	<b>WFABBA</b>	<b>FDeM</b>	<b>FIR</b>
		<b>All dDetectio ns</b>	<b>Filtered</b>	<b>Filtered (Fflags 0-4)</b>	<b>Filtered (Fflags 0-3)</b>		
Number of SEVIRI fire pixels at coincident MODIS overpasses	33414	15610	13008	9736	8832	7664	7151
Number of SEVIRI fire pixels detected by MODIS	29037	14521	12284	9369	8496	7260	6730
Commission error (%)	13	7	6	4	4	5	6
Omission error (%)	77	82	84	87	88	92	95

Formatted Table

Formatted: Centered

Formatted: Centered

Formatted: Centered

Formatted: Centered

Formatted: Font: Bold, Complex Script  
Font: Bold

2665 |

2666 |

2667 |

2668 |

2669 |

2670 |

2671 |

2672 |

2673 |

2674 |



2675  
2676  
2677  
2678  
2679  
2680  
2681  
2682  
2683  
2684  
2685  
2686  
2687  
2688  
2689  
2690  
2691  
2692  
2693  
2694  
2695  
2696  
2697  
2698  
2699  
2700  
2701  
2702  
2703  
2704  
  
2705  
2706  
2707  
2708  
2709  
2710  
2711  
2712  
2713  
2714  
2715  
2716  
2717  
2718

**Table 3:** Summary of the results related to evaluation of the regional bias adjustment factors implemented during the processing of the LSA SAF FRP-GRID product. Slope of the linear best fit between the SEVIRI-predicted regional FRP using the FRP-GRID bias adjustment factors and the FRP measured by MODIS over the same areas are shown, as are the coefficients of determination ( $r^2$ ), at both 5° and hourly resolution (which is the native FRP-GRID product resolution) and also at a weekly resolution accumulated over the entire LSA SAF geographic region.

LSA SAF Region	Abbreviation	Validation Results: Slope ( $r^2$ )	
		5.0° and hourly	weekly and regional
northern Africa	NAfr	1.04 (0.76)	1.15 (0.96)
southern Africa	SAfr	1.02 (0.91)	1.24 (0.97)
South America	SAme	0.97 (0.34)	1.89 (0.83)
Europe	Euro	1.72 (0.19)	4.94 (0.84)

2719  
 2720  
 2721  
 2722  
 2723  
 2724  
 2725  
 2726  
 2727  
 2728  
 2729  
 2730  
 2731  
 2732  
 2733  
 2734  
 2735  
 2736  
 2737  
 2738  
 2739  
 2740  
 2741  
 2742  
 2743  
 2744

**Table 4:** Trace gas and particulate smoke emission factors ( $\eta$ ) for species (s) based on extratropical forest fuels, taken from Andreae and Merlet (2001). \* The emission factor for BC and OC was derived specifically for use in this study (see main text).

Species	Emissions factor (g kg <sup>-1</sup> DM)
Black carbon (BC)	1.7*
Organic carbon (OC)	8.6-9.7
Organic matter (OM)	42*
Total particulate matter (TPM)	17.6±6.4
Fine mode aerosol (PM2.5)	13.0±7.0
Carbon Monoxide (CO)	107±37

2745  
 2746  
 2747  
 2748  
 2749  
 2750  
 2751  
 2752  
 2753  
 2754  
 2755  
 2756  
 2757  
 2758  
 2759  
 2760  
 2761

2762